UNIVERSIDADE FEDERAL DE PERNAMBUCO
CENTRO DE CIÊNCIAS EXATAS DA NATUREZA
PROGRAMA DE PÓS-GRADUAÇÃO EM FÍSICA

Thaís Feliciano Silva

Multiple signatures of criticality explored on V1 neuronal activity

Recife

2023

Thaís Feliciano Silva

Multiple signatures of criticality explored on V1 neuronal activity

Trabalho apresentado ao Programa de Pós-graduação em Física do Centro de Ciências Exatas da Natureza da Universidade Federal de Pernambuco, como requisito parcial para obtenção do grau de Doutor em Física.

Área de Concentração: Dinâmica Não-linear, Caos e Sistemas Complexos

Orientador (a): Pedro Valadão Carelli

Coorientador (a): Michael Okun

Recife

2023

Catalogação na fonte
Bibliotecária: Luiza de Oliveira, CRB4-1316

S586m Silva, Thaís Feliciano
Multiple signatures of criticality explored on V1 neuronal activity / Thaís Feliciano Silva. – 2023.
106 f.: il., fig., tab.

Orientador: Pedro Valadão Carelli.
Coorientador: Michael Okun
Tese (Doutoradodo) – Universidade Federal de Pernambuco. Centro de Ciências Exatas e da Natureza. Programa de Pós-graduação em Física. Recife, 2023.
Inclui referências e apêndice.

1. Criticidade. 2. Avalanches neuronais. 3. Modelos de máxima entropia. 4. Estados corticais. 5. Medidas de complexidade. 6. Silicon Probes I. Carelli, Pedro Valadão (orientador) II. Okun, Michael (coorientador) III. Título

530 CDD (23. ed.) UFPE - CCEN 2023 – 210

THAÍS FELICIANO SILVA

MULTIPLE SIGNATURES OF CRITICALITY EXPLORED ON V1 NEURONAL ACTIVITY

Tese apresentada ao Programa de Pós-Graduação em Física da Universidade Federal de Pernambuco, como requisito parcial para a obtenção do título de Doutora em Física.

Aprovada em: 30/11/2023.

BANCA EXAMINADORA

_____

Prof. Dr. Pedro Valadão Carelli
Orientador
Universidade Federal de Pernambuco

_____

Prof. Dr. Clécio Clemente de Souza Silva
Examinador Interno
Universidade Federal de Pernambuco

_____

Prof. Dr. Renê Rodrigues Montenegro Filho
Examinador Interno
Universidade Federal de Pernambuco

_____

Profa. Dra. Fernanda Selingardi Matias
Examinadora Externa
Universidade Federal de Alagoas

_____

Prof. Dr. Marcelo Bussotti Reyes
Examinador Externo
Universidade Federal do ABC

To my family, Edvaldo, Rosângela and Thiago.

ACKNOWLEDGEMENTS

Having the opportunity to pursue a PhD candidacy demands a great deal of personal effort, but without a support network and favorable financial conditions, none of this would have been possible. Therefore, I would like to express my gratitude to all the individuals and institutions that have assisted me on this journey. Having experienced individuals from diverse scientific backgrounds supporting me was crucial in not only learning how to become a good scientist but also in understanding how to engage with people in the academic community in a constructive manner. In this regard, I extend my sincere appreciation to Dr. Pedro Carelli, my thesis advisor, for his unwavering support, guidance, and invaluable insights throughout my scientific education. I am also grateful to other seasoned researchers, including Dr. Nivaldo Vasconcelos, Dr. Mauro Coppeli, Dr. Michael Okun, and Dr. Fernanda Matias, for their constructive feedback, support, and as sources of inspiration.

Throughout my journey, I had the privilege of working with several individuals who were not only academic collaborators but have also become lifelong friends. My deep gratitude goes out to Dr. Leandro Aguiar, Dr. Antônio Fontenele, Dr. Tawan Carvalho, Bh. Thais Priscilla, Ms. Helena Piuvezam, Daniel Miranda, Nastaran Lotfi, Jheniffer Gonsalves, Felipe Serafim for their contributions and companionship in this academic odyssey.

I also want to acknowledge the financial support provided by the CAPES Institution. Without their funding, my academic pursuit would have been impossible.

Special thanks are owed to my family and friends for their unwavering encouragement and understanding throughout this challenging endeavor. They were essential in helping me stay focused without losing sight of my ultimate goal, providing distraction when I needed to relax, and offering emotional support when tasks seemed overwhelming.

I am filled with a sense of gratitude for having completed this phase of my academic career with the help of everyone, and I feel ready to continue investing in my career, and learning more and more.

ABSTRACT

The hypothesis that the brain self-organizes around a critical point has been under investigation for nearly three decades. This notion posits that extensive neuronal populations can be effectively examined as many-body systems, characterized by principles from statistical physics. According to this analogy, a system near this critical point exhibits certain functional advantages, and the brain already exhibits these characteristics, providing support for the concept of brain criticality. In other contexts, critical point analysis typically explores the transitions between various phases or states of a system, yet the application of this analysis to the dynamics of the brain has remained relatively underexplored. In this study, we propose the evaluation of three distinct signatures of criticality for different cortical states. We define different cortical states based on the level of variability in neuronal population activity, which is closely associated with the degree of synchrony among neurons. The criticality indicators demonstrate greater significance during moments characterized by intermediate levels of synchronization among the neuronal population, as recorded using silicon probes in the visual cortex of anesthetized rats. These findings reinforce investigations into fundamental questions such as the self-organization of brain dynamics around a critical point between assumed brain states and also into the use of synchrony levels in neuronal population activity as an order parameter for a transition associated with the critical point.

Keywords: Criticality. Neuronal avalhanches. Maximal Entropy models. Cortical states. Complexity measures. Rat's Primary Visual Cortex. Silicon Probe.

RESUMO

A hipótese de que o cérebro se autoorganiza em torno de um ponto crítico tem sido objeto de investigação há quase três décadas. Essa ideia postula que grandes populações neuronais podem ser efetivamente examinadas como sistemas de muitos corpos, caracterizados por princípios da física estatística. De acordo com essa analogia, um sistema próximo a esse ponto crítico apresenta certas vantagens funcionais, e o cérebro já exibe essas características, oferecendo suporte ao conceito de criticalidade cerebral. Em outros contextos, a análise de ponto crítico normalmente explora as transições entre várias fases ou estados de um sistema, no entanto, a aplicação dessa análise à dinâmica do cérebro tem permanecido relativamente pouco explorada. Neste estudo, propomos a avaliação de múltiplas assinaturas de criticidade para diferentes estados corticais. Definimos diferentes estados corticais com base no nível de variabilidade na atividade da população neuronal, que está intimamente associada ao grau de sincronia entre os neurônios. Os indicadores de criticalidade demonstram maior significância durante momentos caracterizados por níveis intermediários de sincronização entre a população neuronal, conforme registrado por eletrodos de alta densidade no córtex visual de ratos anestesiados. Essas descobertas reforçam investigações sobre questões fundamentais tais como a autoorganização da dinâmica cerebral em torno de um ponto crítico entre supostos estados do cérebro e também sobre o uso do nível de sincronia na atividade da população neuronal como um parâmetro de ordem para uma transição associada ao ponto crítico.

Palavras-chaves:Criticalidade. Avalanches neuronais. Modelos de Máxima Entropia. Estados corticais. Medidas de complexidade. Córtex visual primário de ratos. Silicon Probes.

LIST OF FIGURES

CONTENTS

1 INTRODUCTION

In the natural world, systems, and objects typically exhibit a distinctive order that lies somewhere between complete order and utter chaos (CRUTCHFIELD, 2011; WHEATLEY, 1992; MADDOX, 1990; GIORBRAN, 2005). This balance between structured organization and randomness is a fundamental characteristic of the world. In the realm of biology, numerous systems display intricate behaviors, which is crucial because it allows these systems the flexibility to adapt, enhance their ability to comprehend new stimuli, incorporate new elements, and eliminate unnecessary components (TOUSSAINT; SEELEN, 2007).

That concept of organization doesn't appear to be the result of any discernible external force or larger system, at least nothing that can be definitively demonstrated. It seems more intellectually sound to consider that organization arises from within the system. Perhaps due to evolutionary processes, biological systems exhibit a tendency to self-organize into an optimal state of functionality, and the brain is no exception to this pattern (BAK, 2013).

The brain has been a subject of study for centuries, and even without prior knowledge, it is evident that the brain's components do not operate in a random, disconnected manner. Conversely, it is also apparent that these components are not in a constant state of synchronization. In such extreme scenarios, it is hard to believe that complex behaviors like speaking, recalling past facts, and investigating the brain's inner workings could emerge.

Physics has a well-established methodology for studying the emergence of complex outcomes from multiple components. For instance, in thermodynamics, a straightforward example illustrates how the positions and velocities of individual particles, along with their interactions, lead to the emergence of collective properties like pressure and temperature. Similarly, in the realm of magnetism, the angular momentum of each particle, or spin, can interact and become organized, resulting in the magnetization of the entire material (GREINER; NEISE; STÖCKER, 2012).

That branch of Physics that deals with systems composed of many particles is called Statistical Physics. It seeks to understand their behavior in terms of statistical laws and probabilities. It provides a bridge between the microscopic world of individual particles and the macroscopic world of everyday observations, helping explain phenomena in thermodynamics, fluid dynamics, and condensed matter physics (TORQUATO; TORQUATO, 2002).

In a simplified perspective, the brain consists of numerous particles, namely neurons, which

interact with each other, giving rise to complex outcomes. This allows for analogies to be drawn between extensive neuronal populations and the many-body particle systems examined in the field of physics.

The inaugural application of statistical physics to the analysis of extensive neuronal populations is frequently credited to John Hopfield's pioneering research in 1982. His work established the groundwork for approaching the study of neural networks through a statistical physics lens and left a profound imprint on the field of neuroscience. Subsequently, the relationship between neuroscience and statistical physics has been further investigated by employing various neuronal datasets and statistical physics methodologies (BIALEK, 2012; HOPFIELD, 1982; KELSO, 1984; PARISI, 1993).

Neuronal data can be obtained through computational models or live recordings. Simulated neuronal network data can vary in form, such as representing individual neuron activity (KASABOV, 2010), network connectivity (SPORNS, 2014), membrane potential traces (HODGKIN; HUXLEY, 1939), or extracellular electrical potential (PARASURAM et al., 2016). These simulations are crucial for testing hypotheses, understanding neural mechanisms, and gaining insights into real neural circuit functioning.

Real-time recordings of neuronal circuits can be obtained through a range of methods. For instance, the use of microelectrodes for extracellular measurements of voltage fluctuations within brain tissue (HAI; SHAPPIR; SPIRA, 2010). Another approach involves employing fluorescent calcium indicators to monitor intracellular calcium levels, which serve as a proxy for neuronal activity (GRIENBERGER; KONNERTH, 2012). Non-invasive techniques, such as fMRI for assessing blood flow and oxygenation (HEEGER; RESS, 2002), MEG for capturing magnetic fields arising from neuronal activity (HALL et al., 2014), and EEG for detecting electrical potentials generated by neurons (KIRSCHSTEIN; KÖHLING, 2009), provide high temporal resolution and are well-suited for clinical neurology and cognitive neuroscience. In contrast, optogenetics, a more recent innovation, integrates genetic engineering with light-sensitive proteins to both control and record specific neuronal activity (YIZHAR et al., 2011). These methods exhibit variations in spatial and temporal resolution, invasiveness, and applicability to specific research inquiries.

The techniques employed to record actual brain activity not only leverage fundamental physics principles like electric circuits, magnetism, and optics, but the subsequent data analysis can also incorporate various physics concepts. Irrespective of the recording method, the analysis of extensive neuronal populations' activity can benefit from the application of statistical physics

Figure 1 – Phase diagram of a fluid.

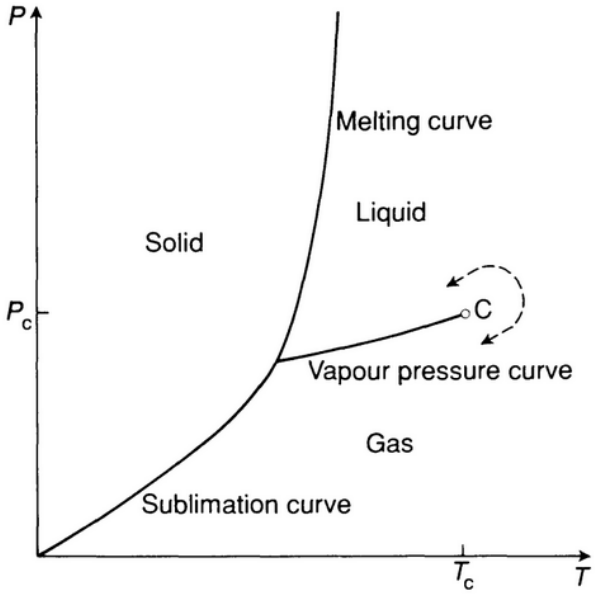

Source: YEOMANS (1992)

methods, as previously discussed.

Statistical Physics has devised techniques for investigating systems comprising numerous microscopic components that manifest diverse types of macroscopic collective behaviors, often referred to as phases, each characterized by distinct levels of internal order (MUNOZ, 2018). Some biological systems may exhibit intermediate levels of organization, not always falling into a state of complete order or complete disorder (HARRIS; THIELE, 2011). Living systems can offer notable functional advantages by operating at critical points that represent delicate balances between phase transitions (SHEW; PLENZ, 2013).

Critical phenomena have been the subject of extensive exploration across a diverse array of systems, including fluid phase transitions (STANLEY, 1971), sandpile dynamics (BAK; TANG; WIESENFELD, 1988b), seismic events (LOTFI; DAROONEH, 2012; REZAEI et al., 2017), bird flock behavior (CAVAGNA et al., 2010), magnetism, condensed matter (SACHDEV; MA, 2011), and beyond. For instance, the phase transition of a fluid can be visually represented in Figure 1, where the lines demarcate the points at which phase transitions may occur. Among these critical points, the specific characteristics of critical point C set it apart, and these distinct attributes serve as key indicators of criticality. They enable us to gauge the system's proximity to this critical region within the phase diagram.

Utilizing theories such as the scaling hypothesis and renormalization group, it becomes

possible to mathematically demonstrate that many characteristics of critical points remain predominantly unaffected by small-scale intricacies. Consequently, one can strongly suggest the existence of universality in large-scale behavior (KADANOFF, 1990).

Extensive investigations have delved into identifying signatures of criticality within living systems (MUNOZ, 2018). The aim of this thesis was to quantitatively analyze these signatures within a system composed of neurons recorded from the cortical region responsible for high-order visual perception processes.

The notion of criticality holds particular allure, especially when applied to extensive neuronal populations, as many of its inherent features, such as long-range spatiotemporal correlations, heightened sensitivity to stimuli, and enhanced information decoding capabilities, align closely with the organization of the brain (SHEW et al., 2011; SHEW et al., 2009).

Statistical physics concepts generally use the thermodynamic limit, wherein the number of particles in the system approaches infinity. When applying statistical physics methods to real neuronal networks, it is vital to consider experimental limitations. The number of neurons that can be recorded depends on the chosen experimental technique, and even the most precise technique will present effects of subsampling (recording fewer neurons than the total number in the target region) (PRIESEMANN et al., 2013; PRIESEMANN et al., 2014).

Fortunately, the scaling hypothesis offers a promising solution to the subsampling predicament. One of the implications of this hypothesis is that the system retains similar structures regardless of the level of detail considered. In essence, if scale invariance can be detected in one part of the system, it is reasonable to infer that other parts of the system exhibit analogous signatures of criticality (HARDSTONE et al., 2012).

This thesis centers on the exploration of criticality signatures within extensive neuronal populations obtained from the visual cortex of rats. The data and subsequent analysis were performed collaboratively by me and colleagues. This collective endeavor aims to illuminate the topic of brain criticality and has yielded noteworthy findings, which are expounded upon in the following chapters.

From this point forward, the structure of this thesis will be as follows: The upcoming chapter will elucidate fundamental neuroscience concepts essential for comprehending the subsequent results. In Chapter Three, we delve into the foundations of the Critical Hypothesis. Chapter Four provides an in-depth description of the methodologies employed to attain our findings. Moving to Chapter Five, a detailed analysis of four published articles by our group, which investigate various criticality signatures computed from electrophysiological data

obtained from V1 rats, will be presented. The final chapter will engage in a discussion of the results and explore potential avenues for future research.

2 ESSENTIAL TOPICS OF FUNDAMENTAL NEUROSCIENCE

2.1 STRUCTURAL ORGANIZATION OF THE NERVOUS SYSTEM

The nervous system is a complex and intricate network of specialized cells, tissues, and structures that coordinate and regulate the activities of the body. It is unanimous that this system is not only responsible for motor behaviors and raw stimulus-response, but also for all the complex cognitive and behavioral acts such as consciousness, speaking, art production, dance, critical thinking, and so on (ARBER; COSTA, 2018; SACKS, 2007; KANDEL; SQUIRE, 2000)

In the animal kingdom, there is an enormous diversity of nervous system organization. In mammals, the nervous system is organized into two main parts: the central nervous system and the peripheral nervous system. All the perception, complex behavior, and stimuli response are coordinated by the central nervous system (CNS) which can be divided into two significant parts, the spinal cord, and the brain. The spinal cord conveys information between the body and brain, both ways, of skin, joints, and muscles. The dorsal part is dedicated to upstream information and The brain is subdivided into 7 main parts: the medulla oblongata (autonomic functions), pons (transmit movement information from the cerebrum to the cerebellum), cerebellum (motor skills), midbrain (eye movement, visual and auditory reflex movements), diencephalon (composed by thalamus and hypothalamus), and cerebrum (composed by cortex, basal ganglia, hippocampus, amygdaloid nuclei), such as illustrated in Figure 2

The cerebrum is the most significant part of the brain and is responsible for integrating and computing high-order functions. This part is divided into 4 functional regions (connectional approach): Frontal lobe (executive functions, decision-making), Pariental lobe (processing sensory information), Temporal lobe (auditory processing, language), and Occipital lobe (visual processing and perception). See figure 3.

The mapping of the brain relies on both its structure and function. Within vertebrates, each region's location is determined by a foundational body plan that outlines the spatial arrangement of structures in three dimensions as depicted in Figure 4. The primary body axis, known as the Rostrocaudal axis, spans from the rostrum to the cauda. The second axis, the Dorsoventral axis, extends from the dorsum to the ventrum. The third axis, the Mediolateral axis, runs from the midline to the animal's lateral margin. These three axes collectively aid in comparing the development of brains within the same species and comprehending the evolution

Figure 2 – The Central Nervous System is divided into seven regions. The Spinal Cord(1), Brain Stem (grouping Medulla Oblongata (2), Pons (3) and Midbrain (5)), Cerebelum(4), Diencephalon (6) (composed by thalamus and hypothalamus) and the cerebrum (7).

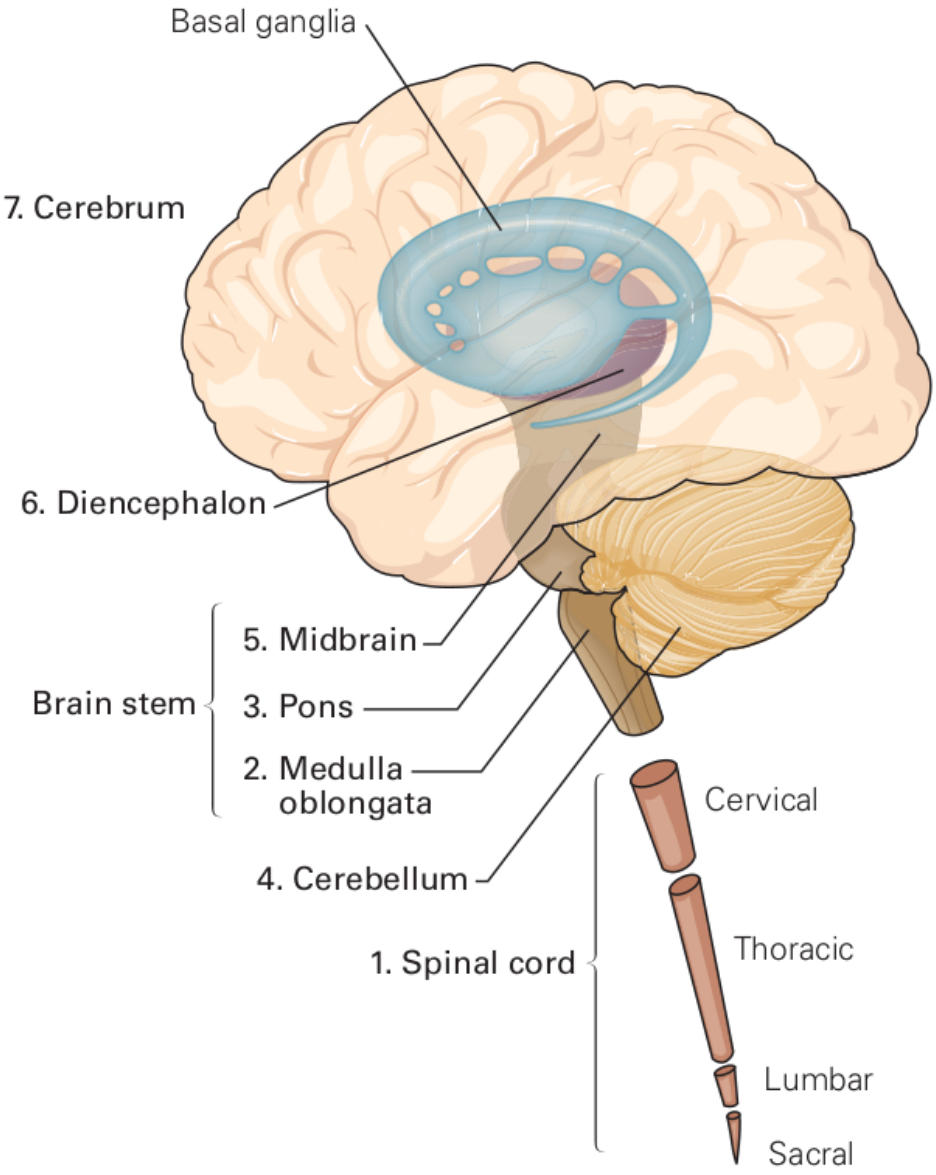

Source: ERIC; JAMES; THOMAS (2000)

of brains across different species (MAI; MAJTANIK; PAXINOS, 2015).

The cerebral cortex, the most superficial region of the cerebrum, is organized in layers in order to increase the efficiency of the sensory information processing (WOOLSEY; LOOS, 1970). The neocortex is what is called the evolutionary more recent part of the cortex encountered in mammals (NORTHCUTT; KAAS, 1995). The neocortex receives inputs from the thalamus, and other cortex regions and its outputs will be spread along the specific cortex regions, going back to the thalamus, basal ganglia, spinal cord, and so on (MORGENSTERN; BOURG; PETREANU, 2016; HARRIS; SHEPHERD, 2015).

Figure 3 – The four lobes of the cerebrum are named after the cranial bones that are located above them. The Central sulcus (furrows on the surface of the brain) delimits the Frontal and Parietal Lobes. The lateral sulcus delimits the Frontal from the Temporal Lobe.

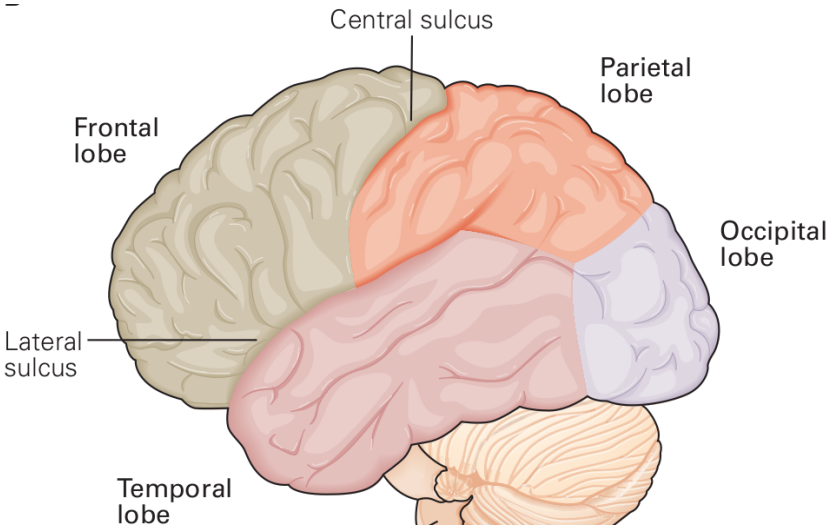

Source: ERIC; JAMES; THOMAS (2000)

Figure 4 – Any part of the central nervous system (CNS) can be accessed using three axes, rostral-caudal, dorsal-ventral, and ventral-dorsal. This three-dimensional space is used for different species and for all the extensions of the CNS.

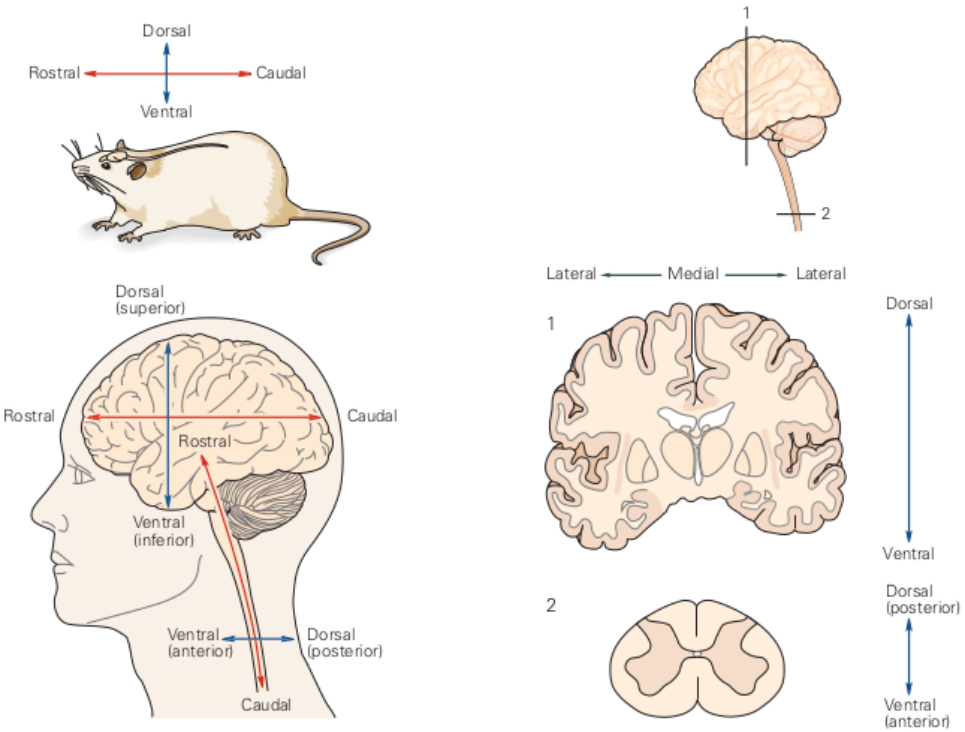

Source: ERIC; JAMES; THOMAS (2000)

The cerebral cortex is composed of a dense sheet of nervous cells called **neurons**. In addition to neurons, the neocortex is an arrangement of other supporting structures such as

Figure 5 – The cell body or soma is where the nucleus and organelles cytoplasmic such as endoplasmic reticulum and the Golgi apparatus are. The dendrites could be found close to the soma or at the end of the axon. They are responsible for the connection between neurons. The axon transmits information in the form of ion concentration, vesicles, proteins, and others. Specifically, the axons could be involved in glial structures called Myelin Sheaths. The synapses are the last part of dendrites responsible for expelling or phagocyte substances.

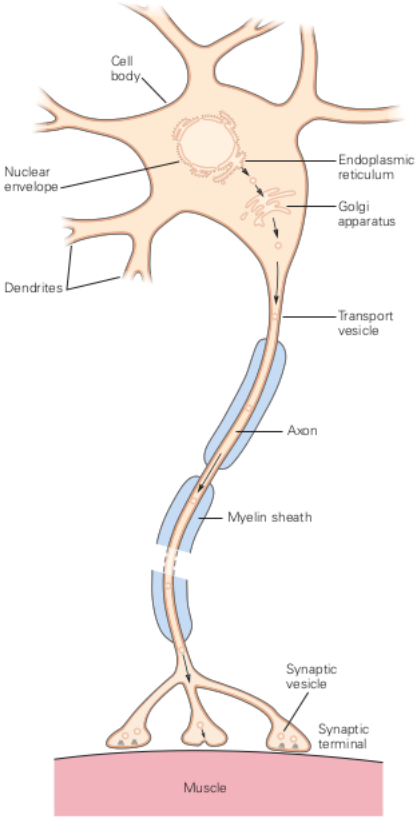

Source: ERIC; JAMES; THOMAS (2000)

glial cells (direct support to signaling), blood vessels (supply essential nutrients and oxygen), endothelial cells (responsible for the blood-brain barrier) and perivascular cells (regulation of cerebral blood flow) (SUR; RUBENSTEIN, 2005).

The neurons are basically composed of the soma, dendrites, and axons. The soma is the metabolic center of the neuron, and it gives rise to several dendrites and one long axon. As with any cell, the soma is composed of cytoplasmic organelles and the cell nucleus embedded by the cytosol. The dendrites are the part of the cell that receives the information coming from the other nerve cells. The axon carries the electrical signal to other cells and extends some distance from the cell body. The extension could be between 0.1mm to 2m. They are crucial for sustaining the function of remote regions. See figure 5 One of the most important structures to signaling in the brain, besides the neurons, are the glial cells. They play diverse roles in neural function. This cell forms the insulating sheaths for the axon, and this insulation is

different between the central nervous system and the peripheral nervous system. See in Figure 6 This type of cell constitutes nearly half the number of brain cells. They nourish neurons and regulate the concentration of extracellular components. Some of them play an important role in the immunological surveillance of the Central Nervous System, poised to react to foreign invaders.

Figure 6 – The glial cell has important roles at the central nervous system's functioning. One of them is the myelinating of neuron which is depicted in this figure. The oligodendrocyte (OL), a type of glial cell, projects myelin sheaths (M) to cover parts of axon segments in order to increase signaling speed. The axon parts not covered it is called nodes of Ranvier (N), they are responsible for the action potential "saltatory conduction". Without the myelin sheaths, the electrical signal would travel continuously along the entire length of the axon, losing amplitude. With this mechanism, the action potentials are renewed from node to node, maintaining the signal properties.

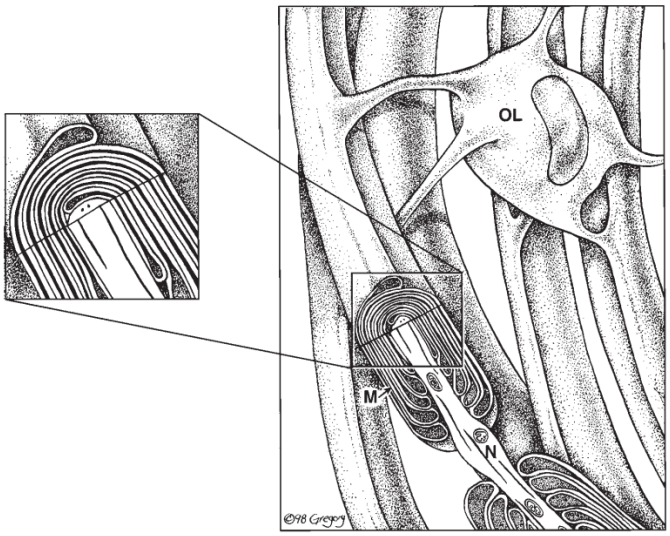

Source: SQUIRE et al. (2012)

2.2 SIGNALING IN THE BRAIN

Neurons serve as the fundamental signaling components of the brain. Understanding their interconnections and information transmission is crucial. Awareness of the electrical properties in certain nerve cells and muscles dates back to Galvani's experiments with frogs in the late 1700s. Physiologists in the late 19th century further demonstrated that the speed of electrical activity conduction along neurons impacts neighboring neuron activity. To gain a deeper understanding of the origin of the brain's electrical signals, it is essential to grasp the structure of the neural membrane.

The cell membrane, present in all cells, including neurons, consists of an insulated lipid bilayer that separates the extracellular environment from the intracellular one. As a result,

ions accumulate intracellularly and extracellularly, potentially creating an electric potential difference due to differences in ion concentration.

Each type of ion contributes to the total electrical potential difference of the cell and the Goldman Equation can quantify this and it is called **membrane potential**.

The Goldman Equation, as denoted in Equation 2.1, takes into account the permeability (rate of solute movement) of the membrane for each ion, which is crucial for the electrical signaling of neurons. Another essential factor in calculating membrane potential is the concentration of each ion both inside (e.g., $[K]_in$) and outside (e.g., $[K]_out$) the cell. P is the permeability of the membrane to a specific ion.

$$V_m \approx -60mV \log_{10} \frac{P_K[\ \mathrm{K}]_{\mathsf{in}} + P_{\mathrm{Na}}[\mathrm{Na}]_{\mathsf{in}} + P_{\mathrm{Cl}}[\mathrm{Cl}]_{\mathsf{out}}}{P_K[\ \mathrm{K}]_{\mathsf{out}} + P_{\mathrm{Na}}[\mathrm{Na}]_{\mathsf{out}} + P_{\mathrm{Cl}}[\mathrm{N}]_{\mathsf{in}}} \tag{2.1}$$

It is important to note that changes in the intra/extracellular ion concentrations are the only factors that can alter the membrane potential. Integral membrane proteins called ion channels, located between the phospholipids composing the cell membrane, are responsible for regulating ion traffic based on specific physical and chemical stimuli. These ion channels possess crucial properties, such as ion selectivity and the ability to open and close in response to electrical, mechanical, or chemical cues, as depicted in Figure 7.

The electrical activity of neurons is related to the movement of ions across the ion channels. There is an event called **Action Potential** which is an abrupt change in the membrane potential detectable through properly calibrated electrodes.

Action potentials exhibit four critical features: a threshold, an all-or-none event, conduction without decrement, and a refractory period. The threshold must be surpassed to initiate an action potential. The second feature ensures that regardless of how much the membrane potential surpasses the threshold, the amplitude and duration of the action potential remain consistent. The third feature guarantees that the action potential propagates over long distances while maintaining its amplitude and frequency. The final feature, the refractory period, denotes the time during which a neuron cannot fire another action potential.

When a neuron is active, it is said to have 'fired,' or a 'spike' has occurred. This activity primarily arises from the harmonious functioning of two ion channels: Sodium and Potassium, whose permeability is directly regulated by the membrane potential. See in Figure 8.

The action potential is how signals are transmitted within a neuron, while the synaptic process dictates communication between neurons. Synapses are specialized zones of contact

Figure 7 – The orange part represents lipid bilayer insulated structure. The blue part represents the specialized ion channels. They control the ion's concentration inside and outside the cell. The rest membrane potential is also controlled by the Na_+/K_+ ionic pump. The electrical potential for each ion is represented in millivolt (mV).

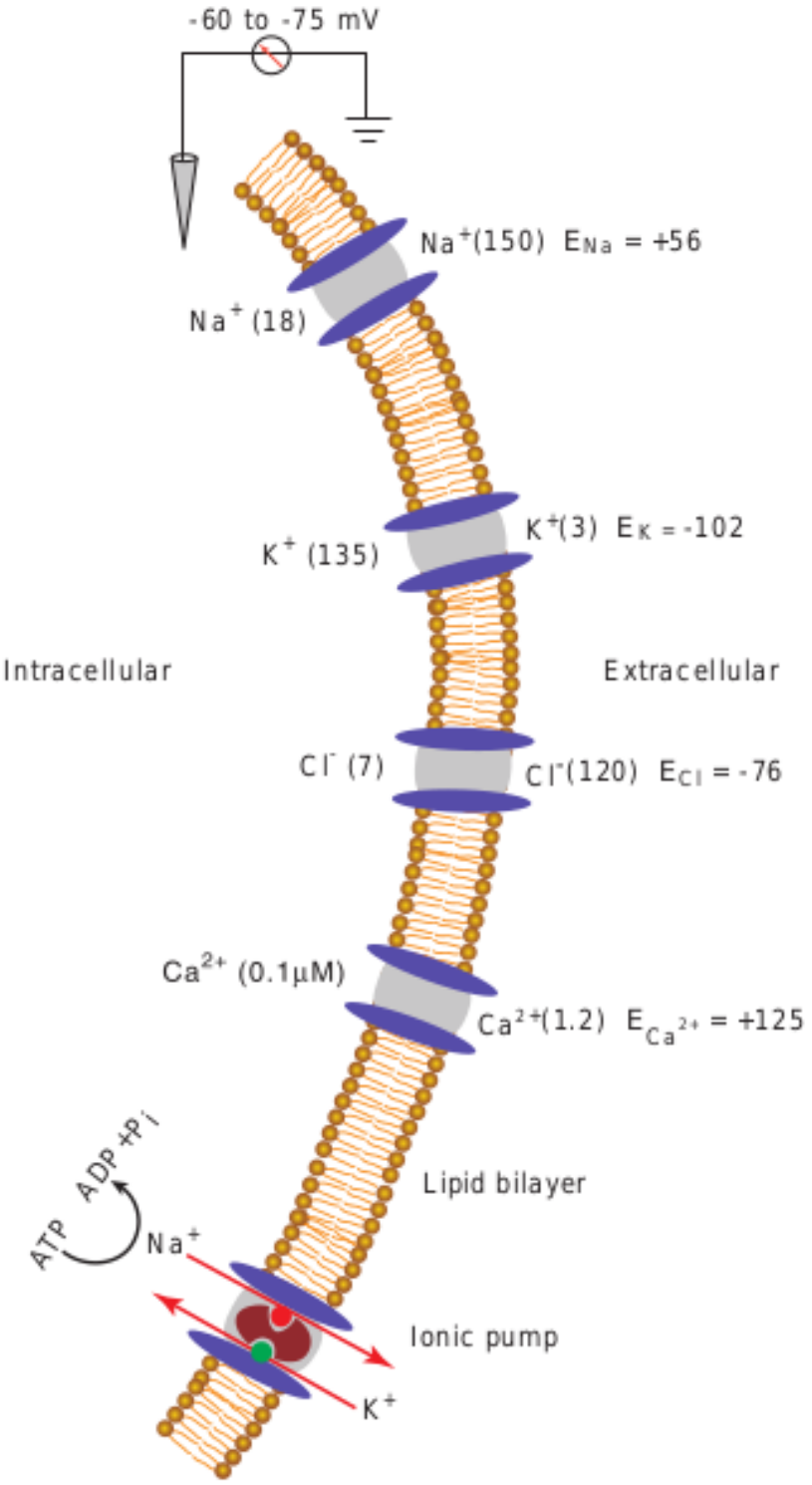

Source: SQUIRE et al. (2012)

Figure 8 – Study of the membrane potential compared with the number of open channels during an action potential. The conductance is defined as the number of open channels per μm^2 located in the neuron's membrane. The figure is showing the conductance for Na_+ and K_+ ions. The action potential event depends on the combination of the two conductances.

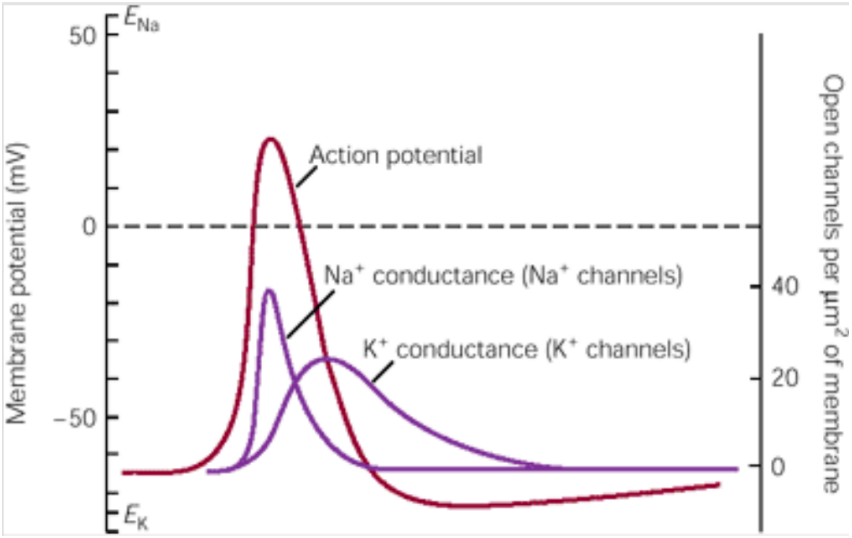

Source: ERIC; JAMES; THOMAS (2000)

where neurons exchange signals and come in two main types: Electrical synapses and Chemical synapses.

Figure 9 – Morphology of electrical synapse. A region rich in pores of presynaptic cytoplasm will connect with a region also rich in pores of the postsynaptic cytoplasm. Ion channels will be formed by the pores in each membrane.

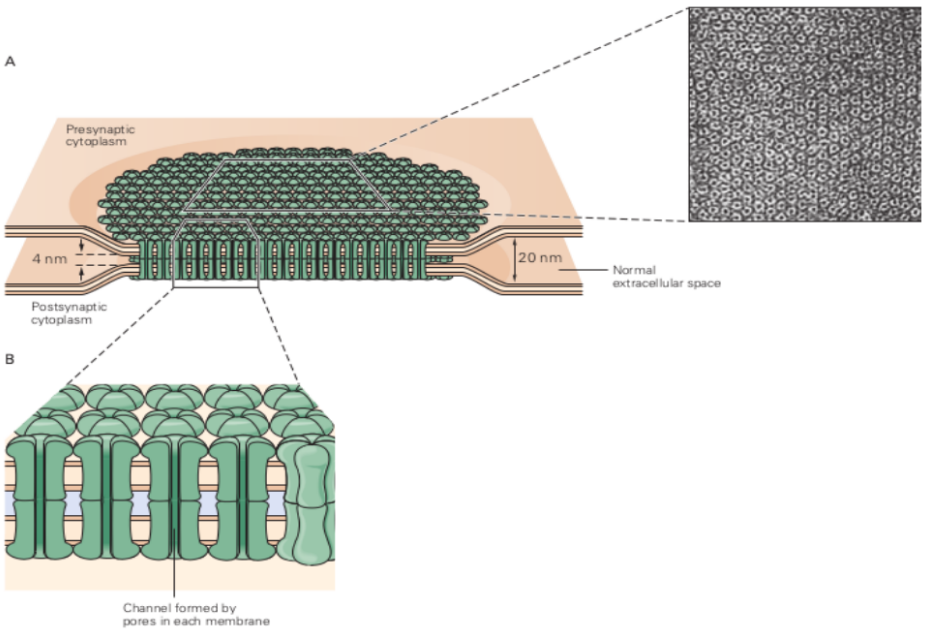

Source: ERIC; JAMES; THOMAS (2000)

Electrical synapses are known for their rapid and specific depolarizing signals (Fig. 9).

They feature a minimal synaptic cleft, approximately 4 nanometers, and a direct cytoplasmic continuity between pre- and postsynaptic cells. These synapses rely on specialized ion channels called gap-junction channels. Signaling transmission at electrical synapses occurs almost instantaneously compared to chemical synapses. Furthermore, changes in the potential of the postsynaptic cell are directly correlated with those in the presynaptic cell. Electrical synapses are typically found in cardiac tissues, muscle tissues, and certain types of glial cells.

Figure 10 – Process of chemical neurotransmission. First, the neurotransmitter is synthesized in the presynaptic neuron (phase 1, and 2). Then, the transmitters are stored in synaptic vesicles (phase 3). The release of the neurotransmitter into the synaptic cleft happens because of external stimuli. After that, neurotransmitters could interact with postsynaptic receptors (phase 4), bind with autoreceptors (phase 5) diffusion from active states (phase 7), or fagocite by glia (phase 8).

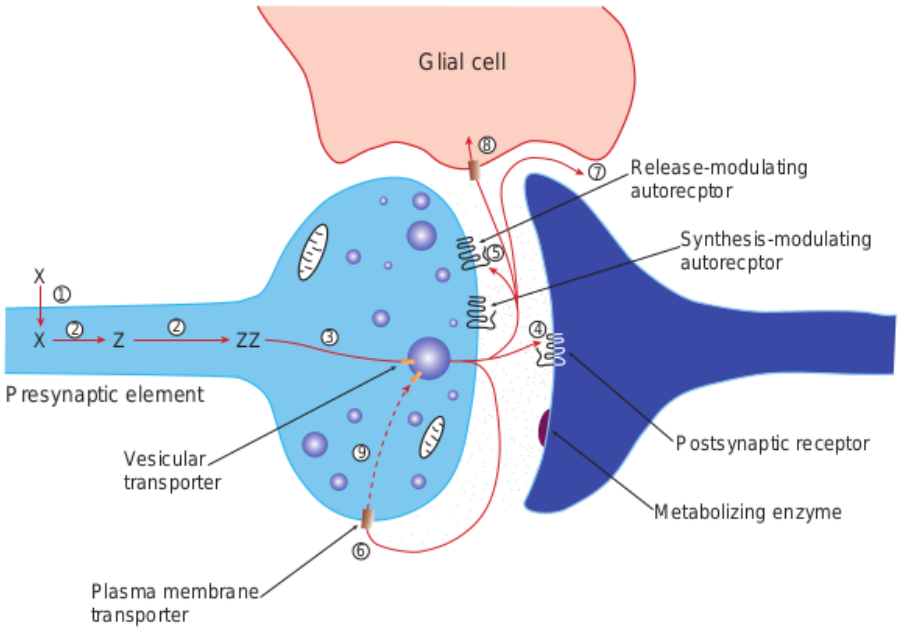

Source: SQUIRE et al. (2012)

Chemical synapses are more prevalent in the nervous system, offering greater response variability and enabling the production of complex responses, which is pivotal for memory and other higher brain functions (Fig. 10). In this type of synapse, neurons are separated by the synapse cleft. An action potential in the presynaptic neuron triggers the release of chemical transmitters, which diffuse across the synaptic cleft to interact with receptors on the postsynaptic cell's membrane. These transmitters affect the membrane potential in a non-linear manner, and if it crosses the cell's threshold, the postsynaptic cell will initiate an action potential

2.3 FUNCTIONAL ORGANIZATION OF NERVOUS SYSTEM

Despite significant advancements in the field of neuroscience over the last 70 years, numerous questions remain unanswered regarding how the nervous system processes information from the environment and how this information is internally communicated to generate responses. Technological progress has enabled the measurement of neuronal-level electrical activity in specific brain areas, allowing for detailed investigations into sensory information processing (STEVENSON; KORDING, 2011; HONG; LIEBER, 2019).

Visual processing involves a large number of brain structures arranged in a hierarchical way. Visual neurons respond selectively to patterns of light and dark, color, shapes, and orientation according to the region in the visual field. In simplicity, the visual processing starts in the retinae. Each one of them has retinal ganglion cells that are responsible for the transduction of luminar stimuli into electrical stimuli. The electrical stimulus will travel around the whole visual pathway until the high levels of the processing. The activity of the retinal cells will travel through the optic nerves, which are axon projections of the ganglion cells, that extend to a midline crossing point called optic chiasm. The axons, after the confluence in the middle point, carry the input from both eyes to the lateral geniculate nucleus of the thalamus. The lateral geniculate, in primates, has 6 layers and each layer receives a specific input from a different part of the eyes. The thalamic neurons receive that mapped information and pass through the primary visual cortex localized in the occipital lobe.

The primary visual cortex or any sensory area of the cerebral cortex is organized based on layers. These layers play distinct roles, ranging from dendritic and axonal connections to sensory input reception and output pathway generation (DOUGLAS; MARTIN, 2004; SAKATA; HARRIS, 2009). Sensory areas of the cerebral cortex have 6 layers. From the most superficial to the deepest layer, they are the molecular layer (Layer I - full of dendrites and axons that travel from and to other areas of the cortex), external granule cell layer (Layer II - Contains small spherical pyramidal neurons), external pyramidal cell layer (Layer III - larger pyramidal cell responsible for intracortical communication), internal granule cell layer (Layer IV - recipient of sensory input, most prominent in sensory areas), internal pyramidal cell layer (Layer V - pyramidal cell which give rise to output pathways of the cortex), and multiform layer (Layer VI - heterogeneous shaped neurons).

One curious feature about cells from Layer V is that these cells drive subcortical structures involved in action, and decide the output of the cortical circuits. The same Layer V influences

Figure 11 – Visual Pathway from the visual field until the layers of Lateral Geniculate Nucleus.

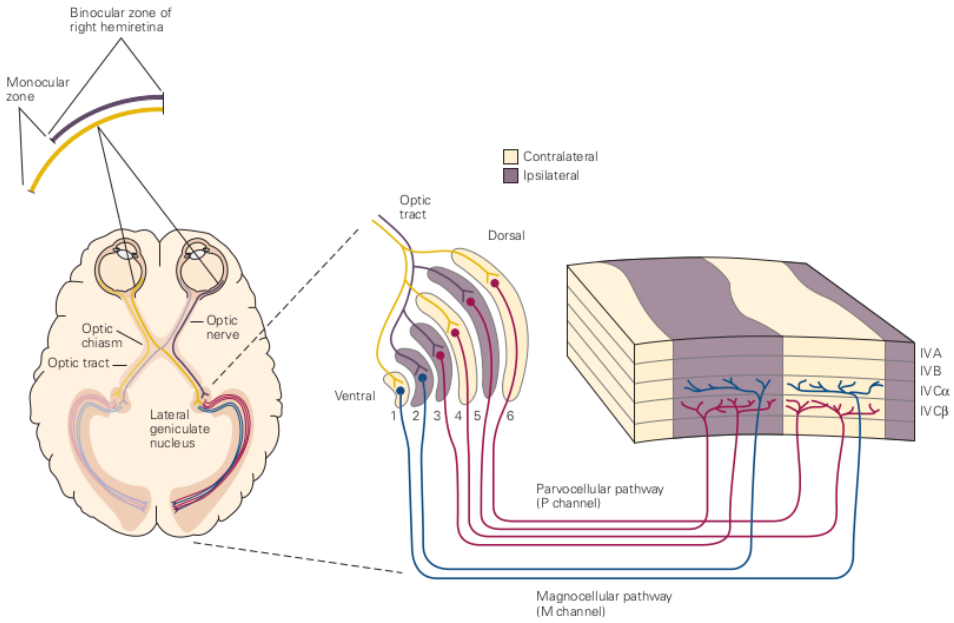

Source: ERIC; JAMES; THOMAS (2000)

input information by the connection with layer VI that connects with thalamic input layers (DOUGLAS; MARTIN, 2004). Also, Communication between layers is dynamic and may vary with cortical states. It is affirmed in (SENZAI; FERNANDEZ-RUIZ; BUZSÁKI, 2019) spike transmission strength between different layers can change during different states, such as waking and non-REM sleep.

Visual processing could be described in many levels of processing. The first one is the low-level visual processing responsible for detecting various types of contrast in complex and dynamic images. The intermediate-level processing is responsible for the identification of contours, fields of motion, and representation of surfaces. High-level visual processing integrates information from a variety of sources and it is responsible for the conscious visual experience.

From the low-level of visual processing to the high-level of visual processing neurons have increasingly larger receptive fields and higher selectivity. As the receptive fields enlarge and the selectivity increases, neural responses depend less on the precise location of the pattern and more on its features. Interestingly, the high levels of visual processing not only recognize patterns, it could be also making inferences from partial information, poorly visible images or occluded objects. In fact, recurrent models could predict which image of some occluded object would be easier for humans to recognize and provide a strong argument of how important the role of recurrent computations is to make visual inferences (TANG et al., 2018).

The sensory processing through which features of a stimulus are represented by neural

Figure 12 – Representation of cell's distribution for all layers of the neocortex. Different stain techniques reveal different structures. Golgi stain shows a subset of neurons including their dendrites and axons. The Nissl stain reveals the soma of neurons and closer dendrites and the Weigert stain displays only myelinated fibers. Source: (ERIC; JAMES; THOMAS, 2000)

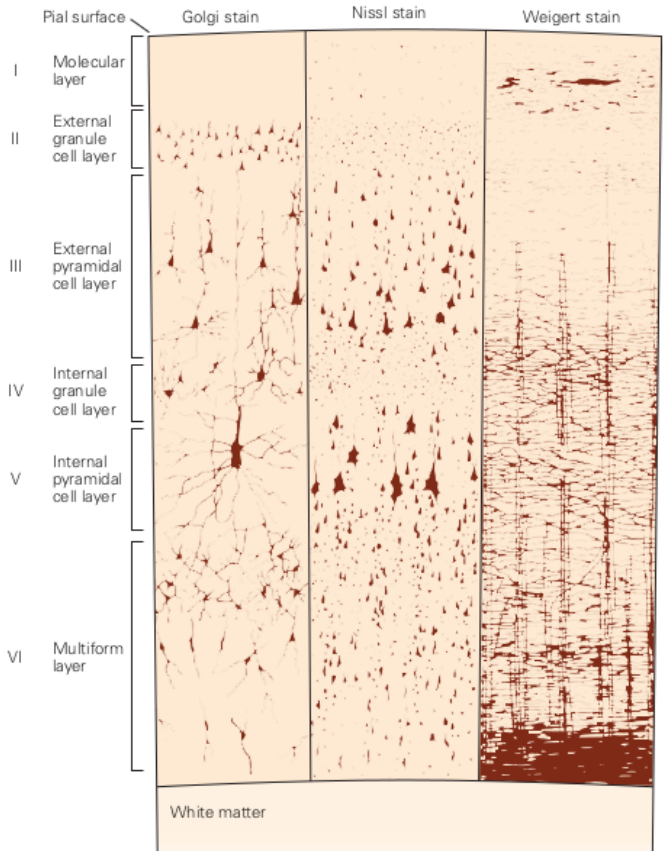

Source: ERIC; JAMES; THOMAS (2000)

activity is called encoding. The sequence of action potentials fired by a neuron in response to a sensory stimulus represents how that stimulus changes over time. Decoding, on the other hand, involves extracting information from neural activity and offers insights into memory, planning, decision-making, and other cognitive functions, with a focus on sensory processing. Neural coding aims to understand both the stimulus features that drive a neuron to respond and the temporal structure of the response and its relationship to changes in the external world.

There are other features used to encode sensory information such as rate code and population code. The first one, the rate code, uses the variation of the number of action potentials per second to communicate the strength of the stimulus and its duration. The second one, the population code, represents the intensity of a stimulus by all active neurons in the receptor population. Also, the patterning of spike trains plays an important role in encoding temporal fluctuations of the stimulus. And another important principle of sensory coding would be the

information conveyed not only when the neurons fire but also when they slow or stop firing.

The response produced by the sensory pathways to encode stimuli is not fixed, there is variability and plasticity associated with it. Such plasticity of cortical maps requires some time to be established and could result from the strengthening of already established lateral connections or from the growth of new connections.

It could be said that the nervous system extracts only certain features of each stimulus while ignoring others. Specific sensory perceptions such as color, tones, odors, and tastes are mental creations constructed by the brain from the sensory experience. There is a process where a specific stimulus energy is converted into an electrical signal and the amplitude and duration of it are related to the intensity and time course of stimulation of the receptor.

One visual stimulus encode is the product of many neurons operating in a specific combination called population code. The number of neurons involved in the perception pathway is important but the nervous system does not represent entire objects by the activity of single neurons. Instead, there is a complex connectivity between cells aligned with signal information coming from action potential patterns and groups of neurons involved.

The number of areas of the cortex involved in visual information processing varies with species. However, it could be said that almost half of the cortex is involved with vision and high processing levels related to visual inputs. In the early 1980s, it was discovered that the sensory information arriving in the primary visual areas is divided into two parallel pathways, the ventral pathway and the dorsal pathway. Both pathways contribute to high-level information processing such as memory mechanisms: semantic memory (talk about objects or persons) and procedural memory (interact about objects or persons)

The ventral pathway (or object recognition pathway) carries the information needed to classify images and generate nouns useful to distinguish persons, places, and objects. The features that identify the object are transmitted through this pathway leading to the temporal lobe and hippocampus. The ventral or object-recognition pathway extends from the primary visual cortex to the temporal lobe;

The other, the Dorsal pathway (or movement-guidance pathway) is responsible for transmitting information essential for immediate actions. This pathway connects the primary visual cortex with the parietal lobe and then with the frontal lobes. It mediates attentional control and visually guided movements.

Interestingly, sensory information processing could be altered by many factors including neurological disorders, aging, traumatic brain injury, chemicals, and so on. More specifically,

Figure 13 – Representation of structures involved in the ventral pathway and dorsal pathway of visual processing. From the primary visual cortex, the visual information flows into two pathways. The ventral pathway carries the visual information about what the stimulus is into temporal lobe. The dorsal pathway directs the visual information about where the stimulus is located into the parietal lobe.

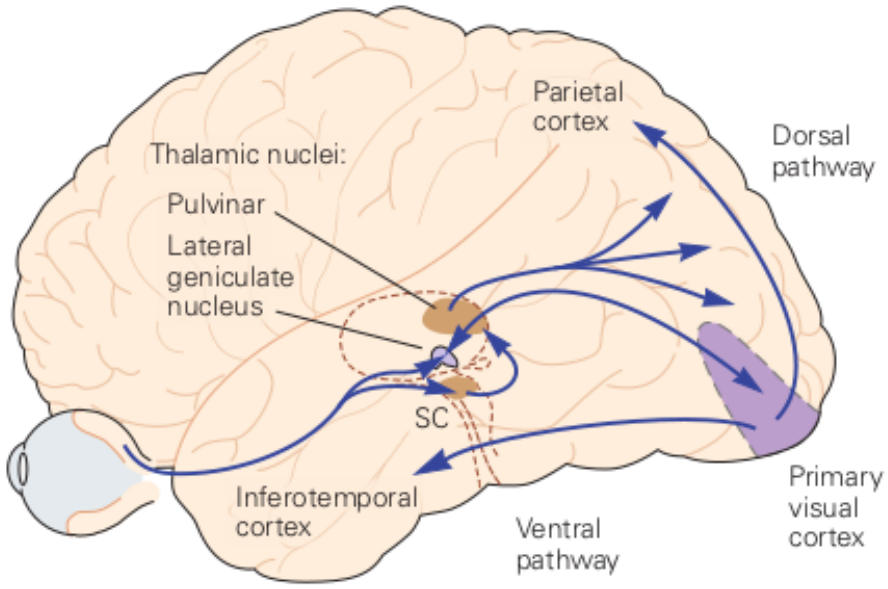

Source: ERIC; JAMES; THOMAS (2000)

drugs such as psychedelics have the capacity to induce states of altered perception, thought, and feelings.

The effects of psychedelics are complex and still not totally understood. It is believed that these compounds altered the dynamic of neurotransmitters and as a consequence the activity of neuronal populations. Over the past few years, the interest in psychedelics increased because many results showed that these drugs could be effective in treatments for depression, drug addiction, post-traumatic stress disorder, and other conditions. Recent studies found more about what changes in the brain activity during psychedelics effects (TAGLIAZUCCHI et al., 2014)(DEARNLEY et al., 2021), the relation between psychedelics and neural plasticity (LY et al., 2018), and using different experimental data (CARHART-HARRIS et al., 2016)(VOLLENWEIDER; KOMETER, 2010).

The constructive nature of visual perception agrees that visual perception is not only an additive combination of color, shape, and brightness coming directly from thalamic output. There is still variability in response per stimulus, and the study of sensory information processing is more complex than expected. It is an active and creative process involving the context and other features in the visual field.

2.4 CORTICAL STATES

Cortical states play a crucial role in shaping neural activity patterns, encompassing population spiking, neuronal correlations, and intracellular potential. These states represent the degree of shared fluctuations in population activity, influencing how information is processed within neuronal populations. These dynamic network activities occur on a timescale of seconds or more.(HARRIS; THIELE, 2011)

Over a specific duration, one can quantify the extent of slow fluctuations in the summed activity of local neurons. Each time window yields a quantitative measure of activity fluctuation amplitude. High fluctuations around the average activity signal highly synchronized moments, while low variability suggests desynchronized activity periods.

Synchronized states exhibit oscillations between up phases, marked by widespread neuronal firing, and down phases, characterized by network quietness. This leads to dramatic fluctuations in the average population firing rate over seconds.

In contrast, **desynchronized states**, also referred to as active or asynchronous states, feature weaker spontaneous fluctuations. It's worth noting that an "active state" doesn't necessarily mean increased firing rates; some neuron subgroups may exhibit decreased activity during these moments.

Rather than being strictly bimodal, cortical states form a spectrum characterized by varying levels of spontaneous activity fluctuations, correlating partially with ongoing behaviors like whisking and locomotion.

Speaking about the relation between the neurons involved in the population, it is trivial to conclude that if a group of neurons share fluctuation in firing rate, their activity will probably be positive correlated. This idea could be proved mathematically.

Mean pairwise correlations indicate significant population rate variance and coordinated global fluctuations, typifying synchronized states. Conversely, desynchronized states show small population activity variance and no pairwise correlations between neurons.

Notably, a mean correlation of zero doesn't imply that every neuron pair is uncorrelated; it suggests a balance between positively and negatively correlated pairs. Correlations were previously thought to arise from shared inputs, but recent findings indicate that asynchronous states can emerge despite shared input.

Fluctuations in spontaneous neuronal activity can vary significantly under different conditions, such as attention (HARRIS; THIELE, 2011), pharmacological effects (MUKAMEL et al.,

Figure 14 – Hypothesis of mechanisms underlying the asynchronous activity and synchronous activity. Figure Ab shows an example of a population asynchronous firing. Figure Ac shows in red the probability distribution of the pairwise correlation for the neurons shown in Ab. Figure Bb displays a raster plot (dot plot of neuron's activity: Xcoordinate = time, Ycoordinate = specific neuron) of a time window with a high level of variability. Figure Bc shows in blue the probability distribution of pairwise correlation in that state and in yellow the probability distribution of pairwise correlation from the concatenate upstate.

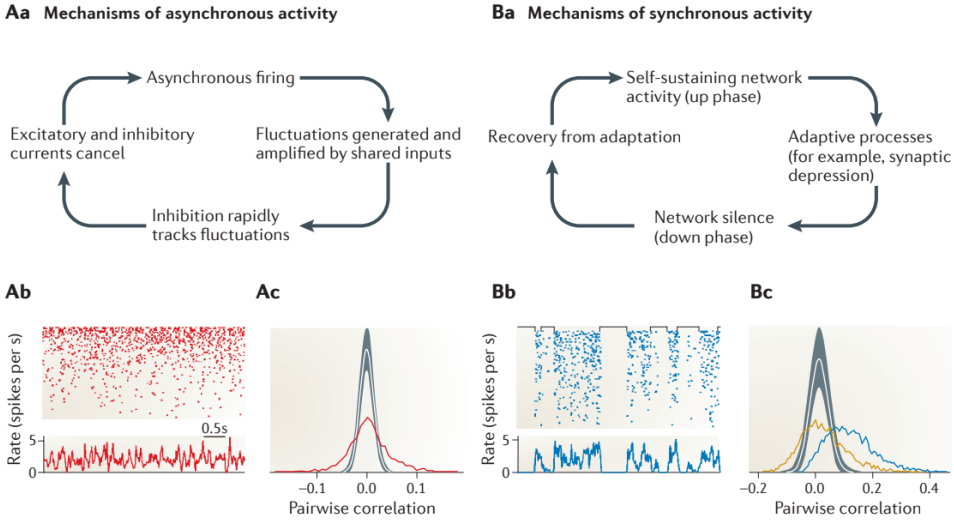

Source: HARRIS; THIELE (2011)

2014), and various brain states (POULET; CROCHET, 2019). However, there must be underlying mechanisms governing the control and maintenance of cortical states (POULET et al., 2012). It is a well-established fact that there exists a relationship between the level of fluctuation in neuronal population activity and the correlation structure, particularly in the asynchronous state. In feedforward network models, it is evident that a substantial quantity of uncorrelated inputs can lead to synchronous spiking activity between pairs of neurons. This finding implies that the correlation between outputs cannot be solely attributed to correlated inputs. Remarkably, experimental datasets have demonstrated that even noise exhibits a non-zero correlation. Taking all this information into account, it raises the possibility that a truly desynchronized state, characterized by a mean correlation of zero, may not exist.

However, recent studies have provided evidence of mean correlations close to zero in the primate visual cortex and in areas S1 (somatosensory cortex) and A1 (auditory cortex) of rats under anesthesia (please include references for these studies). These findings strongly suggest that the cortex possesses mechanisms capable of achieving desynchronized states. One hypothesis is that inhibitory inputs are correlated with excitatory inputs in pairs of neurons. This hypothesis also implies that when the mean correlation is distributed around zero, a substantial number of pairwise correlations deviate from zero, but the balance between positive

and negative pairwise correlations is maintained.

One thought to take into consideration is since there is a relation between correlation structure and variability in the population activity, in moments of highly synchrony, the correlation between pairs will be extremely positive, so how is possible to see fluctuations in population rate of the neural population?

Spontaneous cortical activity persists in isolated cortical slices, implicating intracortical mechanisms in its generation. The mechanism responsible for the down phase is not synaptic inhibition but disfacilitation the temporary absence of synaptic drive. Up phases originate in layer V and propagate to the surface as traveling waves.

In summary, during the up phase, spiking is maintained through recurrent synaptic activity. However, following an extended period of firing, a series of adaptive processes ensue, gradually diminishing the network's excitability. Once sufficient adaptation has taken place, the network's capacity to sustain firing diminishes, resulting in a period of network silence. Subsequently, following an adequate period of rest, the synapses and cells recover, allowing the network to once again support recurrent activity.

(MOCHOL et al., 2015) investigates whether correlations primarily result from neuronal co-activation during brief silent periods when all local network neurons cease firing. Changes in correlation, occurring gradually with brain state variations or abruptly with sensory stimulation, reflect the microcircuit's propensity to transiently stop firing.

3 CRITICALITY

Brain dynamics can be explored from two distinct points, each offering valuable insights. The first approach involves forming hypotheses about the macroscopic level based on microscopic dynamics, while the second approach seeks to decipher microscopic intricacies through macroscopic observations. A theory known as criticality aims to bridge the gap between these scales, drawing parallels from physics where criticality manifests as a specific set of features occurring when a system hovers between phases (HESSE; GROSS, 2014).

In the realm of criticality theory, defining phases relies on measured quantities termed order parameters. Additionally, the control parameter is employed to gauge external influences on system behavior. Ordinarily, gradual adjustments in the control parameter result in smooth shifts in the order parameter. However, certain shifts in the control parameter can trigger abrupt changes in the order parameter, signifying a transition from one phase to another. These changes may manifest as discontinuities or divergences within the phase diagram. Discontinuities indicate a first-order phase transition, while continuous phase transitions with sharp divergences signify a second-order transition.

In cases of second-order phase transitions, systems may find themselves at a point within the phase diagram, positioned between two phases. This delicate point is referred to as the critical state.

Researchers are particularly intrigued by systems existing in this critical state, as they possess the potential for optimal information processing capabilities. This phenomenon has sparked investigations into the concept of criticality within the human brain, exploring how the brain's state might deviate from this critical point due to various pathologies or the presence of chemical substances.

Theoretically, if a system is in the critical state, a set of parameters is tuned to hold at this exact point of the phase diagram. But how can a complex system such as the brain remain at this point? The theory of phase transition in physics is used for infinite elements and in the brain, the system is finite. That way, the critical point is not a point but a region in the phase diagram. There is one hypothesis called self-organized criticality (SOC) which says the brain must organize itself in order to remain in that region, feeding mechanisms to always show signatures of criticality.

To assess self-organized criticality (SOC), certain critical system features are essential.

These include a wide dynamic range of input signals, allowing organisms to interact effectively with their environment, information capacity quantified by the diversity of cortical activity patterns, and the ability to encode stimuli with multidimensional differences.

Signatures of criticality are quantifiable features that could suggest if the system is at the critical point (or region) or how close it is to it. Here, it will be explored four of them. Detrended Fluctuation Analysis, Dynamical Criticality (Neuronal Avalanches), Statistical Criticality (Maximum Entropy Models), and Complexity Measures. Each one of them will be described below.

3.1 DETRENDED FLUCTUATION ANALYSIS

In meteorology, DFA has found application in studying statistics related to stratus cloud liquid water content aiming to enhance meteorological predictability by leveraging the insights gained from DFA (IVANOVA; AUSLOOS, 1999). DFA has been instrumental in characterizing fluctuations in cerebral microvascular hemoglobin concentrations, particularly in studies related to cerebral malaria (SMITH et al., 2023). Also, DFA has been employed in genetic studies to investigate the contributions to long-range correlations in ongoing oscillations observed in EEG signals (LINKENKAER-HANSEN et al., 2007).

To gain insight into the characteristics of scale-free systems and their relationship to criticality, it is crucial to first establish a clear understanding of phenomena associated with characteristic scales and scale-free systems. Phenomena or systems characterized by a specific scale are typically defined through statistical measures such as mean and standard deviation. Examples of such phenomena include the size of specific fruits, the height distribution of young women, or time series data exhibiting white noise 15. In these cases, the characteristic scale presents itself at the expense of rich variability.

In contrast, scale-free phenomena defy simple descriptions through average values and are better elucidated by scale-free probability distributions, often represented by power-law functions with adjustable exponents and constants. These power-law functions serve to capture relationships that span various scales within the system

The absence of a typical or characteristic scale is prevalent in many physiological systems, and it plays a crucial role in enabling a wide range of functional states. For instance, synchronous brain activity has been a subject of investigation, revealing that a population of neurons can spontaneously organize itself around a critical point. This idea has been success-

Figure 15 – Decomposition of a time series into sine waves with different frequencies and amplitudes. The power density is almost uniform for different frequencies. That is an example of the frequency decomposition of white noise.

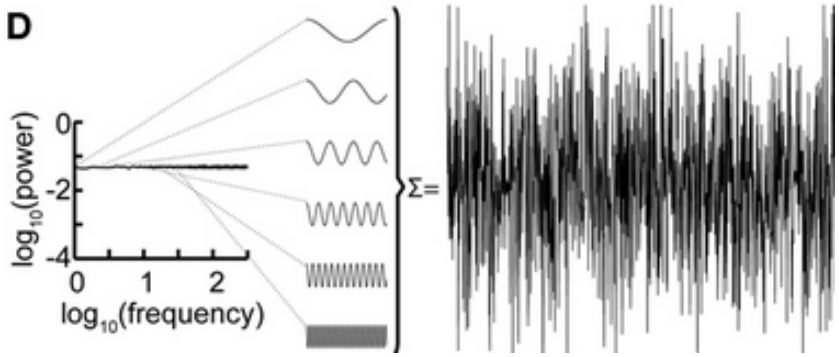

Source: SCHUSTER (2014)

fully tested both in theoretical models and real neuronal data, demonstrating that systems operating at criticality exhibit scale-free probability distributions.

Three key features essential for any critical system are identified. First, having a broad dynamic range of input signals is crucial, as it enhances an organism's ability to interact effectively with its environment. Second, information capacity, which quantifies the diversity of cortical activity patterns available for responding to stimuli, can be measured using the Shannon Entropy equation. Lastly, information capacity also quantifies a network's capability to encode a variety of stimuli with multidimensional differences (SHEW; PLENZ, 2013).

Figure 16 – Decomposition of a time series into sine waves with different frequencies and amplitudes for a scale-free system. In a scale-free system, time series could be decomposed into sine waves with different amplitudes and frequencies. The interdependence of those two characteristics would express a power-law function.

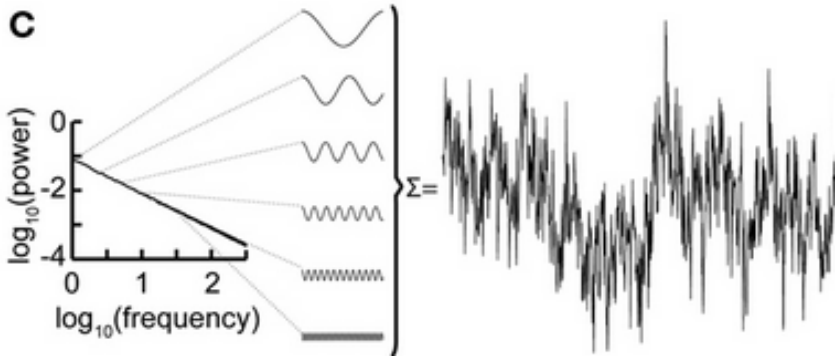

Source: SCHUSTER (2014)

To quantify scaling behaviors in neuronal time series, Detrended fluctuation analysis (DFA) is a commonly used method to quantify scaling behaviors in neuronal time series, grounding

itself in the principles of self-affinity and stationarity.

Self-affinity is a characteristic of fractal time series, where a fractal can exhibit either exact self-affinity, where a small part of the series is identical to the whole series, or statistical self-affinity, where the mean and standard deviation of smaller parts scale with those of larger parts, indicating anisotropic scaling with different dimensions. Self-affine processes result in power-law distributions of measured quantities, defining scale-free systems. For instance, broccoli can be considered a scale-free structure because it lacks a typical size, and the frequency of a specific size is inversely proportional to the size of its flowers, exemplifying the concept of self-affinity in real-world structures.

A **stationary process**, as defined in the context of the book "The Fractal Geometry of Nature" (pg 383 - Degrees of Stationarity), is characterized by the independence of the distribution of X(t) from time (t). This means that the joint distribution of $X(t_1 + \tau)$ and $X(t_2 + \tau)$ is also independent of the time difference τ, and this independence holds for all k variables in the joint distribution of $X(t_1 + \tau)$, $X(t_2 + \tau)...X(t_k + \tau)$. It's important to note that a common misconception is that stationary processes involve samples fluctuating around a fixed average while maintaining statistical consistency. In reality, what remains constant is the underlying generating rule, not the specific data points. To analyze scale-free properties or determine the type of process generating a time series, it's crucial to establish whether the process is stationary or nonstationary. Self-affinity, for instance, only applies to nonstationary processes. To convert a time series generated by a stationary process into one generated by a nonstationary process, a signal profile can be defined as

$$x(t) = \sum_{k=1}^{t} y(k) - \langle y \rangle$$

where $\langle y \rangle$ represents the mean of the time series y(t). This subtraction step removes any global trend from the signal, allowing for scale-free analysis without assuming stationarity.

It is possible to quantify the scale-free nature of a time series, by calculating the fluctuation of a non-stationary signal in windows of different sizes. However, the calculation of the fluctuation could be biased by some steady trend on longer timescales. So, before any analysis based on fluctuations, it is advised to "detrend" the signal. The detrended fluctuation analysis (DFA) can be synthesized as follows (Figure 17):

- Calculate the cumulative sum of the original signal.
- Subtract the mean of the original signal, having the signal profile.

- Define a list of possible window sizes that will be used to separate the time series.
- For one possible window size, the signal profile is segmented into separate "mini" signal profiles which have 50% overlap, w.
- Subtract the linear trend of each mini-signal profile,$w_{detrend}$, and calculated the standard deviation of the detrended signal,$\sigma(w_{detrend})$.
- Compute the mean of all standard deviations coming from the detrended signal which have the same size, $\langle F(t) \rangle = \langle \sigma(w_{detrend}) \rangle$
- Plot the fluctuation function for all window's size, T, on a logarithmic scale.
- The exponent fitted is the DFA exponent α and from this scaling exponent, it is possible to make some assumptions about the system.

The fluctuation scale could be interpreted by its value as follows:

- If $0 < \alpha < 0.5$, the process could have memory and exhibits anticorrelations.
- If $0.5 < \alpha < 1$ the process also has a memory but exhibits positive correlations.
- If $\alpha = 0.5$ the process can be distinguishable from a random process (white- noise).
- If $2 < \alpha < 1$ the process can be seen as non-stationary.

DFA serves as a valuable tool for uncovering scaling behaviors in many complex systems allowing us to explore their scale-free properties effectively, enabling effective exploration of their scale-free properties across a wide range of applications. In the field of neuroscience, DFA has been employed to analyze neuronal time series activity (RIBEIRO et al., 2010), particularly in EEG signals during anesthesia (JOSPIN et al., 2007), providing insights into the measurement of consciousness levels. DFA has been utilized in the analysis of power spectra and frequency distributions in temperature data spanning from the 20th century to the present day (TALKNER; WEBER, 2000). This application aids in resolving controversies related to the low-frequency behavior of power spectral densities.

Figure 17 – Detrended fluctuation analysis step by step. Figure A shows the original time series and right below Figure B displays the cumulative sum subtracted by the time series mean. For each segmented part of the signal profile (Figure C), the linear trend is extracted (Figure D) and the standard deviation is calculated. Each dot of Figure E is calculated by averaging all the standard deviations computed from different window sizes with the same size.

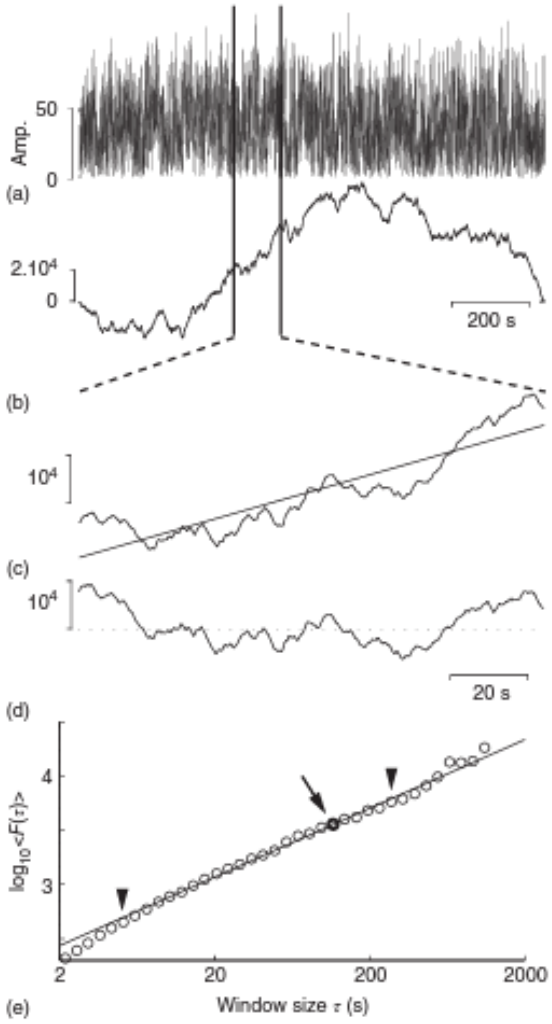

Source: SCHUSTER (2014)

3.2 NEURONAL AVALANCHE

Neuronal avalanches are moments in the activity of some neuronal population in which the beginning is defined when the activity is above the threshold and it finishes when it is below some predefined threshold. The size of this activity and the time between the two threshold-crossing moments vary immensely. These two measures lack characteristic values, making power-law distribution an excellent candidate for modeling the probability distributions of avalanche size and duration.

Systems that exhibit power-law distributions may exhibit a connection with criticality,

although not necessarily a strong one. It's important to note that while power-law distributions can emerge in stochastic dynamics, they alone do not conclusively indicate self-organized criticality (CLAUSET; SHALIZI; NEWMAN, 2009).

Neuronal avalanches could potentially provide compelling evidence supporting the concept of criticality. Nevertheless, certain considerations are essential. Prior to investigating neuronal avalanches, it is crucial to define a specific time window and subsequently binarize the entire time series. Each bin will be characterized by the amplitude of activity within that interval. For instance, if there were 6 spikes from a neuronal population recorded between 0ms and 10ms (using a 10 ms time window), the first bin would be assigned a value of 6, and so forth. It's important to note that altering the bin size will influence the amplitude of activity within each bin. (PRIESEMANN et al., 2014).

Consider a sequence of 10 bins denoted as 3, 2, 6, 18, 3, 6, 0, 1, 13, 0. In this scenario, a threshold is set at 3, and an avalanche is initiated or concluded when a bin registers 3 spikes or fewer. It's important to note that the choice of threshold is arbitrary and can be set to values like 3, 6, or 0. Each threshold selection results in varying numbers of avalanches, different avalanche sizes, and durations, consequently altering the probability distributions and their respective fitted exponents. Any conclusions drawn from these exponents are entirely contingent on the chosen threshold, rendering any statement reliant on this choice somewhat delicate (SHEW et al., 2015),(MUNOZ, 2018).

When using 0 as the threshold, a bin represented by 0 implies an absence of activity during that time window. However, it's unrealistic to expect the entire brain to be completely devoid of activity. Choosing 0 as the threshold for an avalanche implicitly assumes subsampling. In other words, it's impossible to have a moment of absolute silence if the recording encompasses the activity of all neurons in a given region. In experimental data, subsampling is an unavoidable constraint. Each experimental technique has its inherent limitations, and this factor impacts the study of neuronal avalanches. To address this limitation, neuronal networks are often simulated to approximate a fully sampled network as closely as possible (CARVALHO et al., 2021).

The hypothesis of a critical brain using neuronal avalanches is based on the scale invariance seen in descriptive probability distributions (KHALUF et al., 2017). The property of scale invariance describes situations where the essential structural (space) or dynamical (time) properties remain unchanged when considering the system at different scales.

If it is used f(x) to describe the structure or dynamics of any system as a function of the

variable x, a scale-invariant system f(x) must satisfy the condition

$$f(\lambda x) = C(\lambda) f(x)$$

There are two types of scale invariance, a continuous scale invariance in which λ can take any real value and a discrete scale invariance in which it takes only discrete values. The discrete case corresponds to fractal-like, self-similar systems. Some apparently discrete scale-invariant systems can actually correspond to specific statistical samplings of a continuous scale-invariant probability distribution.

Scale-invariant systems typically have no characteristic scale, since any specific scale that defines them would have to appear in the function f(x), making the transformation described in the equation above impossible. Such scale-invariant systems are referred to as being scale-free.

Systems with scale-invariant dynamics can be defined as having either local activity that displays scale-invariant correlations in space or global activity that displays scale-invariant correlations in time.

Critical systems require scale invariance and one of the measures for it is to find probability distributions fitted by power-laws. The power-law distribution has two variables open for fitting, The constant C and the exponent α. The exponent cluster systems according to their values, and other characteristics define the universality classes. Each class has some features that it is expected for the system to follow.

Scaling theory predicts the functional forms of the histograms of avalanche sizes and durations from experiments near a critical point.

$$P(S) \sim S^{-\tau}$$

$$P(T) \sim T^{-\tau_t}$$

$$\langle S \rangle (T) \sim T^{1/\sigma\nu z},$$

where P is the probability distribution for avalanche sizes (P(S)) and durations (P(T)). $\langle S \rangle (T)$ is the average size conditioned on a given duration. τ, τ_t and $\sigma\nu z$ are the critical exponents and it is also expected that they follow a specific equation among them, according to the scaling theory (FRIEDMAN et al., 2012) .

$$\frac{\tau_t - 1}{\tau - 1} = \frac{1}{\sigma\nu z}$$

The first result for critical exponents in neuronal avalanches was encountered by Beggs and Plenz and the critical exponents documented were $\tau = 3/2$ and $\tau_t = 2$. These values match with a specific universality class called mean field-direct percolation (MF-DP).

In mean-field direct percolation, the term "mean-field" indicates that the interactions between nodes are approximated by assuming that each node interacts independently with some average or mean properties of the entire system. This simplification allows for mathematical tractability and analytical solutions, which might not be achievable in more complex, realistic scenarios where interactions are more intricate.

Due to its simplicity, the critical branching process has become a canonical model for understanding criticality in the brain.

Beggs and Plenz (2003) found in cultured slices of cortex power-law distributions for the size and duration of avalanches and used these findings to advocate the hypothesis of signatures of criticality in the brain.

Understanding criticality in neural networks involves exploring power-law distributions, scale invariance, and the dynamics of neuronal avalanches. While power laws offer insights, scale invariance, and critical exponents provide a deeper understanding of the brain's behavior near critical points. Studying criticality in neural networks is a complex endeavor, but it holds the potential to uncover fundamental principles of brain function.

3.3 MAXIMUM ENTROPY MODELS

There is a growing interest in applying the principles of thermodynamics criticality to understand the dynamics of the brain. This intriguing application draws its foundations from commonalities shared between large groups of neurons and complex systems. These shared features include the immense number of neurons found in the cortex, their relatively uniform basic operations, weak correlations among individual neurons in a probabilistic manner, and the presence of functional characteristics resembling critical systems. These critical system features encompass extreme sensitivity to external stimuli, highly complex activity patterns even in the absence of stimuli, and transitions between distinct macroscopic states.

To establish a precise analogy, it is essential to introduce key concepts. The primary concept in this context is that of spin models. In general, each element in such models is characterized by two states: 1 when active (spin "up") and -1 when deactivated (spin "down"). The state of one element can influence nearby or functionally connected elements, and the extent of

this influence can be quantified. These interactions, along with the overall system's state, collectively define the energy of each state. States with higher energy are less likely to occur because thermodynamic systems tend to minimize their energy (theoretically true only for insulated systems.

$$E(\boldsymbol{\sigma}) = -\left(\sum_i \theta_i \sigma_i + \sum_{(i<j)} \theta_{ij}\sigma_i\sigma_j + \sum_{(i<j<k)} \theta_{ij_k}\sigma_i\sigma_j\sigma_k + \cdots\right)$$

θ_i, θ_{ij} and θ_{ij_k} are the interaction terms between each element's pairs, triplets, and so on. θ's sign dictates which configuration has the lower energy and as a consequence bigger probability.

The likelihood of a particular state can be calculated using the Gibbs-Boltzmann distribution.

$$p(\boldsymbol{\sigma}) = \frac{1}{Z} e^{\frac{-E(\boldsymbol{\sigma})}{T}}$$

This distribution provides a description of the probability of various configurations based on the interactions between elements. In a system with N elements, each having two possible states, the number of possible configurations is 2^N.

In the context of the Gibbs-Boltzmann distribution, the parameter T can represent either temperature or the significance of internal constraints in describing the collective behavior of the system. A lower T signifies a stronger influence of these constraints, resulting in greater heterogeneity in the Gibbs-Boltzmann probability distribution. T, in a sense, quantifies the degree of randomness in the system. As T increases, system randomness also increases, and the probability distribution approaches uniformity.

At this point, the discussion shifts to three critical quantities that serve as indicators of a system's proximity to a critical state:

Magnetization: This quantity measures the ensemble average of the element's state and reflects the overall activity level. The collective behavior of individual elements determines the system's overall magnetization.

$$M = \frac{1}{N}\sum_{i=1}^{2^n} p_i \sum_{j=1}^{n} \sigma_j^i$$

Where p_i is the probability of the i system's state and σ_j^i is the j element's state of the i system's state. A critical point occurs when temperature induces a transition in magnetization from ± 1 to 0.

$$M \sim |t|^{\beta}$$

where t is the reduced temperature based on the critical temperature defined by

$$t = \frac{(T - T_{\mathrm{c}})}{T_{\mathrm{c}}}$$

Susceptibility: Susceptibility measures the system's sensitivity to external perturbations.

$$\chi = \left.\frac{\partial M}{\partial H}\right|_{H=0}$$

At the critical point, susceptibility diverges because input sensitivity is maximized.

$$\chi \sim |t|^{-\gamma}$$

The γ exponent expresses how the changes in the susceptibility are related to the reduced temperature. In the thermodynamic limit, when the number of elements tends to infinite when the temperature T tends to the critical temperature T_C, the susceptibility diverges meaning that in these conditions the input sensibility is maximized.

Specific Heat: Specific heat measures the internal complexity or diversity of system configurations. It is calculated based on the variation in internal energy with temperature changes. This derivative can be expressed in terms of the mean of all possible energies.

$$C = \frac{1}{N}\frac{\partial U}{\partial T} = \frac{\langle E_i^2 \rangle - \langle E_i \rangle^2}{nT^2}$$

The specific heat is related to the diversity of system configurations because the variance of the logarithm of a probability distribution signifies a system's capacity to represent and store information. Near the critical temperature, specific heat exhibits a unique relationship with the reduced temperature.

$$C \sim |t|^{-\alpha}$$

Exactly in $T = T_C$, the specific heat diverges for infinitely large systems. And this exponent α is different from the one defined on the detrended fluctuation analysis

Notably, at $T = T_C$ (the critical temperature), specific heat diverges for infinitely large systems. However, when the system has a finite size, determining a precise value for T that exhibits a discontinuity in magnetization (M), divergence in susceptibility (chi), and specific

heat (C), along with their respective exponents, is not straightforward. These quantities approximate power-law relations with reduced temperature only when the system contains an infinite number of elements. Nonetheless, valuable insights into T_C and the critical exponents can still be derived from finite-size systems.

It is evident that properties like C(T) systematically change with the number of elements involved, and the T value that maximizes C(T) approaches T_C as the number of elements increases. Extrapolating this behavior to an infinite number of elements (N) enables the prediction of the critical temperature (T_C).

In the context of statistical physics, this process of finding T_C and critical exponents for finite-size systems is referred to as "finite-size scaling" (FSS).

However, when it comes to the practical application of manipulating the "temperature" (T) in the brain to observe changes in thermodynamic properties, the methodology remains unclear. In this regard, a method known as the "single-histogram method" has been employed.

To conclude, complex systems, whether the brain or other systems, are characterized by numerous elements that interact weakly. Consequently, it is often challenging to isolate individual elements to understand the collective behavior of the entire system

3.4 COMPLEXITY

There is no universal definition of complexity. Over the years different measures have been proposed based on different definitions. However, in general, statistical complexity must describe somehow intricate patterns hidden in the dynamics, emerging from a system that itself is much simpler than its dynamics. Complexity could be seen as a measure of off-equilibrium "regularity" and "order", not associated with very regular structures.

The possible definitions of complexity are categorized into three options. The first class the complexity grows with increasing disorder, the second class is small for high levels of order and disorder. The last one grows with increasing order. The complexity measure highlighted in here, the Martín-Platino-Rosso (MPR) statistical complexity, belongs to the second class (MARTIN; PLASTINO; ROSSO, 2006).

Any information measure can be seen as a characterization of a given probability distribution. For example, the Shannon entropy can be explained as a measure of the uncertainty associated with some probability distribution. If it is certain all the outcomes from the system, the knowledge about the system is maximal. However, ignorance about the system will achieve

its maximum when the probability distribution is uniform.

The quantity calculated to represent complexity must not indicate only the level of disorder or information quantity. It could be more useful to define a measure to quantify how far the probability distribution that describes the system is from the uniform distribution. The statistical complexity will be then the combination of the disequilibrium Q (reflecting the system's architecture) and the entropy H (information stored in the system) (TIMME et al., 2016).

The entropy is given by

$$H[P] = \frac{S[P]}{S[P_e]}$$

where P_e represents the system's uniform probability distribution. MPR complexity measure is defined as follows

$$C[P] = Q_J\left[P, P_e\right] \cdot H[P].$$

The $Q_J\left[P, P_e\right]$ is defined in terms of the Jensen-Shannon divergence as

$$Q_J\left[P, P_e\right] = Q_0 J\left[P, P_e\right],$$

where

$$J\left[P, P_e\right] = S\left[\frac{(P + P_e)}{2}\right] - \frac{S[P]}{2} - \frac{S\left[P_e\right]}{2},$$

and Q_0 is the inverse of the maximum value of $J\left[P, P_e\right]$.

4 EXPERIMENTAL PROCEDURES IN DATA ANALYSIS

This chapter not only discusses the methodology employed to obtain the results but also the evolution of our group's journey in acquiring the necessary resources to conduct these experiments. Personally, I had the privilege of contributing to the laboratory's development, which involved procuring materials, establishing a rat vivarium, and mastering the creation and implementation of experimental protocols.

Initially, our experiments entailed electrophysiological recordings within the primary visual cortex. We utilized multi-electrodes for this purpose, a technology funded by Hubel (HUBEL, 1957) used over the decades to study single neurons and receptive fields. They were manufactured in our laboratory and consisted of 32 tungsten electrodes arranged in an 8x4 matrix (Fig.18). These electrodes were connected to a PCB board via Omnetics ™connectors, enabling us to conduct tests involving visual stimuli, including assessments of contrast and gratings, in anesthetized rats.

Figure 18 – A) Stereotaxic used to position the animal and have access to accurate coordinates axis. B) Long Evans, animal model used for all experiments. C) Skull exposed. The bregma (intersection between digital and coronal sutures) is used as the coordinate origin. The primary visual cortex of the rat can be found using stereotaxic coordinates coming from the rat atlas (D) that provide the three coordinates. E) Manufactured multielectrode matrix used to record electrical activity in the visual cortex of rats. F) TDT system of acquisition. The left equipment is the head stage responsible for transforming the analog signal into a digital signal. The zip clip compared with a coin connects the multielectrode with the TDT system. The right equipment is responsible for synchronizing possible stimuli with the digital signal acquired and sent to the computer. G) Spike sorting interface integrated into the TDT system.

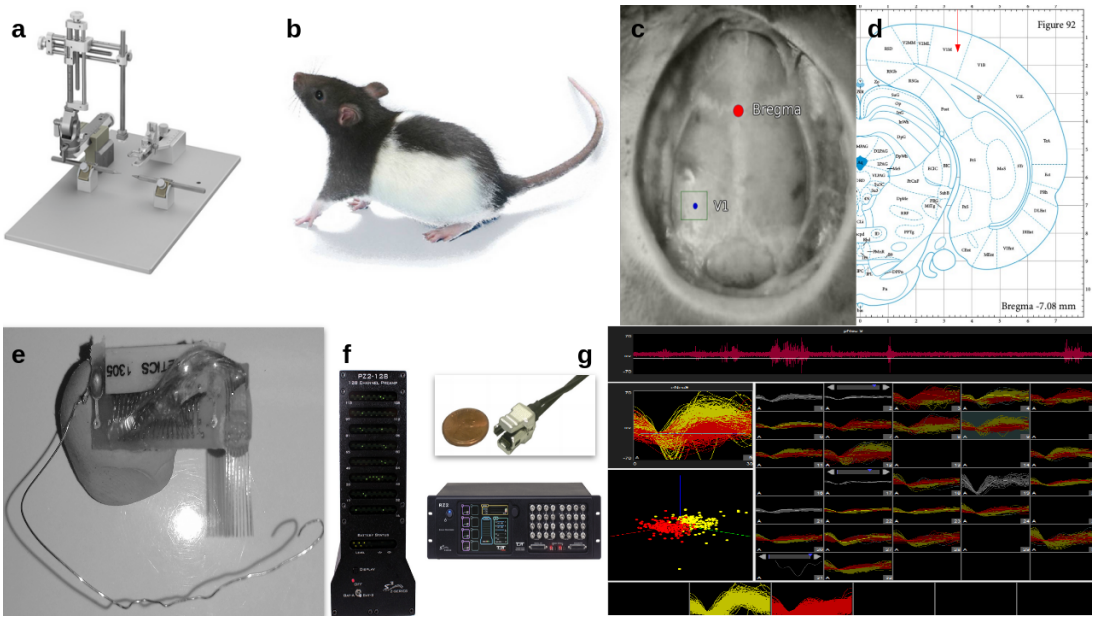

Source: The author (2023)

After a couple of years, the lab adopted a novel technique that incorporated high-density multi-electrode silicon probes, the Neuronexus ™. The primary objective of this technique was to enable the simultaneous recording of a larger number of neurons closely positioned to one another. The initial silicon probe employed featured 32 electrodes distributed across 4 shanks, with 8 electrodes on each shank (Fig. 19). Subsequently, a more advanced silicon probe was acquired, boasting 6 shanks, each equipped with 10 electrodes, and an additional 4 channels for enhanced recording capabilities.

Under this innovative approach, the lab conducted a series of recordings. Rats were anesthetized using urethane, and the recordings were extended for a duration of 3 hours within the primary visual cortex, conducted in the absence of external stimulation. These datasets were subsequently utilized in the formulation of four published articles (LOTFI et al., 2020; LOTFI et al., 2021; FONTENELE et al., 2019; CARVALHO et al., 2021). The following section will provide a comprehensive account of the experimental protocol that was consistently applied across all the aforementioned publications.

4.1 DETAILED EXPERIMENTAL PROTOCOL

The recordings were conducted in anesthetized Long-Evans male rats, which were typically 3-4 months old. To prepare for surgery, the rats underwent a 24-hour food restriction period. urethane was chosen as the anesthetic agent due to its capacity to induce a broad range of spike variability. Anesthesia was administered using a dosage of 1.58 grams of urethane (HARA; HARRIS, 2002) per kilogram of the animal's body weight, diluted to a concentration of 20% in saline. Once the animals reached the desired level of anesthesia and local anesthesia was applied, the process of skull exposure commenced. Using the cranial suture lines as reference points, the coordinates of the visual cortex were marked.

The craniotomy, which involves creating an opening in the skull, and the durotomy, which entails exposing the brain by withdrawing the dura, were both carried out within a designated 1mm x 1mm square region (Figure 18c,d). The center of this square had coordinates of [AP (anteroposterior) = 7.2, ML (mesolateral) = 3.5] (PAXINOS; WATSON, 2006). Electrophysiological recordings were conducted using Neuronexus equipment equipped with 64 channels, distributed across 6 silicon shanks. Each shank contained 10 channels, with an additional 4 channels evenly spaced in height within one of the shanks (Fig.19b). The surface area of each channel measured 160 square micrometers, and they were arranged in a staggered configuration

Figure 19 – A) Sketch of the Open Ephys system for acquisition of electrophysiology data. The Intan chip is connected to the silicon probe and it is responsible for transforming the analog signal into digital signal. The acquisition system is responsible for taking the digital signal, synchronizing it with possible stimuli devices, and load in the computer. The open ephys has an online interface that makes it possible to see the "live" raw data, change the sample acquisition, modify the bandpass filter, build a different channel map, and so on. The output data files will be saved for posterior analysis. B) Real picture of a 64-channel silicon probe. C) Sketch of dimension specifications of the silicon probe. D) Real picture of a silicon probe acute implant in the rat's primary visual cortex. E) Example of two clusters detected by the klusta software. The top one is considered SUA cluster and the down is considered a MUA cluster.

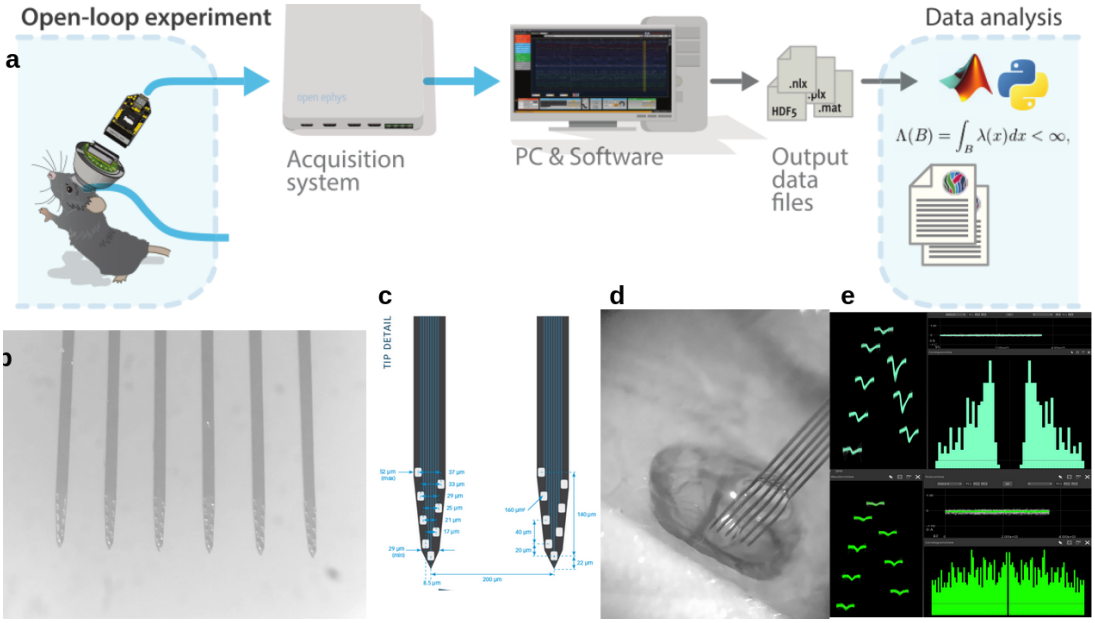

Source: SIEGLE et al. (2017)

with 20-micrometer spacing between them. The shanks themselves were positioned at intervals of 200 micrometers from one another (Fig.19c). The Neuronexus probe was introduced 1-1.2 mm cortex deep, aiming at visual cortex layer V (Fig.19d). The surgical and recording procedures were approved by the Federal University of Pernambuco (UFPE) Committee for Ethics in Animal Experimentation (23076.030111/2013-95 and 12/2015).

The acquisition system employed was Open Ephys, which consists of several components. This system includes a single acquisition board, designed as an open-source interface for capturing up to 512 channels of extracellular electrophysiology data through a USB connection. It also incorporates a headstage, responsible for detecting and acquiring weak electrical signals from living tissue, utilizing an Intan amplifier chip. The Graphical User Interface (GUI) serves as the open-source software interface (Fig.19a). The acquisition sample rate is set at 30 kHz, and signal quantization is based on 16-bit precision (Fig. 20).

During the recording sessions, measures were taken to isolate the animal from extraneous noise and light to the greatest extent possible. Subsequently, the acquired raw data underwent

Figure 20 – Analog-to-digital conversion. The signals the channels capture are amplified and the data sample is quantized. The example of the figure shows the quantization process with 3 bits. 3 bits allow the system to generate 8 codes to translate the analog signal to digital information. Each code, for instance 001, represents a voltage interval and if the analog value is in this interval, this sample will be represented by 001. The system used in this project is 16 bits, so it will have 2^16 possible levels to represent the input signal.

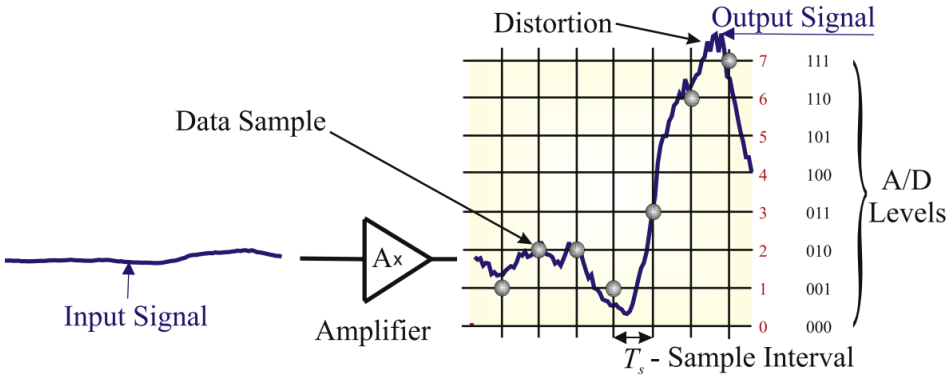

Source: DRONGELEN (2018)

filtering into two distinct frequency bands: the Low-Frequency Potential (LFP) band, ranging from 0 to 300 Hz, and the Action Potential (AP) band, covering frequencies from 500 to 3000 Hz. The AP band facilitated the detection of action potentials. This was achieved by establishing a threshold value, and when the filtered signal crossed this threshold, both the timing and the waveform of the action potential (spike) were recorded (Fig.21). This initial step was carried out by an open-source software tool known as Klusta.

Figure 21 – Illustration of action potential detection. Raw data is filtered, excluding low-frequency components from the frequency spectrum. The filtered data will easily show when the action potential happens. In order to mark the spike time, a linear threshold, represented by the red line, is applied and the time sample that crosses the threshold is saved.

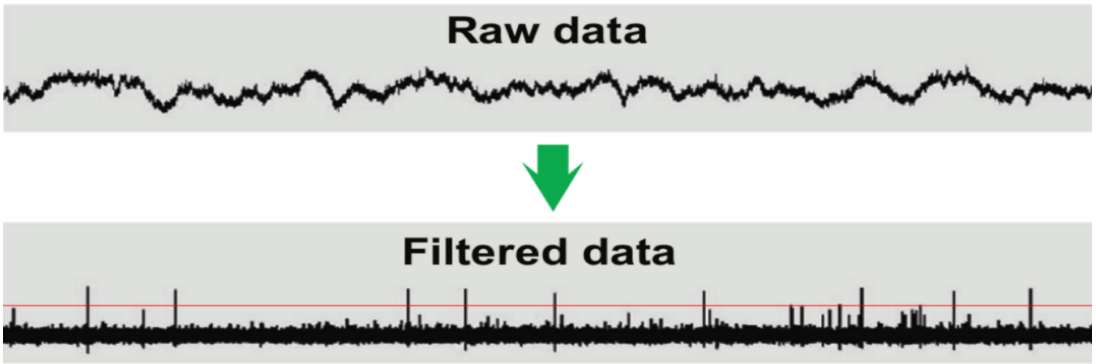

Source: REY; PEDREIRA; QUIROGA (2015)

Due to the placement of the channels, it's common for a single action potential to be detected by multiple channels. This overlap is visibly evident even in the raw data (Fig. 22). To handle these multi-channel detections, spikes are treated as spatiotemporally connected components. For signals to be considered part of the same spike, they must meet specific criteria. Namely, the filtered signals involved in a single spike must collectively exceed a relatively weak threshold (set at 2 standard deviation units), and at least one signal from the nearest channel must surpass a stronger threshold (equivalent to 4 standard deviation units). This approach enables the retention of vital information, including the spike's timing, which channels detected the same spike, and the waveforms displayed on each channel at that precise moment for each spike.

Figure 22 – Action Potential felt in adjacent channels. A) Layout of 32 channels organized in a silicon probe used to collect the data displayed in B. B) Segment of the recorded data explained in (ROSSANT et al., 2016). The rectangles highlighted the spike moments felt by more than one channel.

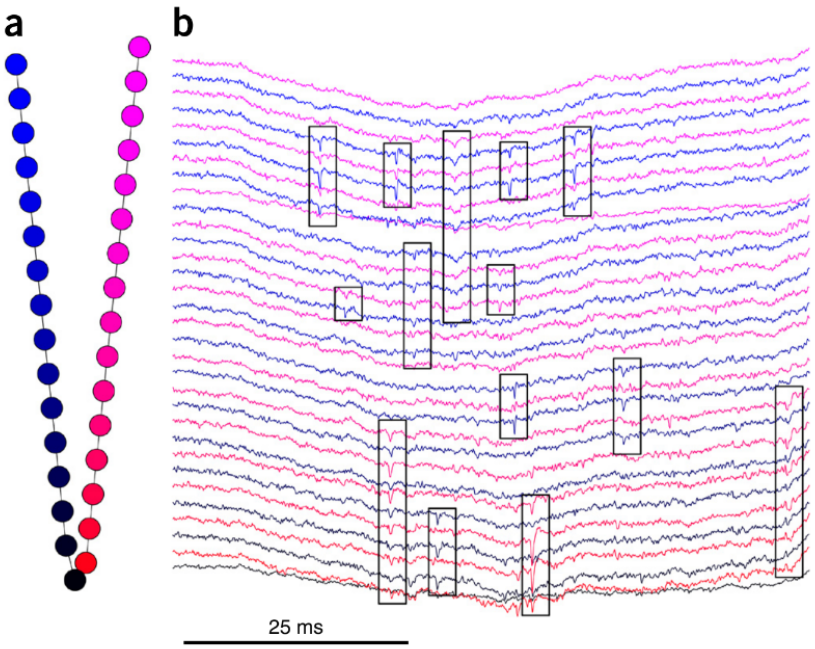

Source: ROSSANT et al. (2016)

The second step of spike sorting is unsupervised clustering. In this part, the detected spikes will be judged and grouped into similar neuronal sources according to the features saved for each spike.(Fig.23).

Following this, the next step involved using Klustaviewa, a graphical interface, for the supervised phase of spike sorting. During this stage, the clusters formed automatically were subjected to analysis to determine whether they represented Single Unit Activity (SUA) or Multi-Unit Activity (MUA).

Figure 23 – Process illustrated of clustering detected spikes. Each spike has a set of features responsible for characterizing the spike such as waveform, amplitude ratio, spike duration, refractory period, etc. Plotting a dot for each spike and the dot's coordinates as the set of features, it is possible to see cluster clouds forming and they could be called the activity of a putative neuron.

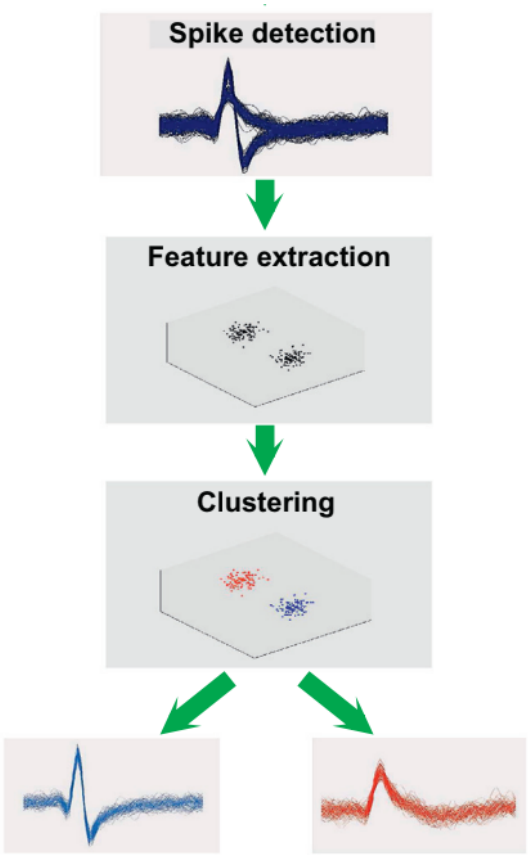

Source: REY; PEDREIRA; QUIROGA (2015)

A Single Unit Activity cluster signifies that the unsupervised spike sorting process successfully grouped a collection of spikes with similar characteristics, indicating that these spikes originated from the same neuron. In contrast, Multi-Unit Activity clusters encompass a combination of neuronal activities, but it remains uncertain whether these activities derive from a single, unique neuron. To differentiate between SUA and MUA clusters, specific features must be identified.

Single Unit Activity (SUA) clusters are characterized by distinct waveforms, with minimal variations among the 100 randomly selected spikes displayed in the WaveformView tab (Fig.24A). In these clusters, one channel typically exhibits the highest spike amplitude, while adjacent channels display lower spike amplitudes.

The FeatureView tab (Fig.24B) offers a visualization of an n-dimensional space, where each dot represents an individual spike. The 'n' denotes the number of features used in the Principal Component Analysis (PCA) to create the clusters. This tab provides insight into the

proximity of spikes in this space. The closer the dots are, the more alike they are, supporting the notion that these dots represent the activity of a single neuron.

The CorrelogramView tab (Fig.24C) exhibits an auto-correlogram density distribution of spikes. It operates by selecting one spike as a central time reference and then creating 25ms bins (with a bin size of 0.2ms) before and after this reference point. The count of spikes occurring in each bin relative to the central spike is calculated for all spikes. For SUA clusters, it is essential that the bins surrounding the central point remain empty or exhibit counts below the average. This criterion is necessary to classify a cluster as SUA, primarily due to the refractory period. In the case of spikes from the same neuron, no spike should occur before the refractory period, thus ensuring a clear distinction.

Figure 24 – Example of cluster considered Single Unity Activity. Print screen of KlustaViewa software interface. This data was collected in our laboratory. A) WaveformView tab. B) FeatureView tab. C) CorrelogramView tab.

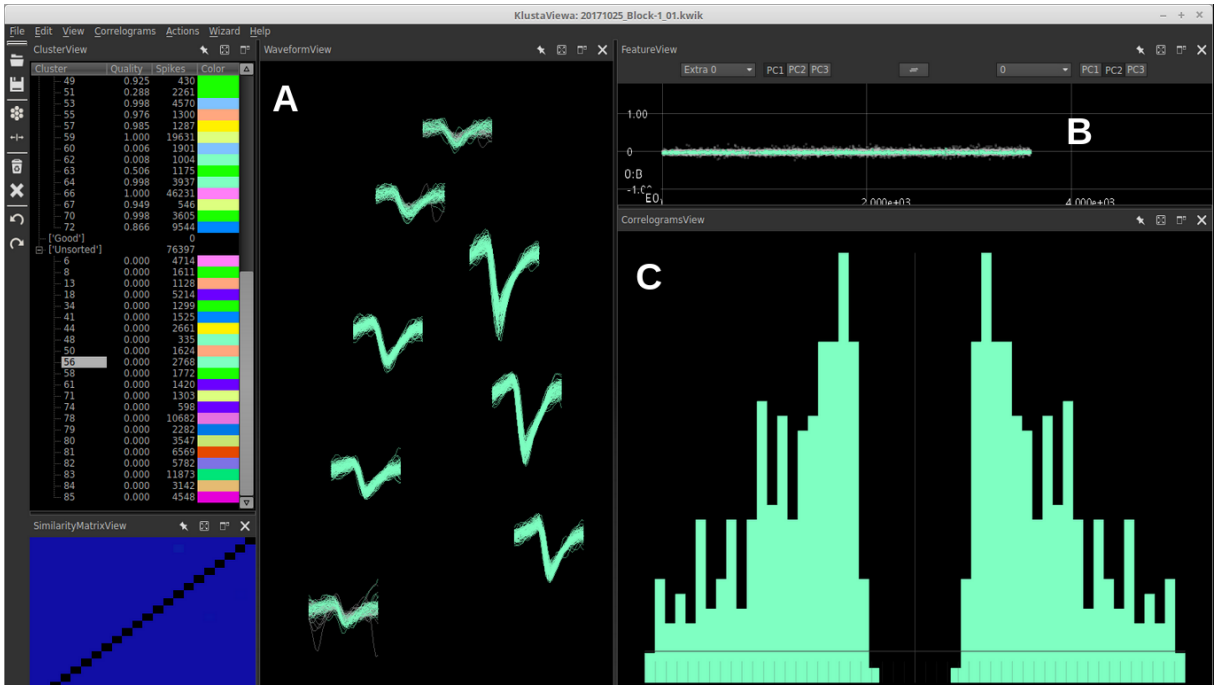

Source: The author (2023)

Multi-Unit Activity (MUA) clusters exhibit distinct characteristics as well. In the WaveformView tab (Fig. 25a), it's typical to observe all the channels detecting nearly identical spike amplitudes, indicating the likelihood of multiple neuron activities originating farther from the silicon probe.

The FeatureView tab (Fig. 25b) tends to reveal dispersed clusters that are further from the center. These more diffuse clusters suggest a greater diversity in the characteristics of spikes

within the MUA group.

The CorrelogramView tab (Fig. 25c) often displays an auto-correlogram that doesn't conform to the refractory period. This deviation from the refractory period is a key indicator of MUA, reflecting the simultaneous firing of spikes from multiple neurons.

Figure 25 – Example of cluster considered Multi-Unit Activity. Print screen of KlustaViewa software interface. This data was collected in our laboratory. A) WaveformView tab. B) FeatureView tab. C) CorrelogramView tab.

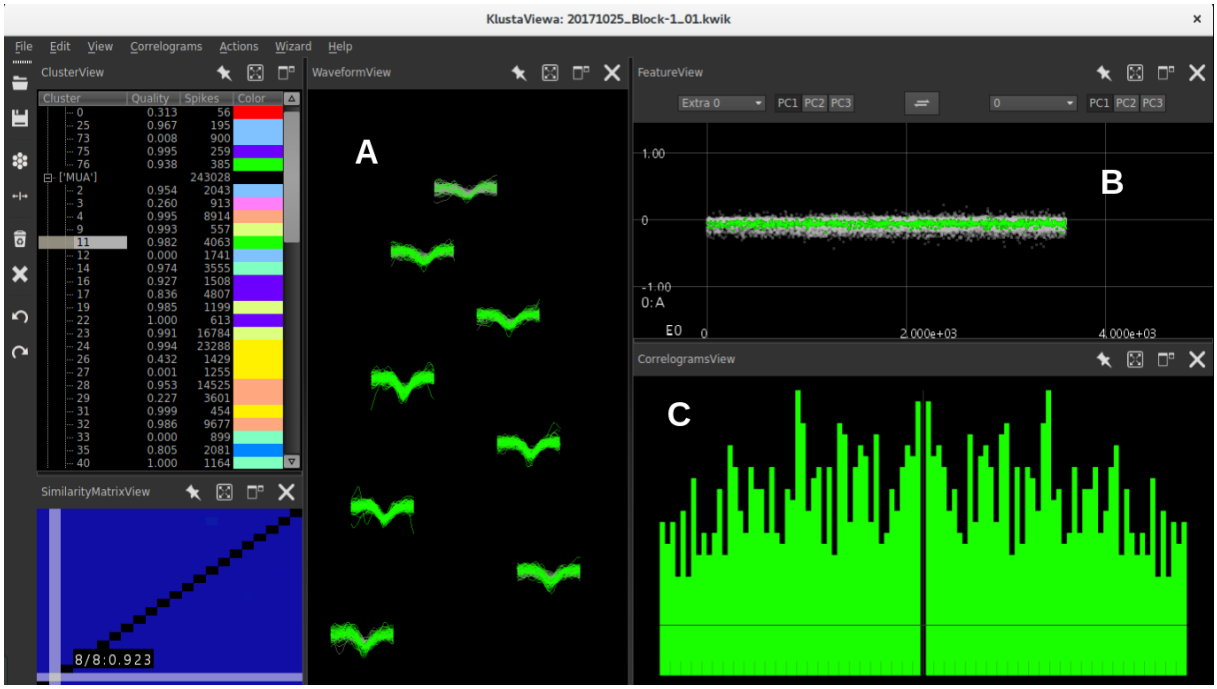

Source: The author (2023)

In addition to categorizing each cluster as SUA, MUA, or noise, the supervised spike sorting process provides the flexibility to merge clusters when they appear to originate from the same neuron or to split a cluster when there are spikes that deviate significantly from the majority, allowing for the potential removal of such outliers (Fig. 26).

The initial analysis of electrophysiological data recorded with silicon probes begins with unsupervised spike sorting, a process that identifies spikes in the raw data and groups them into clusters representing potential neuronal activity. These clusters are subsequently classified as either single-unit or multi-unit activity based on a set of distinct features. Finally, the accumulated information can be condensed into a time series, as illustrated in the figure 27. Subsequently, this time series data will be employed in various ways, depending on the subsequent phases of analysis.

Figure 26 – Example of two clusters shown together. The manual decision is made based on waveform similarities, auto-correlations, and cross-correlations. The Featureview could also be used to help in the decision to merge clusters.

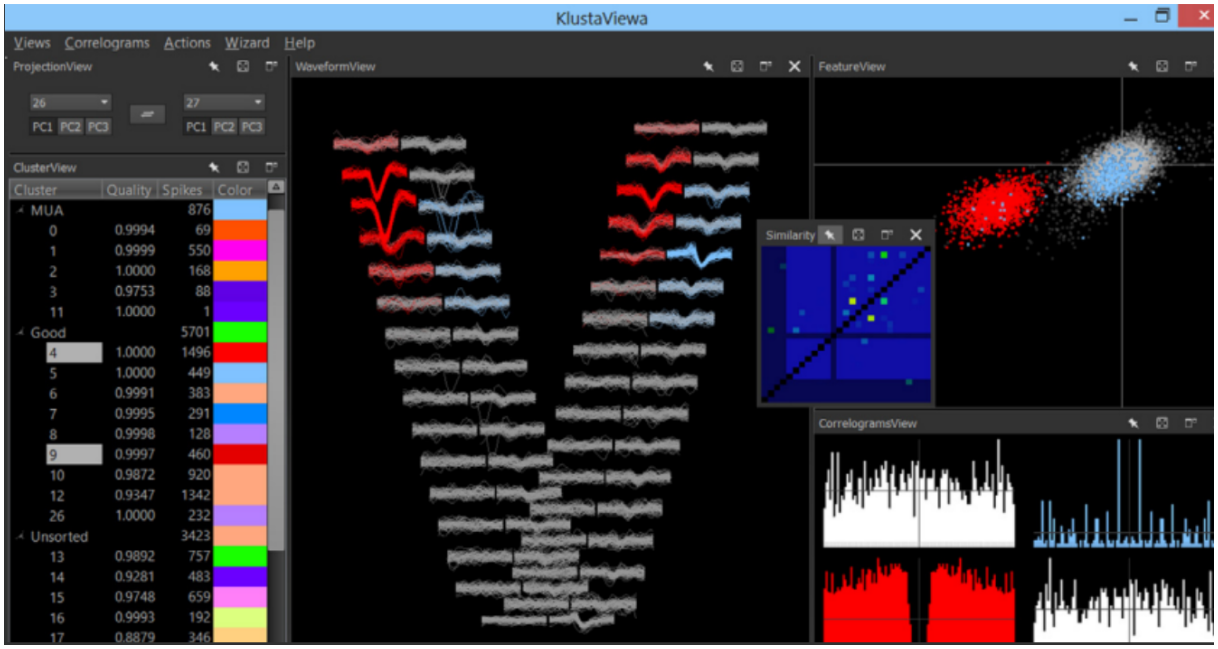

Source: ROSSANT et al. (2016)

Figure 27 – Possible format for the final data after the spike sorting. Four columns could be created. The first one (time(s)) is composed of the time in seconds of each spike for all clusters and shanks. The second column (cluID) gives the information about to which cluster that spike belongs. The third column says which shank that cluster was detected. The fourth column says for each cluster which channel the putative neuron is closer judged by the maximum amplitude.

time(s)	cluID	shankID	chanMAX
0.331533	36.0	2.0	4.0
0.340567	34.0	2.0	1.0
0.369567	44.0	4.0	2.0
0.379733	33.0	2.0	3.0
0.410267	47.0	4.0	2.0
0.441300	30.0	2.0	3.0
0.446267	68.0	5.0	5.0
0.446833	40.0	3.0	7.0

Source: The author (2023)

5 RESULTS

5.1 PUBLISHED ARTICLES

5.1.1 Criticality between Cortical States, PRL, 2019

Criticality in the brain and its manifestations have been investigated across various contexts (LIU et al., 2014),(WORRELL et al., 2002), (VYŠATA et al., 2014), (MAREŠ et al., 2013),(TINKER; VELAZQUEZ, 2014). , involving diverse species (GIREESH; PLENZ, 2008; PETERMANN et al., 2009; ZIMMERN, 2020) and models (CHALLET; MARSILI, 2003; KINOUCHI; COPELLI, 2006; LEVINA; PRIESEMANN, 2017). In this particular study of ours (FONTENELE et al., 2019), a specific facet of criticality, namely neuronal avalanches, was thoroughly examined. According to the critical brain hypothesis, systems operating at a critical point exhibit scale-invariant characteristics (BAK; TANG; WIESENFELD, 1988b; BAK; TANG; WIESENFELD, 1988a).

One of the seminal findings that reinforced the critical brain hypothesis was the 2003 study by Beggs and Plenz published in the Journal of Neuroscience. Their research emphasized the significance of the concept of self-organized criticality and the extensive examination of this theory in various contexts (BEGGS; PLENZ, 2003). According to Beggs and Plenz, this theory asserts that systems consisting of numerous interconnected and nonlinear elements can naturally self-organize into a critical state, where avalanches exhibit scale invariance and adhere to a power-law probability distribution.

The spike data analyzed in our paper were intentionally diverse to underscore the robustness of the results. The data sources included *ex vivo* cortex of turtles (SHEW et al., 2015), cortical slices of the rat brain (FRIEDMAN et al., 2012), freely moving mice (SENZAI; FERNANDEZ-RUIZ; BUZSÁKI, 2019), an anesthetized monkey (KOHN; SMITH, 2016), and anesthetized rats administered with urethane. The experimental protocol I was involved in pertained to anesthetized rats treated with urethane. The electrophysiological recordings were acquired using Neuronexus with 32 channels, 8 channels in each of 4 silicon shanks according to the methodology presented in Chapter 3 (Fig. 28a).

Our study examined the criticality signature within segments of spike data separated based on the variability levels associated with cortical states. The separation was achieved by calculating the coefficient of variation (CV) for each 10-second interval of neuronal population activity (HARRIS; THIELE, 2011). Figure 28b depicts the temporal series of CV, revealing a no-

tably wide dynamic range for this metric according to the density distributions for CV values. In Figure 28c, we can observe three 10-second raster plots that illustrate three distinct levels of variability. The purple window corresponds to a 10-second interval with the lowest coefficient of variation (CV) in the dataset. The red window represents an intermediate level of CV, while the green window signifies a period characterized by the highest level of synchrony.

The article by Harris et al. (2011) elucidates the mathematical connection between fluctuation and correlation. Consequently, one can anticipate distinct pairwise spiking correlation density functions for each of the three levels of variability, as depicted in figure 28d. The mean and standard deviation of these density functions exhibit a direct proportionality to the level of variability, as one would naturally anticipate.

Figure 28 – Study of signatures of criticality in V1 cortex. Figure A sketches the experimental and acquisition setup. Figure B shows the CV time series with 10 seconds of window per sample. The plot on the right shows the density distribution of CVs. Figure C is a representation of how the raster plot of 10 seconds of population activity looks like for three different values of CV. In Figure D, the data was segregated into three CV levels, and their correlation structure was calculated. The plot displays the density distribution over the structure correlation values. Figure E is graphically explaining how the avalanche is defined, and how its size and its duration are calculated. Figures F and G show the probability distribution of specific sizes and durations respectively for three different levels of CV. Figure H represents the AIC criterion to test if the fit corresponds more to a log-normal function or a power-law function depending on CV levels.

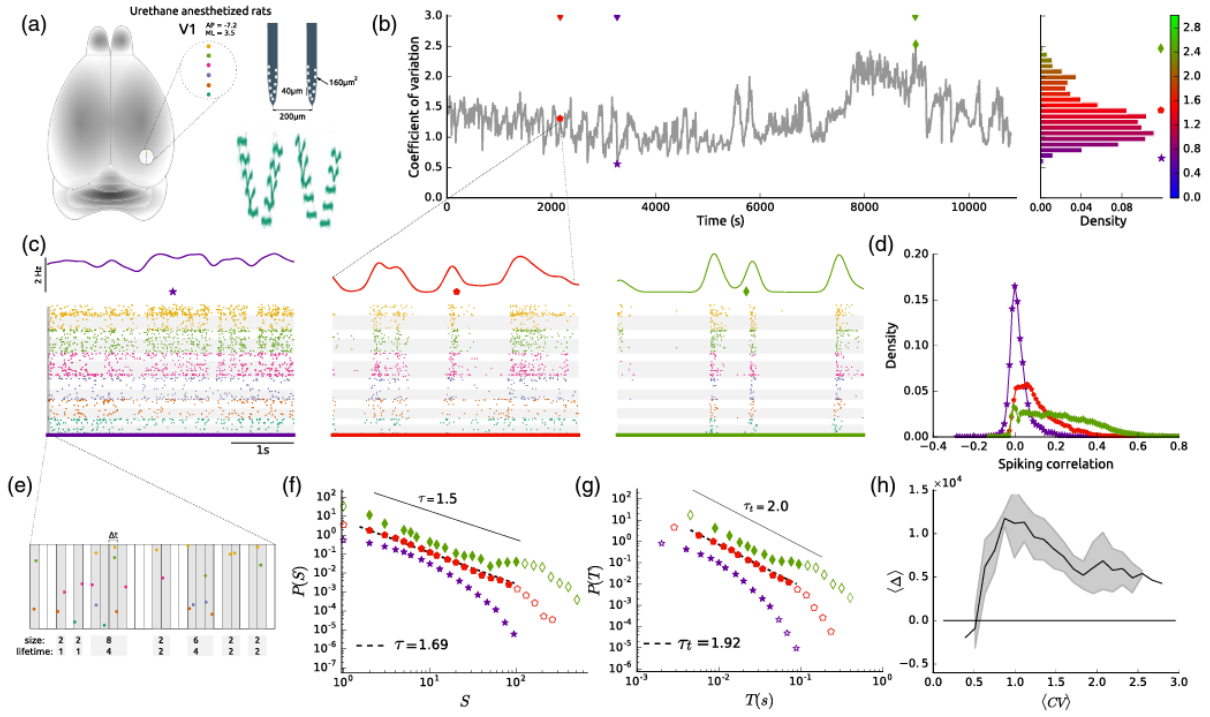

Source: FONTENELE et al. (2019)

Neuronal avalanches are defined as population spikes that are preceded and followed by periods of silence. The population spike is partitioned into non-overlapping time bins. The

duration of these time bins is determined by the average inter-spike interval, denoted as $\langle ISI \rangle$ (approximately 2-4 ms). Figure 28e provides a graphical explanation of how to quantify the size (number of spikes) and duration (number of bins between two empty bins) of a neuronal avalanche. Our study demonstrated that the probability distributions of both size (Fig. 28f) and duration (Fig. 28g) of neuronal avalanches can follow a power-law distribution when considering only the segments of spiking activity with CV values falling within the intermediate range. The fitting of this supposedly power-law distribution yields a fitted exponent.

At the critical point, another critical exponent that could be calculated is the fitted function of average size conditioned on a given duration. For example, given an avalanche duration of 0.03s, the avalanche could have a size of 3 spikes, or 100 spikes, depending on how many neurons are involved in that specific avalanche. Then the size of avalanches could be averaged for every specific avalanche duration. Figure 29c shows that for different levels of variability, the fitted exponents are different.

Relations involving exponents derived from size and duration distributions can provide insights into the criticality signatures investigated in the brain (SETHNA; DAHMEN; MYERS, 2001).

Another noteworthy outcome pertains to the scaling relations. The exponents for both size and duration align with the exponent obtained from the relationship between the average avalanche size and the average avalanche duration. That equality is only theoretically satisfied at the critical point.

$$\frac{\tau_t - 1}{\tau - 1} = \frac{1}{\sigma \nu z}$$

In our findings, the degree of this alignment depends on the level of variability in spike activity, as characterized by the coefficient of variation (CV). Figure 29a shows that the scaling relations hold true for anesthetized rats when the coefficient of variation (CV) falls within the intermediate range, as displayed. In Figure 29b, the dashed line illustrates the CV density distribution, indicating that a majority of the spike activity time series exhibits intermediate CV values. Notably, the median of the CV distribution coincides with the point at which the scaling relations equate. Figure 29e and figure 29f show the same plot as in figure 29a but for freely moving mice and anesthetized monkeys respectively.

It is conceivable to classify systems based on their fitted exponents and their interrelations. Systems sharing identical exponents may be regarded as belonging to the same universality class, and there has been considerable debate regarding which universality class the brain might

Figure 29 – Signatures of criticality for different experimental and artificial data. Figure A, B, E, and F represent the relation between the scaling relation and CV for (A)anesthetized rats, (E) freely moving mice, and (F)anesthetized macaque monkey. Figure B is the same as A, but an average of all the datasets of anesthetized rats. The dashed range of CV represents where the curves crossed taking into account the standard deviation. The dotted curves in Figures B and E are the density distribution of CV. Figure C is the plot between the avalanche's duration and its average size for different levels of CV. Figure D shows the relation between the DFA exponents and the difference between the scaling relations. Figure G combines all datasets used in this article to show that regardless of the nature of the data, the parametric relation between τ and τ_t remains and it is different from what one expects from MF-DP university class, for example.

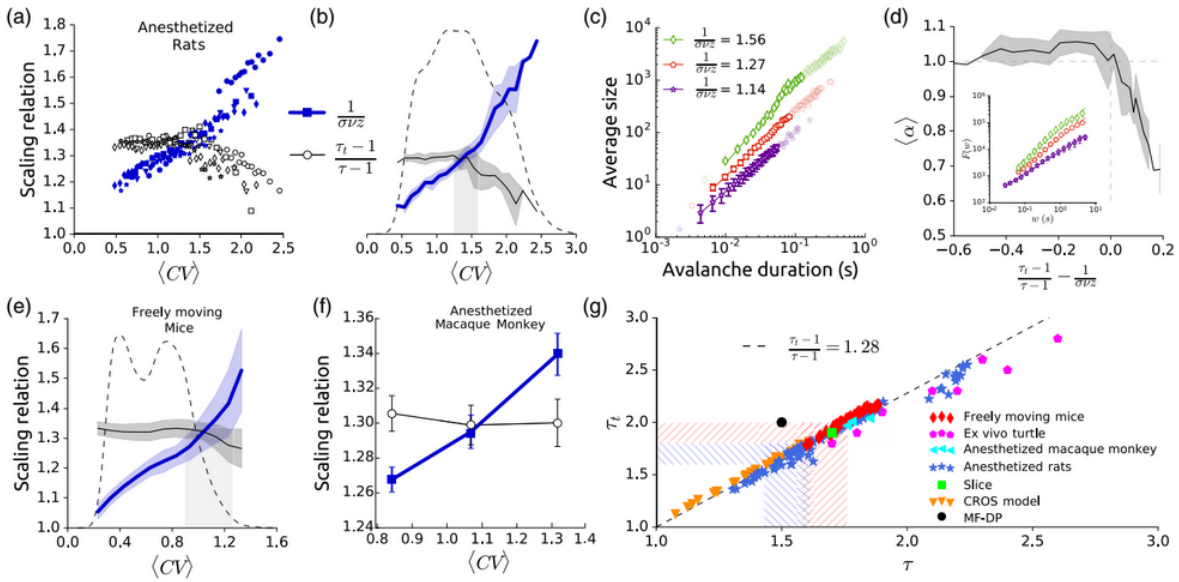

Source: ?? (**??**)

belong to (FRIEDMAN et al., 2012).

Another feature explored was the detrended fluctuation analysis. The fluctuation measured F(w) is also different for different levels of variability as shown in the inset of the figure 29d. That figure also shows the DFA exponent average in the function of the scaling relation equality distance and the equality happens when the DFA exponent α converges to one.

According to the findings of our paper, it is not a singular pair of exponents (size and duration) that stands out, but rather a consistent relationship between them, as shown in Figure 29g. Upon thorough data analysis, it becomes apparent that the scaling relations are only upheld when the coefficient of variation (CV) is situated at an intermediate level. This suggests that CV levels may serve as a proxy for an order parameter responsible for the transition from a less synchronized state to a more synchronized one. The critical point manifests itself when CV reaches an intermediate level, thereby signifying the presence of criticality signatures.

In this article, clear signatures of criticality were identified in the spike activity of the V1

cortex in urethane-treated rats. The critical point appears to be inaccessible when the neuronal population is highly synchronized or highly asynchronous. However, at intermediate levels of synchrony, it is robustly observed across different animals, anesthesia conditions, and brain regions.

These findings also challenge the notion that the critical point solely marks the transition between the absorbing (zero activity) and active phases (non-zero activity), as predicted by the direct percolation universality class. Instead, it is more precise to describe the transition as occurring between the active and oscillatory phases, especially since the CROS model successfully mimicked the results derived from spike data, and its structural basis is rooted in collective oscillations. The CROS model has both excitatory and inhibitory stochastic spiking neurons arranged in an $L \times L$ square lattice, each neuron interacting with a controlled random fraction of its neighbors within a small $l \times l$ region.

An additional noteworthy result is the discovery of a linear relationship between the fitted exponents from the size and duration distributions. This relationship holds true only for intermediate levels of the coefficient of variation (CV), and this phenomenon was consistent across all datasets analyzed, including the CROS model.

All of these findings give rise to more questions than they resolve. For instance, considering that the CROS model respects the relationship between the exponents, can this model predict additional features of the data? Can both anesthetized and unanesthetized animals be effectively described by the same model? And if so, does this model represent the most parsimonious explanation for the observed data?

5.1.2 Signatures of brain criticality unveiled by maximum entropy analysis across cortical states, PRE, 2020

The pioneering article that applied maximum entropy models to neuronal data was published in 2006 in Nature by E. Schneidman and colleagues. In this study, they demonstrated that despite the relatively weak pairwise correlations between neurons, a model using only these correlations could account for over 90% of the information within the system (SCHNEIDMAN et al., 2006).

These models belong to the class of maximum entropy models, which are probabilistic models designed to adhere to specific constraints while describing the system without making assumptions about any unknown features. An insightful analogy was drawn between a group

of neurons and a lattice of spins.

The maximum entropy model employed in this analogy was the Ising Model, where each spin represented a neuron, and the state of each neuron was described as either active ($+1$) or non-active (-1 or 0), akin to the quantum state of spins.

The Hamiltonian for this model incorporated interaction strengths between pairs of neurons and the "external field" strength of each neuron, both of which were adjusted based on data until the model accurately reflected the data. This adjustment process was guided by Monte Carlo algorithms, resulting in a probability distribution of states from the data closely resembling the probability distribution from the simulated model data.

The project I engaged in for my master's degree leveraged these tools to detect signatures of criticality in the Ising model derived from neuronal data. Once the model was fitted, it became possible to calculate the specific heat from the Hamiltonian, with this quantity diverging as the system approached the critical point.

Following the groundbreaking work in 2006, a new field emerged, with numerous articles adopting various approaches and slightly different models within the maximum entropy model class (TKAČIK et al., 2013; GARDELLA; MARRE; MORA, 2016; TKAČIK et al., 2014).

The article discussed below seeks to identify signatures of criticality in a maximum entropy model that accounts for the relationship between past and present firing rates. Building on the idea presented by Fontenele et al. in 2019, this article explores the hypothesis of detecting criticality, now including specific heat divergence, among different cortical states.

This article utilized two types of electrophysiological recordings from the ongoing activity of the V1 cortex, employing Neuronexus probes as the electrodes. A total of eight datasets were analyzed in this study. Five of these datasets were collected at the Life and Health Institute, University of Minho, while the remaining three were recorded in our laboratory. Notably, the data from Recife and Portugal exhibit similarities, albeit one set employed 32-channel silicon probes and the other 64-channel silicon probes. The 64-channel probes enable the simultaneous recording of more neurons, while maintaining consistent recording quality and data processing protocols.

As previously mentioned, following the groundbreaking work in 2006, numerous researchers drew inspiration from it, leading to the exploration of a variety of maximum entropy models for analyzing neuronal data. In 2016, Tierry Mora and Oliver Mare published a paper identifying signatures of criticality using a model distinct from the original Ising Model, yet still belonging to the maximum entropy models class. The probability distribution in this alternative model

takes the form of a Boltzmann distribution (MORA; DENY; MARRE, 2015).

$$P_\beta\left(\{\sigma_{i,t}\}\right) = \frac{1}{Z(\beta)} e^{-\beta E(\{\sigma_{i,t}\})}$$

This new system's energy still relies on two components: 'h' and 'J.' These components are respectively associated with the probability of 'K' neurons being active simultaneously, denoted as $P(K)$, and the joint probability of 'K' neurons being active at time 't' and 'K" neurons being active at time 't+u,' expressed as $P(K_t, K_{t+u})$.

$$E = -\sum_t h(K_t) - \sum_t \sum_{u=1}^{\nu} J_u(k_t, K_{t+u})$$

The concept is to adjust 'h' and 'J' until the probability distribution $P(\sigma_{i,t})$ derived from the model aligns with the one obtained from the data. Once the algorithm converges to the optimal probability distribution that accurately represents the data, the specific heat can be calculated. Specific heat is defined as

$$c(\beta) = \frac{\beta^2}{NL}\left(\left\langle E^2\right\rangle_\beta - \left\langle E_\beta^2\right\rangle\right)$$

Specific heat is anticipated to exhibit divergence when β equals one and as the number of elements increases.

All calculations related to specific heat, as well as the generation of probability distributions from the model and data, were executed using a code compilation provided by the authors of the paper, Thierry Mora and Olivier Mare.

To validate the code's functionality, specific heat was computed for all full recordings. As depicted in Figure 30 on the left, it is evident that the peak in specific heat becomes more prominent and approaches the critical beta as the number of neurons increases. This behavior is a well-known characteristic in spin systems and has been previously examined in neuronal data.

A similar analysis was carried out on shuffled data, and the unique feature of specific heat, its divergence near T equals one, is visible in Figure 30 on the right.

The primary objective of this study was to investigate the concept proposed by Fontenele et al. in 2019, which suggested that signatures of criticality, specifically features related to neuronal avalanches, might be more pronounced at intermediate levels of variability. In this context, the chosen signature of criticality was the divergence of the specific heat, and this metric was computed across a range of cortical states, spanning from the most asynchronous to the most synchronized.

Figure 30 – Specific heat calculated for subgroups of neurons. Left: Specific heat measured in 5 different size subgroups of neurons. Right: The same subgroups were analyzed however the spike trains were shuffled.

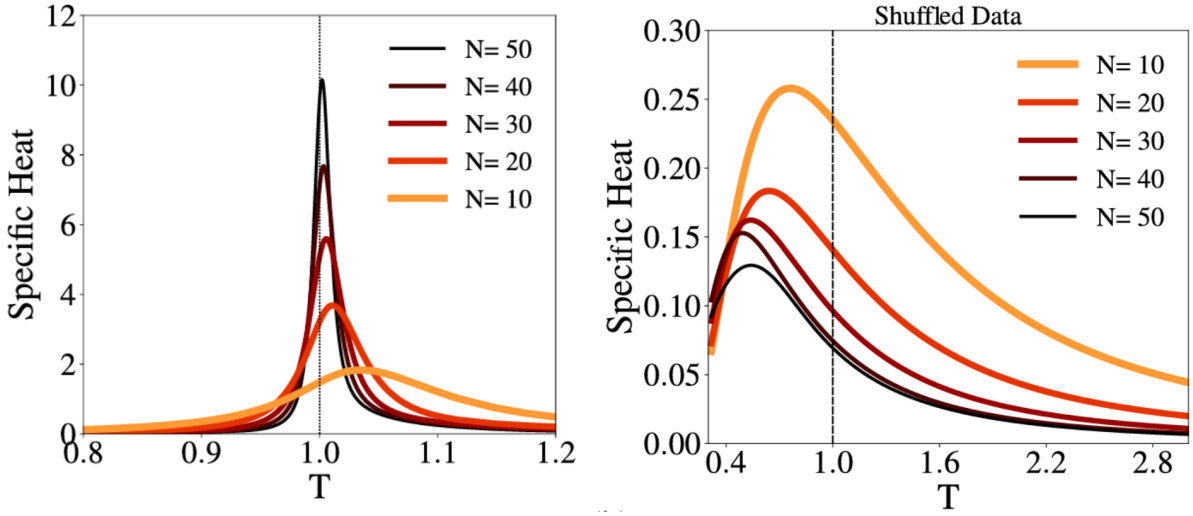

Source: LOTFI et al. (2020)

Figure 31 – Specific heat of the whole neuron population for different levels of variability. T^* is the value of T when the specific heat is maximum. Remembering that the "real value of c is for T equals 1, the rest of the values come from the model.

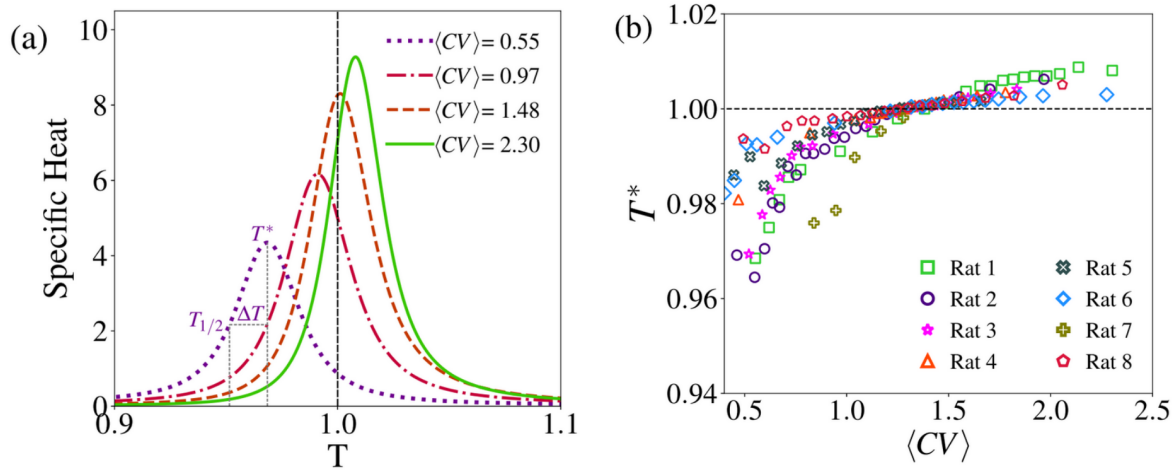

Source: LOTFI et al. (2020)

In Figure **??**a, it is evident that for lower levels of CV, the specific heat values are lower, the curve shape is less pronounced, and the parameter T^* is below T=1, indicating a subcritical state. As the CV values increase, the specific heat curves become more distinct, with their peaks approaching T=1.

Upon reaching a certain point, corresponding to a higher level of variability indicative of a more synchronized state, the specific heat curve peaks when the parameter T is greater than one, implying that for this level of synchrony, the observed group of neurons would have self-organized into a supercritical state.

The most remarkable finding is that the level of CV at which $T^* = 1$ is approximately $CV \simeq 1.48$, a value closely resembling what Fontenele et al. discovered as the threshold for identifying signatures of criticality using neuronal avalanches.

The specific heat was calculated for the same datasets as in Fontenele et al.'s work. Figure **??**b depicts the values of T^* for each range of CV. In comparison to Figure **??**a, each point in Figure **??**b corresponds to the value of T where the specific heat attains its maximum value.

Within the same figure, all the datasets are presented, and it's evident that T^* converges towards one as the mean CV value approaches 1.48. This outcome underscores the consistency across various animal samples and different laboratory settings.

Figure 32 – Relation of new quantity τ with levels of variability of spiking activity quantified by coefficient of variation, CV. Right: τ value in function of CV for the animals. Left: Same measure but the data was shuffled before.

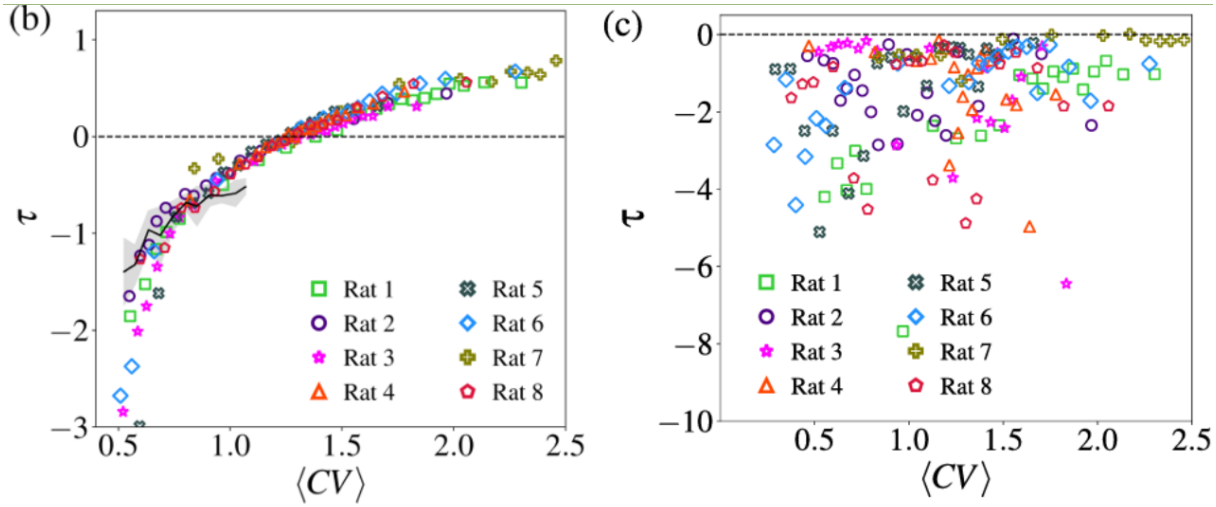

Source: LOTFI et al. (2020)

Another innovative concept introduced in this paper was the development of a novel measure that connects two key values: the temperature associated with the maximum specific

heat and the temperature that aligns with half of the maximum specific heat. The proposed equation was

$$\tau \equiv \frac{T^* - 1}{T^* - T_{\frac{1}{2}}}$$

where $T_{\frac{1}{2}}$ is defined as $c(T_{\frac{1}{2}}) = \frac{c(T^*)}{2}$.

Once again, it is evident that all the animals in Figure 32 exhibit a consistent pattern. It's worth noting that three of these rat datasets were recorded and analyzed in our laboratory, while the other five were shared data from Portugal.

This new measure illustrates that the manner in which specific heat changes with CV is consistent across all datasets, and the critical τ (which equals zero) is achieved for all datasets when the average CV is approximately 1.48.

The findings of this paper were particularly intriguing because they not only confirm the results of Fontenele et al. but also reignite a significant debate about whether measures of cortical states can effectively serve as a control parameter for phase transitions.

In general, the use of specific heat curves strengthens the argument that the system approaches criticality as the number of elements involved increases, as previously observed in Figure 30.

However, the unique aspect is how the system's proximity to criticality for a specific CV range is unprecedented and supports the relationship between variability levels and criticality. Furthermore, this relationship is consistent across all datasets, whether from Recife or Portugal.

Another significant result is how the relationship between T^* and the average CV appears to collapse into a single, distinct curve when a new parameter, τ, is introduced. This parameter is a function of T^* and accounts for how close the specific heat peak is to T=1 and the sharpness of the curve. Once again, all datasets seem to follow a well-defined pattern, and this phenomenon is not observed in shuffled data.

The results from Fontenele et al. in 2019 and Lotfi et al. in 2020 may lead one to consider that CV levels could serve as a plausible control parameter for identifying a critical point. This hypothesis aligns with biological reasoning, as the brain might not be able to achieve its maximum information processing potential under either extreme level of synchrony.

It is essential to acknowledge the existence of a level of complexity and non-linearity in how a group of neurons interacts. Not all neurons will be fully synchronized or entirely asynchronous. Thus, an intermediate level of synchrony, quantified by the coefficient of variation,

may intuitively be sensible for expanding the dynamic range of stimulus responses, enhancing information capacity, and optimizing information transmission.

The next question posed by our research group was: is there a model capable of replicating the results from the data? Moreover, could this model enhance our understanding of criticality signatures and cortical states? The following section will delve into another project that seeks to address these questions.

5.1.3 Subsampled directed-percolation models explain scaling relations experimentally observed in the brain, Frontiers in neural circuits 2021

Tawan Carvalho was a PhD student in our research group from 2019 to 2021 and played a pivotal role in an intriguing and groundbreaking project. Leveraging his background in computational Statistical Physics, he applied a modeling approach to explore the critical relationship between cortical states and real neuronal data.

This pioneering project exclusively utilized datasets collected in our laboratory, led by me and Dr. Leandro Alcantara, along with the valuable contributions of Bh. Thais Priscila. A total of five datasets were meticulously analyzed in this study, following the same experimental protocol as in Fontenele et al. 2019.

The focal point of this research was a spiking neuronal network model that incorporated both excitation and inhibition (GIRARDI-SCHAPPO et al., 2020). Each neuron in this model adhered to a stochastic leaky integrate-and-fire equation, a well-known model that plays a significant role in the mean-field direct percolation (MF-DP) university class (TEETER et al., 2018).

Within each universality class that exhibits criticality, it is anticipated that certain common features will emerge. One such example is the exponents derived from probability distributions based on neuronal avalanches (YAGHOUBI et al., 2018).

The specific model used in this study was parameterized to enable the resulting artificial neuronal activity to exhibit criticality signatures. While criticality signatures from the MF-DP class were discernible in this model, they were notably absent in the real data (RIBEIRO et al., 2010). This discrepancy suggests that the real neuronal data may not align with this specific universality class, or that the model does not accurately replicate the behavior of neurons in the visual cortex.

These intriguing findings will be the focus of further investigation in this work, offering

impressive insights that challenge assumptions implied by our two previous studies.

To generate the artificial data, we employed a spiking neuronal network with an excitation and inhibition network, as described in (GIRARDI-SCHAPPO et al., 2020). Each neuron within the network, consisting of N neurons, had its membrane voltage denoted as V_t, and it was governed by the following equation:

$$V_t^{\mathrm{E/I}}(t+1) = \Bigg[\mu V_1^{\mathrm{E}/l}(f) + I_\varepsilon + \frac{J}{N}\sum_{j=1}^{N_E} X_f^{\mathrm{E}}(t) - \frac{gJ}{N}\sum_{j=1}^{N_{\mathrm{I}}} X_j^{\mathrm{I}}(t)\Bigg]\left(1 - X_1^{\mathrm{E/I}}(t)\right),$$

Time is discretized in a 1 ms window, where μ represents the leak time constant, I_e signifies the external current, J stands for the synaptic coupling strength, and g denotes the inhibition-to-excitation coupling ratio. The variable X(t) reflects the current state of the neuron, taking a value of 0 when it's inactive and 1 otherwise. The ratio between the populations of inhibitory (N_i) and excitatory (N_e) neurons is established at 0.2 and 0.8, respectively, in accordance with the findings outlined in (SOMOGYI et al., 1998)

The voltage membrane, in turn, plays a pivotal role in determining whether neurons will become active in the subsequent millisecond, utilizing a piecewise linear sigmoidal probability function.

$$\Phi(V) \equiv P(X = 1 \mid V) = \Gamma(V-\theta)\Theta(V-\theta)\Theta\left(V_S - V\right) + \Theta\left(V - V_S\right)$$

where θ is 1 and it is defined as a firing threshold, Γ is the firing gain constant, Θ is the Heaviside step function and $V_S = \frac{1}{\Gamma+\theta}$ is the saturation potential.

The model exhibits a direct percolation critical point at a specific inhibition-to-excitation coupling ratio, denoted as g. The critical value of g, represented as g_c, is determined to be 1.5 (for $J = 10$ and $\Gamma = 2$). When g falls below 1.5, it signifies an active excitation dominance, while values above g_c indicate a phase dominated by inhibition in the model. We employed two distinct methods to obtain two types of data: one derived from a stochastic model, extensively investigated by Giradirno, and the other obtained from electrophysiological data. Both datasets were subjected to an analysis that focused on the levels of variability in neuronal population activity. The coefficient of variation (CV) was computed at 10-second intervals within the time series of neuronal population activity.

This CV value allowed us to track changes in variability over time for both real and simulated data. Within each 10-second window, we performed neuronal avalanche analysis.

To accomplish this, the large 10-second time window was divided into smaller bins, where the bin size was determined based on the average inter-spike interval. A neuronal avalanche was defined as the population activity occurring between two bins with zero activity. We quantified the number of spikes within each avalanche (referred to as the "size of avalanche") and the number of bins separating the empty bins (referred to as the "duration of avalanches").

Consequently, for each 10-second interval, we obtained a unique CV value, a size vector, and a duration vector encompassing all avalanches that occurred within that interval. These size vectors were combined with other vectors that shared similar CV values, thereby creating a larger vector containing all avalanche sizes within a comparable range of CV. This same process was repeated for avalanche durations.

With these concatenated vectors organized by CV values, we could calculate the probability of an avalanche involving, for example, 5 spikes, by tallying the occurrences of such avalanches and dividing by the total number of avalanches.

Subsequently, we scrutinized the shape of the probability distribution for these avalanche characteristics. The exponent yielding the best fit for these probability distributions was computed using the Maximum Likelihood Estimator (MLE) procedure (MYUNG, 2003). Once the most suitable exponent was identified, we conducted a test to determine whether the fit resembled a power-law distribution or a log-normal distribution. This test, known as the Akaike Information Criterion (HU, 2007), guided our selection. All further analyses only considered probability distributions that exhibited a superior fit to a power-law distribution.

The Girardini model we've discussed is primarily characterized by its parameter, g, which signifies the inhibition-to-excitation coupling ratio. Notably, the stationary firing density within the artificial population undergoes changes as g varies, as illustrated in Figure 33a. Intriguingly, even small fluctuations in g can lead to a rapid transition of the system from an active state (non-zero activity) to an absorbing state (zero activity). This phase transition can be precisely quantified and analyzed by examining the exponent obtained from the power-law fit of probability distributions (Fig. 33b,c,d).

Here, τ represents the exponent derived from the probability distribution of avalanche sizes, while τ_t corresponds to the exponent associated with avalanche durations. For this model, when g equals 1.5, it is a well-established fact that τ equals 1.5 and τ_t equals 2. With these specific exponent values, it is reasonable to conclude that this model belongs to the MF-DP university class.

The model can effectively replicate the level of variability observed in real data by reducing

Figure 33 – Spiking neuronal network with excitation and inhibition with 10^5 neurons for different values of g. Figure A shows the stationary density of firing, $\widetilde{\rho}$, in function of the inhibition to the excitation coupling ratio, g. Figure B displays the probability distribution of all possible sizes for avalanches for three different values of g. In Figure C, the same calculation is made as in B but now for avalanche duration. Figure D shows the average size of avalanches related to their respective duration. In Figure E, it is possible to see the time series of instant density firing for each of the three values of g.

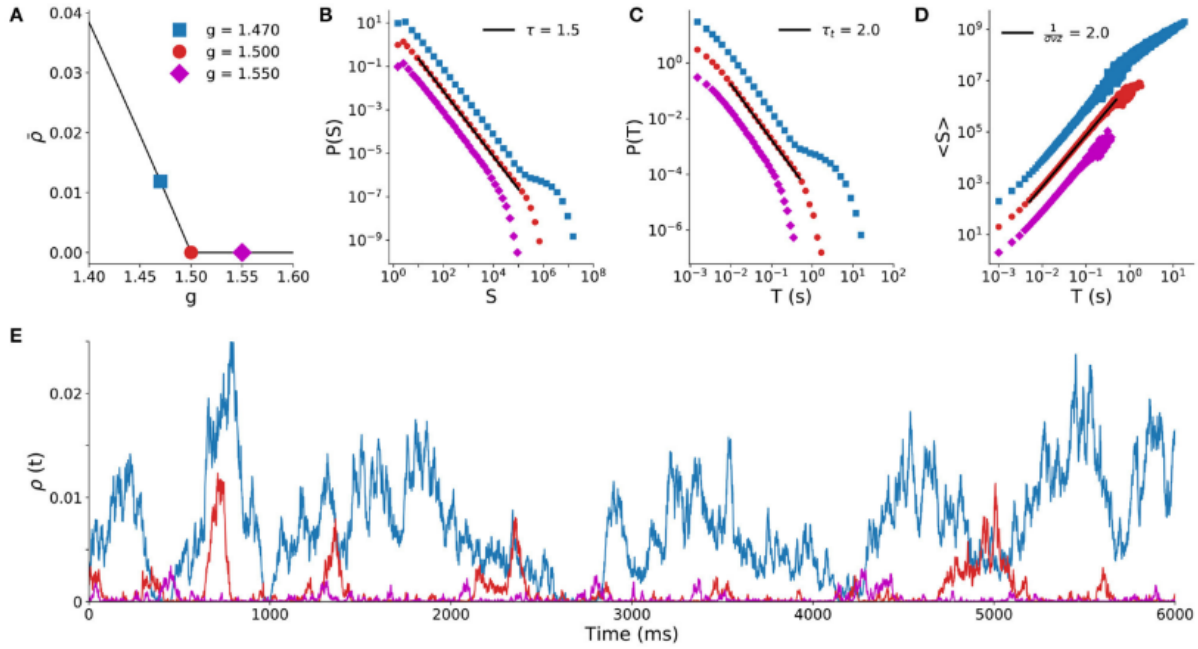

Source: CARVALHO et al. (2021)

the number of neurons to 100. With this constraint, it becomes possible to achieve three distinct states of low, intermediate, and high coefficient of variation (CV) by making minor adjustments to the values of g around 1.5, as illustrated in Figure 34a and 34d, left panel. The model's resemblance to real data can also be confirmed by examining the probability distributions of avalanches (Fig. 34c,f).

Values of g below 1.5 result in artificial spike trains that exhibit characteristics akin to concatenated segments of real spike trains with a low CV. Conversely, when g exceeds 1.5 in the artificial data, it closely resembles high CV real spike trains. These characteristics mentioned are indicative of the criticality signatures investigated by Fontanelle et al. in 2019.

Both the model and the real data exhibit identical criticality signatures, including the scaling relation dependent on the coefficient of variation (CV) and the linear correspondence between τ and τ_t (Fig. 35). These findings strongly imply that this spiking neuronal network, featuring both excitation and inhibition, stands as a promising candidate for accurately replicating results obtained from real neuronal data.

The article also delved into the impact of the sampling fraction and time bin size on the

Figure 34 – Two panels to show the similarity between the real data acquired in our lab and the data the model simulated for 100 neurons. Figure A show the time series of CV for almost 3 hours of recording. Each point is the CV value for 10s of neuronal population activity. On the same figure on the left, there is a density distribution of CV. Three CV extremes values were highlighted and used to exemplify how these three levels behave. Figure B shows the raster plots for 10 seconds of population activity for two different states. On the left, this window has a low value for CV, and clearly, this group of neurons has a low level of synchrony. On the right side, it was chosen a high value of CV that shows how deeply synchronized the neurons are. In Figure C, blocks of 10 seconds with similar values of CV were concatenated, and the avalanche analysis was calculated displaying a distinction between the probability distributions of the three different ranges of CV. Figures D, E, and F are the same analysis as A, B, and C in the data generated by the model.

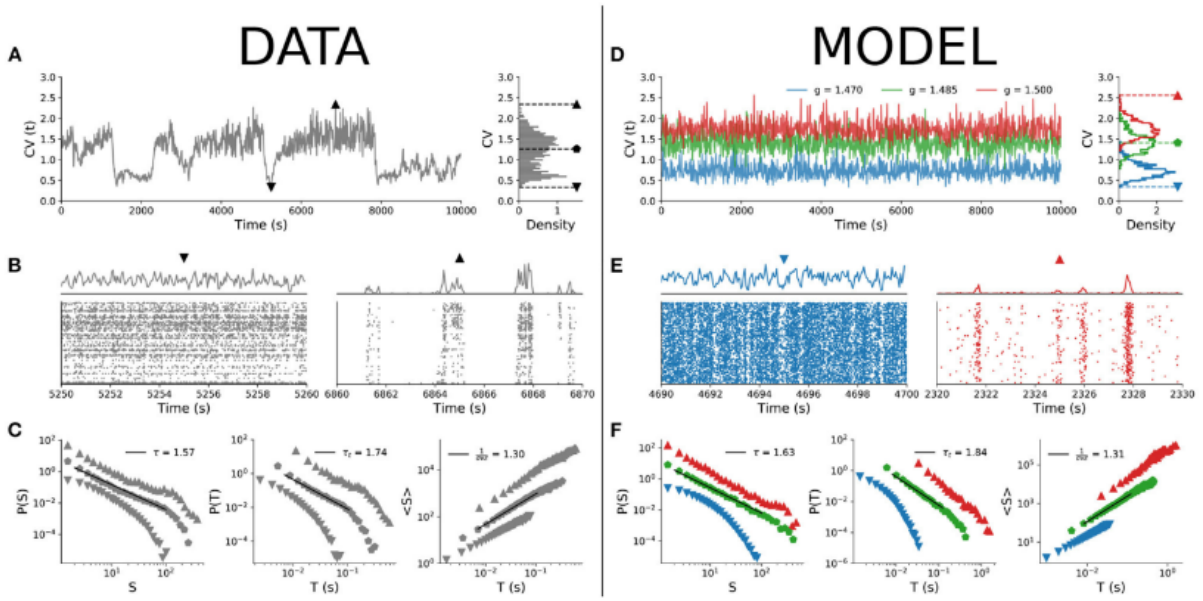

Source: CARVALHO et al. (2021)

observed criticality signatures. When the time bin is set equal to the inter-spike interval (ISI), an intriguing pattern emerges as the population size N increases. The relationship between τ and τ_t becomes progressively more akin to that observed in real data (Fig. 36a). However, employing ISI as the time bin width has its limitations. Specifically, a minimum of 30 artificial neurons is necessary, or else the power-law fits fail to meet the Akaike Information Criterion (AIC) criterion. Furthermore, a significant subgroup of neurons experiences ISIs of less than 1 ms, which is unsuitable for avalanche calculations given the model's time scale of 1 ms.

Conversely, when a fixed bin size of 1 ms is employed across all subgroup sizes, an intriguing phenomenon surfaces in Figure 36c. The scaling relation holds with consistent accuracy for both a small fraction of neurons (1.3) and the entire neuron population (MF-DP=2), albeit with differing values. Nevertheless, as the fraction of artificial neurons increases from the minimum value, the scaling relation diminishes (Fig. 36b).

Figure 36d provides further insight, indicating that as the fraction of neurons utilized for

Figure 35 – Signatures of criticality measured for real data and artificial data. Figures A (real data) and C (artificial data) show two features depending on CV. One feature is a single value relating τ and τ_t by the equation $\frac{\tau_t - 1}{\tau - 1}$. The second feature is the exponent fitted by the relation between the average size of avalanches and their duration. Figures B (real data) and D (artificial data) show that τ and τ_t obey a linear relation of 1.3 for CV values around 1.5. The same behavior is encountered in the artificial data except for values of g slightly bigger than $g = 1.5$.

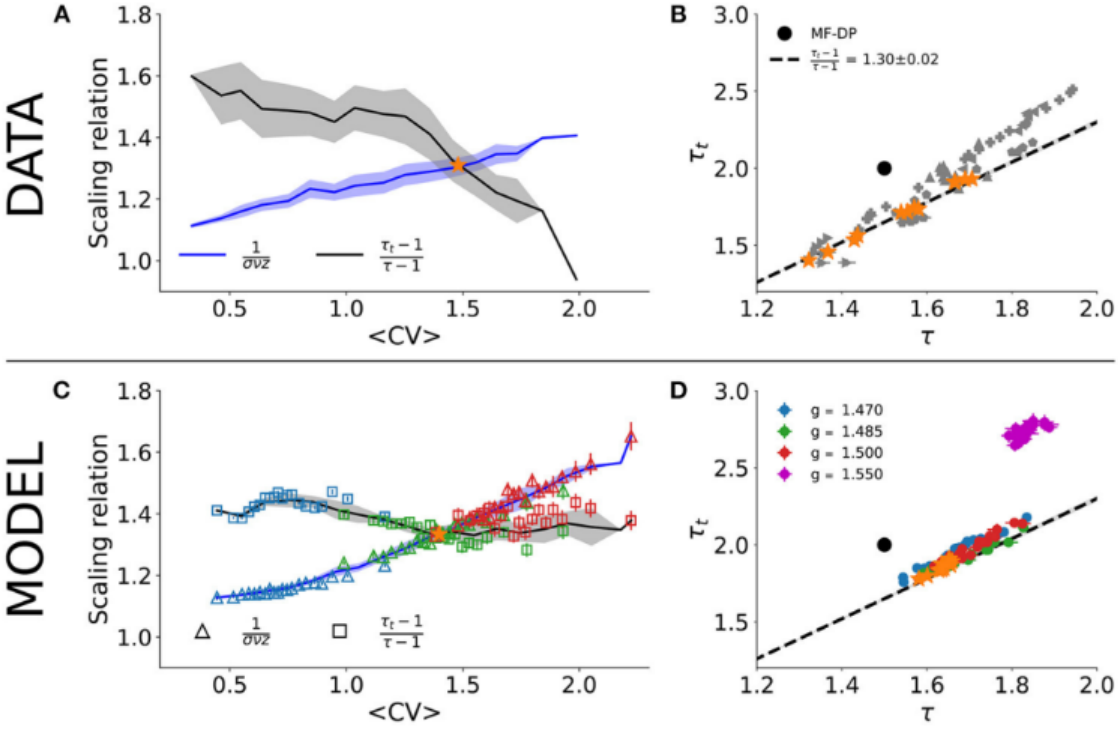

Source: CARVALHO et al. (2021)

calculating τ and τ_t expands, these exponents progressively tend toward the values associated with the MF-DP class.

One of the greatest highlights of this paper was finding a model and its specific parameters that could reproduce the real data, its cortical state density distribution, and also the avalanche dynamics. The key parameters responsible for adjusting the model to the real data were the inhibition to the excitation coupling ratio, g, and the number of neurons N involved in the calculations.

With this adjusted E/I spiking neuronal network, it is possible to investigate deeply the central question of this field: "If the brain is critical, what is the phase transition? ". Fontanele et al, 2019, suggested that the level of variability of the neuronal population activity could have an effect on how close the system will be from the critical point.

Tawan's article effectively challenged a previously held notion when it demonstrated that a well-established model could reproduce a broad spectrum of changes in CV by slightly

Figure 36 – Dependence of the number of neurons and time bin width on signatures of criticality for artificial data. Figure A and C calculate the scaling relation for any CV in function of the fraction of neurons involved in the sub-network with (A) time bin equal to the ISI and (B) time bin equal to 1 ms. Figures B and D show the parametric relation between τ and τ_t for different numbers of neurons and with (B) time bin equal to the ISI and (D) time bin equal to 1 ms.

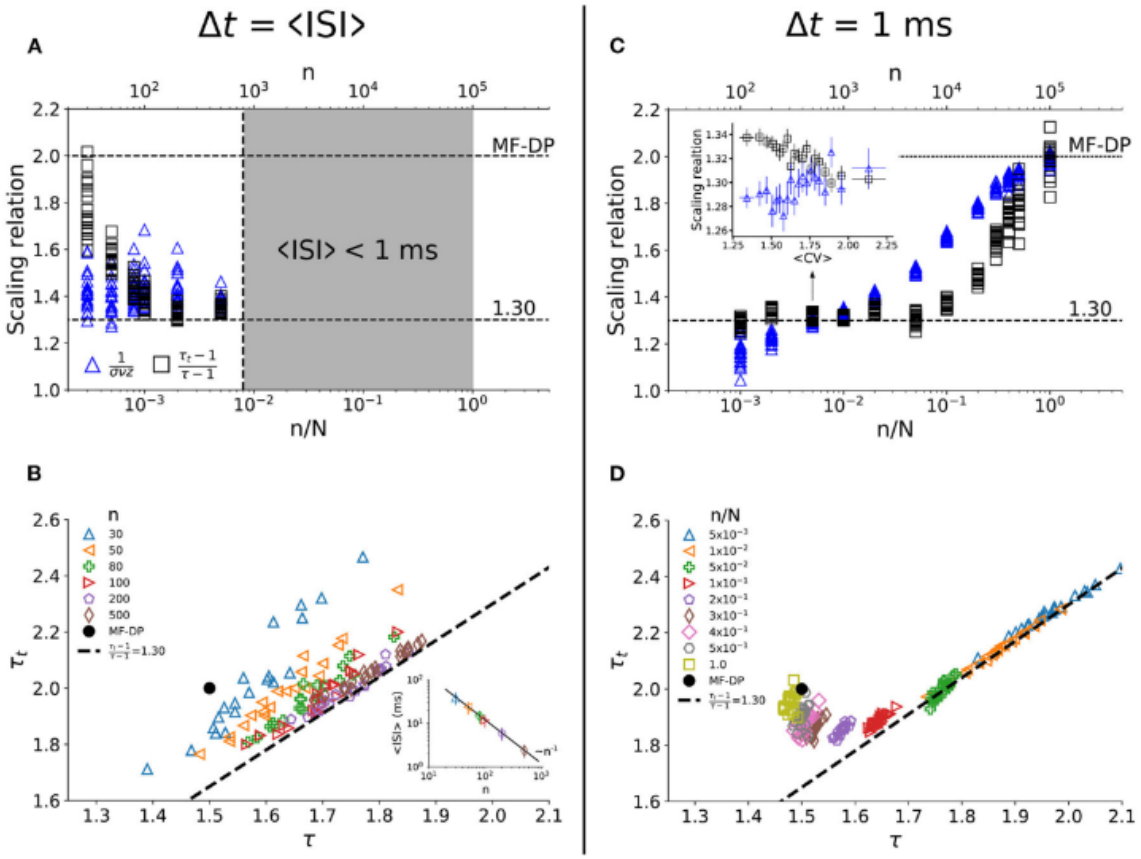

Source: CARVALHO et al. (2021)

adjusting the model's control parameter, denoted as 'g,' responsible for characterizing the model's criticality.

It is evident, from an electrophysiological perspective, that data obtained through neuronal recordings with electrodes inherently represents a subsample of the entire neuronal population. In other words, when utilizing available techniques for recording neuronal activity, it is practically impossible to ensure the recording of every single neuron within a specific area.

The subsampled data generated by the model remarkably mimics the criticality signatures observed in real data. However, the complete artificial dataset exhibits characteristics in line with expectations from models associated with the MF-DP university class. This paper played a pivotal role in enhancing our research group's comprehension of how to approach criticality and its relationship with cortical states.

5.1.4 Statistical complexity is maximized close to criticality in cortical dynamics, PRE, 2021

Complexity lacks a universally precise definition; however, various complexity measures have been proposed and employed, including Kolmogorov complexity (MING; VITÁNYI, 1990), Crutchfield's complexity, and Young's complexity (CRUTCHFIELD; YOUNG, 1989). The statistical complexity employed in this study was the Martín-Platino-Rosso (MPR) complexity (MARTIN; PLASTINO; ROSSO, 2006). To conduct the calculations, it was necessary to represent the time series as a probability distribution, achieved in this case using the Bandt-Pompe recipe (BANDT; POMPE, 2002).

With this probability distribution, complexity and entropy could be charted in a phase plane, based on the variability of time series segments. For highly desynchronized or synchronized data segments, the complexity takes on a value of zero. In contrast, Shannon entropy assumes values between 0 and 1, reflecting the degree of synchrony, ranging from most desynchronized to most synchronized.

The complexity-entropy phase plane proved to be a valuable tool for studying the relationship between these two measures and criticality. An investigation revealed a connection between criticality and complexity, indicating that complexity peaks when the system is poised near criticality (TIMME et al., 2016).

To explore this relationship, a symbolic information-theoretical approach was applied to time series of neuronal population activity, enabling the calculation of permutation entropy and MPR complexity across a range of cortical state values.

To compute any information-theoretical metric, like Shannon's entropy or the MPR complexity measure, it is imperative to derive a probability distribution function for the system. Let X(t) denote the time series that characterizes the system. We can segment the time series into symbols, each of which can then have its frequentist probability calculated. This, in turn, enables the use of Shannon's entropy, expressed as follows:

$$S[P] = -\sum_{j=1}^{N} p_j ln(p_j)$$

When a system is entirely predictable, its entropy equals zero. Conversely, when a system is entirely unpredictable, its entropy assumes the maximum possible value. We can define the normalized Shannon's entropy, which is

$$H[P] = \frac{S[P]}{S[P_e]}$$

where P_e represents the system's uniform probability distribution. Another information-theoretical metric that can be employed to characterize the system is the MPR complexity measure. It is defined as follows

$$C[P] = Q_J\left[P, P_e\right] \cdot H[P].$$

The $Q_J\left[P, P_e\right]$ is defined in terms of the Jensen-Shannon divergence as

$$Q_J\left[P, P_e\right] = Q_0 J\left[P, P_e\right],$$

where

$$J\left[P, P_e\right] = S\left[\frac{(P + P_e)}{2}\right] - \frac{S[P]}{2} - \frac{S\left[P_e\right]}{2},$$

and Q_0 is the inverse of the maximum value of $J\left[P, P_e\right]$.

To assess the probability distribution function, the Bandt-Pompe symbolization technique was applied to the system's time series. This technique involves extracting patterns of length D associated with each observable in the system. For instance, when D=3, a set of 6 symbols can be generated, such as (012), (021), (102), (120), (201), (210). The figure 37 displays an example. Consider a system's time series approximately given by X(t)=5,10,8,4,5,3,8,2,10,7.

The initial symbol corresponds to the sequence (5,10,8), represented as (0,2,1). Subsequently, the next sequence, (10,8,4), is symbolized as (1,2,0), and so forth. The domain size of the probability distribution function is 6, and each symbol's frequency is counted. The probability distribution is then computed based on these counts. Although the symbolic representation discards the amplitude information from the time series, it effectively retains the temporal structure and temporal correlations.

The exploration of the hypothesis of criticality in the brain has spanned almost three decades, necessitating the identification of quantitative signatures for this hypothesis. Complexity measures have been proposed as potential signatures of criticality (TIMME et al., 2016). Previous studies from our research group have investigated the impact of different cortical states on criticality signatures, such as the scale invariance observed in neuronal avalanches (FONTENELE et al., 2019) and the divergence in thermodynamic quantities (LOTFI et al., 2020). In this work, we aimed to characterize cortical states using the Martín-Platino-Rosso statistical complexity.

Figure 37 – Construction process of the probability distribution function used to calculate the complexity and entropy measure. A) Possible symbols to represent the time series. B) Segment of time series representation. C) Probability distribution of symbols used to describe the time series.

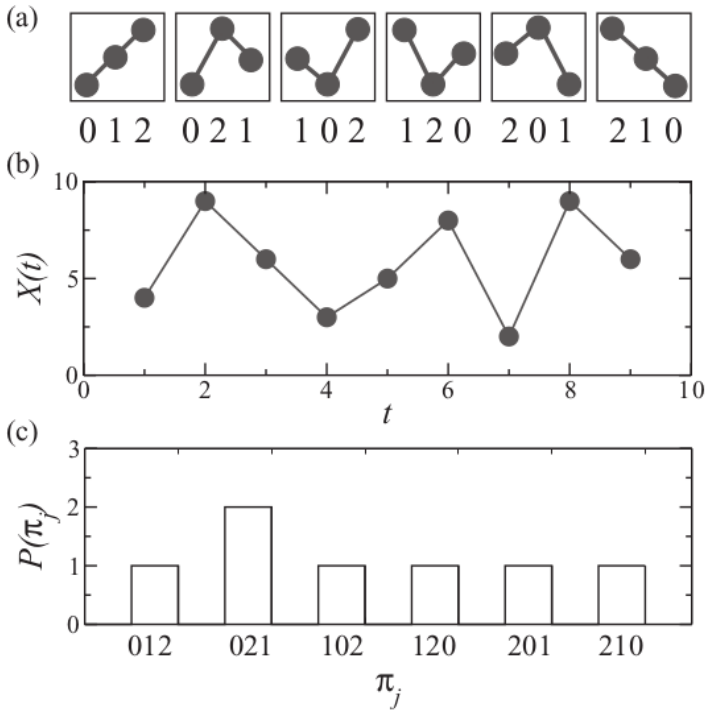

Source: LOTFI et al. (2021)

Figure 38 – Three segments of the time series with different levels of variability. The first line of plots **a** shows the population firing rate of 274 recorded clusters and the second line is the raster plots for the same three specific time windows. The green column represents a time window with high spiking variability (CV=2.60). The red column presents a time window with an example of intermediate value of CV (CV=1.30) and the blue represents a moment of low variability, a desynchronized state with CV=0.484.

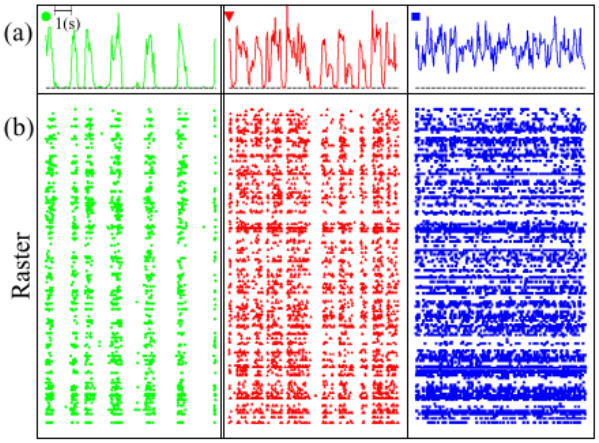

Source: LOTFI et al. (2021)

Initially, cortical states were characterized using datasets from anesthetized rats. At 10-second intervals, we calculated the coefficient of variation (CV) to quantify the level of vari-

ability, allowing us to observe the temporal evolution of CV (Fig. 38). Using the same time window, we also computed entropy (H) and complexity (C) over time (refer to Fig. 39).

Figure 39 – Three quantities were calculated along the recording session at each non-overlapping 10 seconds. The first plot shows CV time series. The second plot shows Shannon's entropy at each non-overlapping 10 seconds window. The third column presents the complexity measure at each non-overlapping 10 seconds. And the density distribution of each time series is on the side. The time windows presented in figure 38 are pointed with the corresponding color dots.

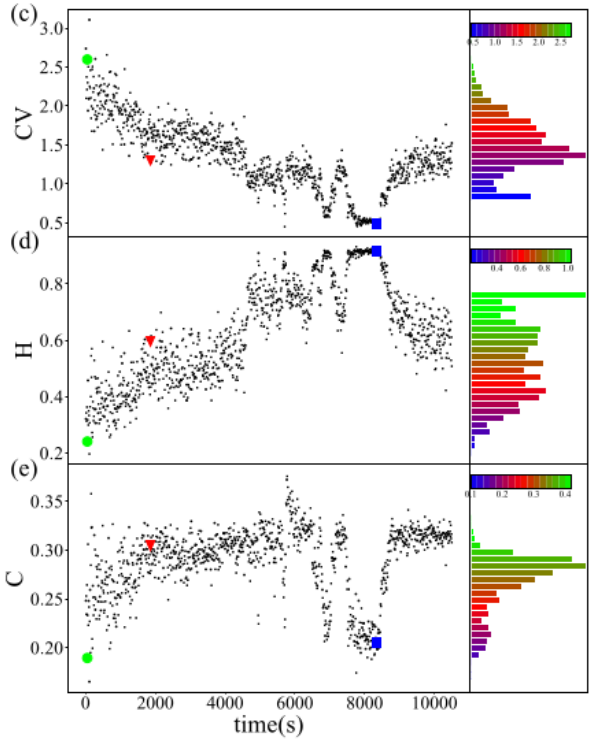

Source: LOTFI et al. (2021)

A visual inspection of the temporal series of CV, H, and C may suggest correlations between these measures. In the f igure 40a (top), a clear relationship is observed between entropy and the level of variability, where entropy decreases with higher spiking variability. Remarkably, all experiments exhibit the same trend (Fig. 40a down). Additionally, Fig. 40b demonstrates that statistical complexity is maximized between synchronized and desynchronized cortical states, a pattern consistently observed in all experiment datasets. The relationship between entropy and complexity is non-trivial, and all experiments adhere to this relationship within theoretical upper and lower boundaries (Fig. 40c).

To enhance the robustness of the complexity measure, we computed it for surrogate data, revealing that the dependence between complexity and cortical states diminishes (Fig. 41).

Our investigation into complexity as a measure of criticality suggests that statistical complexity is maximized in proximity to the phase transition in a probabilistic cellular automata

Figure 40 – Information-theory measures for different levels of CV calculated for different recording sessions. The first column displays the relation between Shannon's entropy and the mean values of CV. The second column shows the relation between the MPR complexity measure and the mean values of CV. The third column shows the relation between the MPR complexity measure and Shannon's entropy. The first line of plots corresponds to one recording session. The second line of plots shows the group's result for 7 different rats.

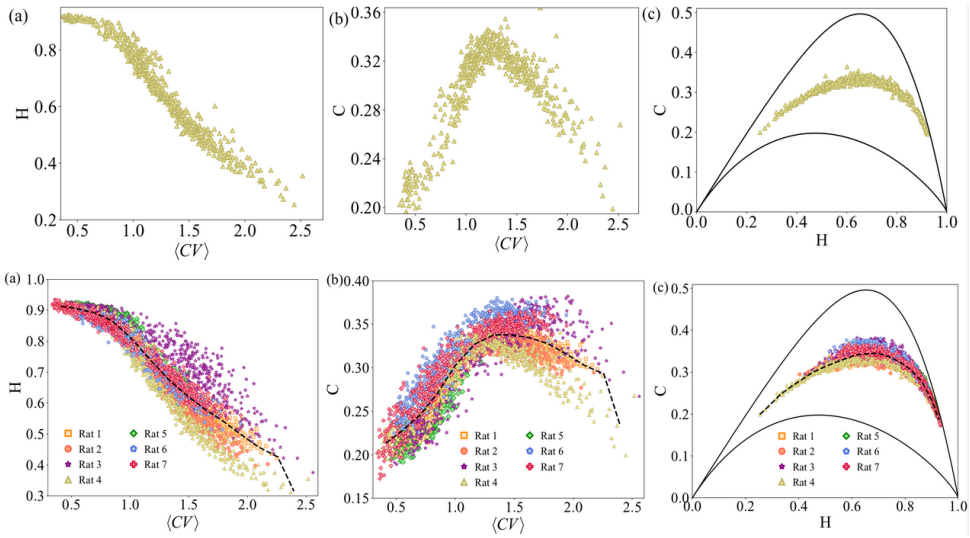

Source: LOTFI et al. (2021)

Figure 41 – Information-theory quantifiers calculated for the surrogate data. The gray line is the mean of all experiments displayed in the figure 40 and the gray shadow represents the standard deviation. The blue dashed line is the mean over all the surrogated datasets and the blue shadow is the correspondent standard deviation. The left plot shows the relation between Complexity and CV. The right plot shows the relation between complexity and entropy for the data and the surrogated data.

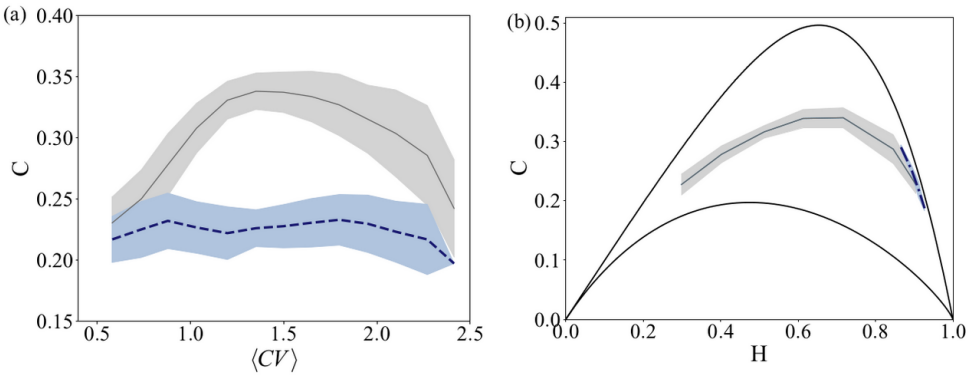

Source: LOTFI et al. (2021)

network (KINOUCHI; COPELLI, 2006) (Fig. 42).

The study demonstrated a non-trivial relationship between cortical states and the information-theory quantifiers computed in this work. Both quantifiers utilize the probability distribution function derived from the symbolic characterization of neural population activity, which is based on the Bandt-Pompe recipe.

Figure 42 – Comparison between experimental data and simulated data. The probabilistic cellular automata network model was simulated with 10^5 neurons and the control parameter σ is varied from 0.996 to 1.010 as depicted in the figure.

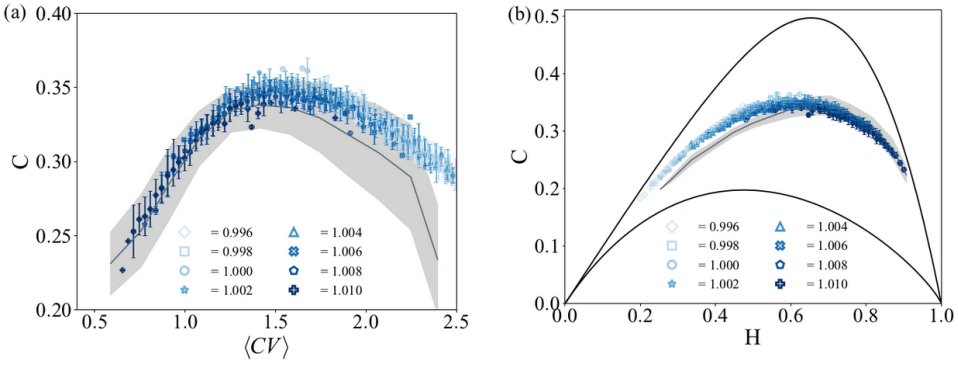

Source: LOTFI et al. (2021)

The findings revealed that complexity reaches its peak at intermediate levels of coefficient of variation (CV), coinciding with the levels associated with neuronal avalanches and maximum entropy models exhibiting criticality signatures. The same pattern was observed in simulated data generated by a probabilistic cellular automata network model. These results lend support to the hypothesis of criticality in the brain, introducing complexity as a significant signature of criticality in this context.

6 FINAL CONSIDERATIONS

The central objective of this thesis was to investigate the brain criticality hypothesis by employing diverse signatures of criticality (SCHUSTER, 2014) within datasets collected in our laboratory. These datasets were obtained from the visual cortex of anesthetized rats using highly dense electrode arrays (BUZSÁKI, 2004) and from that investigation four articles were published.

The initial study, published in the Physical Review Letters in 2019, yielded a pivotal result. It revealed a significant relationship between cortical states and neuronal avalanches, showing a distinct signature of criticality. Neuronal avalanches were studied based on brain states however, the scale invariance was not verified for awaken rats exploring novel objects (RIBEIRO et al., 2010). Neuronal avalanches were analyzed based on the level of variability in neuronal population activity. Notably, it was observed that higher levels of synchrony and asynchrony lacked scale invariance properties in the detected neuronal avalanches. In contrast, intermediate levels of variability exhibited scale invariance, as evidenced by power-law fits in the probability distributions of avalanche size and duration.

Another crucial discovery from this work was the scaling relation between the exponents calculated in the power-law fits for avalanche duration and size. From previous works, the scaling relation obtained over the neuronal activity of acute slices of rat cortex indicated scaling relations compatible with the direct percolation university class, but they were not seen in our data (BEGGS; PLENZ, 2003). However, the relationship encountered in our data held consistently across various datasets, encompassing experimental data from different animals and brain regions, as well as computational data from distinct models. This study suggested that the critical point may be linked to the transition between order (synchronized neurons) and disorder (asynchronous neurons), with the signatures of criticality being most prominent at intermediate levels of variability.

The subsequent article, published in the Physical Review E in 2020, explored another signature of criticality from the perspective of statistical criticality. The neuronal population was treated as a regular lattice of spins, analogous to the Ising model, where "spin-up" represented an active neuron and "spin-down" an inactive one. This approach led to the calculation of the energy function and the specific heat, with the expectation of a specific heat divergence at the critical point. The results demonstrated that the divergence of the specific heat was

more pronounced not only for larger groups of neurons (TKAČIK et al., 2015; MORA; DENY; MARRE, 2015) but for data segments with intermediate levels of variability in the neuronal population activity, and that was validated across seven datasets analyzed. The datasets used were the cortical spiking data of urethene-anesthetized rats and the recordings were made using 64-channels silicon probes inserted in the primary visual cortex.

The third study was focused on complexity measures applied in data segments with different cortical states. More specifically, the measure chosen was the Martín-Platino-Rosso (MPR) measure which is a combination of Jensen-Shannon divergence and Shannon entropy. The relationship between complexity and criticality has been investigated and the complexity is maximized for systems poised at critical points (TIMME et al., 2016). Impressively, the complexity measure was maximized for intermediate levels of variability in the neuronal population activity across all datasets analyzed.

The most intriguing aspect of the combined results from these three studies is that they converge around the same level of variability. This poses a fundamental question: if criticality signatures emerge, does the system operate near a critical point? (CHIALVO, 2010).This critical point is typically defined as the transition point between at least two phases. In this context, the hypothesis suggests that the order parameter governing this transition is the level of variability quantified by CV, with the extreme phases being highly synchronized and highly asynchronous states.

To explore this hypothesis further, a fourth project compared the results from the first project with artificial data generated by a spiking neuronal network model, manipulated by the control parameter g, the inhibition-to-excitation coupling ratio. Remarkably, the model could replicate the variability levels seen in the real data with slight variations in g. This could lead to the conclusion that neuronal self-organization around a critical point might occur independently of the cortical state. However, the challenge of detecting signatures of criticality for all variability levels remained due to inherent subsampling limitations in real neuronal data.

The experimental datasets were derived from the spiking activity of neurons in the primary visual cortex of anesthetized rats. The silicon probes used for recording featured high-density electrode arrays. Nevertheless, the methodology had spatial limitations, resulting in subsampling constraints that must be acknowledged in the interpretation of scientific questions and results.

Despite these technical constraints, the results obtained were significant, offering insights

into a wide range of research inquiries. The combined impact of the four articles is reflected in their more than 200 citations, underscoring their contribution to our understanding of the Brain Criticality hypothesis.

REFERENCES

ARBER, S.; COSTA, R. M. Connecting neuronal circuits for movement. *Science*, American Association for the Advancement of Science (AAAS), v. 360, n. 6396, p. 1403–1404, jun 29 2018. Available at: <http://dx.doi.org/10.1126/science.aat5994>.

BAK, P. *How nature works: the science of self-organized criticality*. [S.l.]: Springer Science & Business Media, 2013.

BAK, P.; TANG, C.; WIESENFELD, K. *Scale invariant spatial and temporal fluctuations in complex systems*. [S.l.]: Springer, 1988.

BAK, P.; TANG, C.; WIESENFELD, K. Self-organized criticality. *Physical review A*, APS, v. 38, n. 1, p. 364, 1988.

BANDT, C.; POMPE, B. Permutation entropy: a natural complexity measure for time series. *Physical review letters*, APS, v. 88, n. 17, p. 174102, 2002.

BEGGS, J. M.; PLENZ, D. Neuronal avalanches in neocortical circuits. *Journal of neuroscience*, Soc Neuroscience, v. 23, n. 35, p. 11167–11177, 2003.

BIALEK, W. *Biophysics: searching for principles*. [S.l.]: Princeton University Press, 2012.

BUZSÁKI, G. Large-scale recording of neuronal ensembles. *Nature neuroscience*, Nature Publishing Group US New York, v. 7, n. 5, p. 446–451, 2004.

CARHART-HARRIS, R. L.; MUTHUKUMARASWAMY, S.; ROSEMAN, L.; KAELEN, M.; DROOG, W.; MURPHY, K.; TAGLIAZUCCHI, E.; SCHENBERG, E. E.; NEST, T.; ORBAN, C. et al. Neural correlates of the lsd experience revealed by multimodal neuroimaging. *Proceedings of the National Academy of Sciences*, National Acad Sciences, v. 113, n. 17, p. 4853–4858, 2016.

CARVALHO, T. T.; FONTENELE, A. J.; GIRARDI-SCHAPPO, M.; FELICIANO, T.; AGUIAR, L. A.; SILVA, T. P.; VASCONCELOS, N. A. D.; CARELLI, P. V.; COPELLI, M. Subsampled directed-percolation models explain scaling relations experimentally observed in the brain. *Frontiers in neural circuits*, Frontiers Media SA, v. 14, p. 576727, 2021.

CAVAGNA, A.; CIMARELLI, A.; GIARDINA, I.; PARISI, G.; SANTAGATI, R.; STEFANINI, F.; VIALE, M. Scale-free correlations in starling flocks. *Proceedings of the National Academy of Sciences*, National Acad Sciences, v. 107, n. 26, p. 11865–11870, 2010.

CHALLET, D.; MARSILI, M. Criticality and market efficiency in a simple realistic model of the stock market. *Physical Review E*, APS, v. 68, n. 3, p. 036132, 2003.

CHIALVO, D. R. Emergent complex neural dynamics. *Nature physics*, Nature Publishing Group UK London, v. 6, n. 10, p. 744–750, 2010.

CLAUSET, A.; SHALIZI, C. R.; NEWMAN, M. E. Power-law distributions in empirical data. *SIAM review*, SIAM, v. 51, n. 4, p. 661–703, 2009.

CRUTCHFIELD, J. P. Between order and chaos. *Nature Physics*, Springer Science and Business Media LLC, v. 8, n. 1, p. 17–24, dec 22 2011.

CRUTCHFIELD, J. P.; YOUNG, K. Inferring statistical complexity. *Physical review letters*, APS, v. 63, n. 2, p. 105, 1989.

DEARNLEY, B.; DERVINIS, M.; SHAW, M.; OKUN, M. Stretching and squeezing of neuronal log firing rate distribution by psychedelic and intrinsic brain state transitions. *bioRxiv*, Cold Spring Harbor Laboratory, p. 2021–08, 2021.

DOUGLAS, R. J.; MARTIN, K. A. Neuronal circuits of the neocortex. *Annu. Rev. Neurosci.*, Annual Reviews, v. 27, p. 419–451, 2004.

DRONGELEN, W. V. *Signal processing for neuroscientists*. [S.l.]: Academic press, 2018.

ERIC, R. K.; JAMES, H. S.; THOMAS, M. J. *Principles of neural science. Vol. 4*. [S.l.]: New York: McGraw-hill, 2000.

FONTENELE, A. J.; VASCONCELOS, N. A. de; FELICIANO, T.; AGUIAR, L. A.; SOARES-CUNHA, C.; COIMBRA, B.; PORTA, L. D.; RIBEIRO, S.; RODRIGUES, A. J.; SOUSA, N. et al. Criticality between cortical states. *Physical review letters*, APS, v. 122, n. 20, p. 208101, 2019.

FRIEDMAN, N.; ITO, S.; BRINKMAN, B. A.; SHIMONO, M.; DEVILLE, R. L.; DAHMEN, K. A.; BEGGS, J. M.; BUTLER, T. C. Universal critical dynamics in high resolution neuronal avalanche data. *Physical review letters*, APS, v. 108, n. 20, p. 208102, 2012.

GARDELLA, C.; MARRE, O.; MORA, T. A tractable method for describing complex couplings between neurons and population rate. *eneuro*, Society for Neuroscience, v. 3, n. 4, 2016.

GIORBRAN, G. The Two Opposing Types of Order in Nature. 2005.

GIRARDI-SCHAPPO, M.; BROCHINI, L.; COSTA, A. A.; CARVALHO, T. T.; KINOUCHI, O. Synaptic balance due to homeostatically self-organized quasicritical dynamics. *Physical Review Research*, APS, v. 2, n. 1, p. 012042, 2020.

GIREESH, E. D.; PLENZ, D. Neuronal avalanches organize as nested theta-and beta/gamma-oscillations during development of cortical layer 2/3. *Proceedings of the National Academy of Sciences*, National Acad Sciences, v. 105, n. 21, p. 7576–7581, 2008.

GREINER, W.; NEISE, L.; STÖCKER, H. *Thermodynamics and statistical mechanics*. [S.l.]: Springer Science & Business Media, 2012.

GRIENBERGER, C.; KONNERTH, A. Imaging calcium in neurons. *Neuron*, Elsevier, v. 73, n. 5, p. 862–885, 2012.

HAI, A.; SHAPPIR, J.; SPIRA, M. E. In-cell recordings by extracellular microelectrodes. *Nature methods*, Nature Publishing Group US New York, v. 7, n. 3, p. 200–202, 2010.

HALL, E. L.; ROBSON, S. E.; MORRIS, P. G.; BROOKES, M. J. The relationship between meg and fmri. *Neuroimage*, Elsevier, v. 102, p. 80–91, 2014.

HARA, K.; HARRIS, R. A. The anesthetic mechanism of urethane: the effects on neurotransmitter-gated ion channels. *Anesthesia & Analgesia*, LWW, v. 94, n. 2, p. 313–318, 2002.

HARDSTONE, R.; POIL, S.-S.; SCHIAVONE, G.; JANSEN, R.; NIKULIN, V. V.; MANSVELDER, H. D.; LINKENKAER-HANSEN, K. Detrended fluctuation analysis: a scale-free view on neuronal oscillations. *Frontiers in physiology*, Frontiers Media SA, v. 3, p. 450, 2012.

HARRIS, K. D.; SHEPHERD, G. M. The neocortical circuit: themes and variations. *Nature neuroscience*, Nature Publishing Group US New York, v. 18, n. 2, p. 170–181, 2015.

HARRIS, K. D.; THIELE, A. Cortical state and attention. *Nature reviews neuroscience*, Nature Publishing Group UK London, v. 12, n. 9, p. 509–523, 2011.

HEEGER, D. J.; RESS, D. What does fmri tell us about neuronal activity? *Nature reviews neuroscience*, Nature Publishing Group UK London, v. 3, n. 2, p. 142–151, 2002.

HESSE, J.; GROSS, T. Self-organized criticality as a fundamental property of neural systems. *Frontiers in systems neuroscience*, Frontiers Media SA, v. 8, p. 166, 2014.

HODGKIN, A. L.; HUXLEY, A. F. Action potentials recorded from inside a nerve fibre. *Nature*, Nature Publishing Group UK London, v. 144, n. 3651, p. 710–711, 1939.

HONG, G.; LIEBER, C. M. Novel electrode technologies for neural recordings. *Nature Reviews Neuroscience*, Nature Publishing Group UK London, v. 20, n. 6, p. 330–345, 2019.

HOPFIELD, J. J. Neural networks and physical systems with emergent collective computational abilities. *Proceedings of the national academy of sciences*, National Acad Sciences, v. 79, n. 8, p. 2554–2558, 1982.

HU, S. Akaike information criterion. *Center for Research in Scientific Computation*, North Carolina State University Raleigh, NC, v. 93, p. 42, 2007.

HUBEL, D. H. Tungsten microelectrode for recording from single units. *Science*, American Association for the Advancement of Science, v. 125, n. 3247, p. 549–550, 1957.

IVANOVA, K.; AUSLOOS, M. Application of the detrended fluctuation analysis (dfa) method for describing cloud breaking. *Physica A: Statistical Mechanics and its Applications*, Elsevier, v. 274, n. 1-2, p. 349–354, 1999.

JOSPIN, M.; CAMINAL, P.; JENSEN, E. W.; LITVAN, H.; VALLVERDÚ, M.; STRUYS, M. M.; VEREECKE, H. E.; KAPLAN, D. T. Detrended fluctuation analysis of eeg as a measure of depth of anesthesia. *IEEE transactions on biomedical engineering*, IEEE, v. 54, n. 5, p. 840–846, 2007.

KADANOFF, L. P. Scaling and universality in statistical physics. *Physica A: Statistical Mechanics and its Applications*, Elsevier, v. 163, n. 1, p. 1–14, 1990.

KANDEL, E. R.; SQUIRE, L. R. Neuroscience: Breaking down scientific barriers to the study of brain and mind. *Science*, American Association for the Advancement of Science, v. 290, n. 5494, p. 1113–1120, 2000.

KASABOV, N. To spike or not to spike: A probabilistic spiking neuron model. *Neural Networks*, Elsevier, v. 23, n. 1, p. 16–19, 2010.

KELSO, J. Phase transitions and critical behavior in human bimanual coordination. *American Journal of Physiology-Regulatory, Integrative and Comparative Physiology*, v. 246, n. 6, p. R1000–R1004, 1984.

KHALUF, Y.; FERRANTE, E.; SIMOENS, P.; HUEPE, C. Scale invariance in natural and artificial collective systems: a review. *Journal of the royal society interface*, The Royal Society, v. 14, n. 136, p. 20170662, 2017.

KINOUCHI, O.; COPELLI, M. Optimal dynamical range of excitable networks at criticality. *Nature physics*, Nature Publishing Group UK London, v. 2, n. 5, p. 348–351, 2006.

KIRSCHSTEIN, T.; KÖHLING, R. What is the source of the eeg? *Clinical EEG and neuroscience*, SAGE Publications Sage CA: Los Angeles, CA, v. 40, n. 3, p. 146–149, 2009.

KOHN, A.; SMITH, M. A. Utah array extracellular recordings of spontaneous and visually evoked activity from anesthetized macaque primary visual cortex (v1). *CRCNS. org*, v. 10, p. K0NC5Z4X, 2016.

LEVINA, A.; PRIESEMANN, V. Subsampling scaling. *Nature communications*, Nature Publishing Group UK London, v. 8, n. 1, p. 15140, 2017.

LINKENKAER-HANSEN, K.; SMIT, D. J.; BARKIL, A.; BEIJSTERVELDT, T. E. van; BRUSSAARD, A. B.; BOOMSMA, D. I.; OOYEN, A. van; GEUS, E. J. de. Genetic contributions to long-range temporal correlations in ongoing oscillations. *Journal of Neuroscience*, Soc Neuroscience, v. 27, n. 50, p. 13882–13889, 2007.

LIU, X.; WARD, B. D.; BINDER, J. R.; LI, S.-J.; HUDETZ, A. G. Scale-free functional connectivity of the brain is maintained in anesthetized healthy participants but not in patients with unresponsive wakefulness syndrome. *PLoS One*, Public Library of Science San Francisco, USA, v. 9, n. 3, p. e92182, 2014.

LOTFI, N.; DAROONEH, A. The earthquakes network: the role of cell size. *The European Physical Journal B*, Springer, v. 85, p. 1–4, 2012.

LOTFI, N.; FELICIANO, T.; AGUIAR, L. A.; SILVA, T. P. L.; CARVALHO, T. T.; ROSSO, O. A.; COPELLI, M.; MATIAS, F. S.; CARELLI, P. V. Statistical complexity is maximized close to criticality in cortical dynamics. *Physical Review E*, APS, v. 103, n. 1, p. 012415, 2021.

LOTFI, N.; FONTENELE, A. J.; FELICIANO, T.; AGUIAR, L. A.; VASCONCELOS, N. A. de; SOARES-CUNHA, C.; COIMBRA, B.; RODRIGUES, A. J.; SOUSA, N.; COPELLI, M. et al. Signatures of brain criticality unveiled by maximum entropy analysis across cortical states. *Physical Review E*, APS, v. 102, n. 1, p. 012408, 2020.

LY, C.; GREB, A. C.; CAMERON, L. P.; WONG, J. M.; BARRAGAN, E. V.; WILSON, P. C.; BURBACH, K. F.; ZARANDI, S. S.; SOOD, A.; PADDY, M. R. et al. Psychedelics promote structural and functional neural plasticity. *Cell reports*, Elsevier, v. 23, n. 11, p. 3170–3182, 2018.

MADDOX, J. Order in the midst of chaos. *Nature*, Springer Science and Business Media LLC, v. 347, n. 6292, p. 421–421, 10 1990.

MAI, J. K.; MAJTANIK, M.; PAXINOS, G. *Atlas of the human brain*. [S.l.]: Academic Press, 2015.

MAREŠ, J.; VYŠATA, O.; PROCHÁZKA, A.; VALIŠ, M. Age-dependent complex noise fluctuations in the brain. *Physiological Measurement*, IOP Publishing, v. 34, n. 10, p. 1269, 2013.

MARTIN, M.; PLASTINO, A.; ROSSO, O. Generalized statistical complexity measures: Geometrical and analytical properties. *Physica A: Statistical Mechanics and its Applications*, Elsevier, v. 369, n. 2, p. 439–462, 2006.

MING, L.; VITÁNYI, P. M. Kolmogorov complexity and its applications. In: *Algorithms and complexity*. [S.l.]: Elsevier, 1990. p. 187–254.

MOCHOL, G.; MOCHOL, G.; HERMOSO-MENDIZABAL, A.; SAKATA, S.; HARRIS, K. D.; HARRIS, K. D. M.; ROCHA, J. de la. Stochastic transitions into silence cause noise correlations in cortical circuits. *Proceedings of the National Academy of Sciences of the United States of America*, 2015.

MORA, T.; DENY, S.; MARRE, O. Dynamical criticality in the collective activity of a population of retinal neurons. *Physical review letters*, APS, v. 114, n. 7, p. 078105, 2015.

MORGENSTERN, N. A.; BOURG, J.; PETREANU, L. Multilaminar networks of cortical neurons integrate common inputs from sensory thalamus. *Nature neuroscience*, Nature Publishing Group US New York, v. 19, n. 8, p. 1034–1040, 2016.

MUKAMEL, E. A.; PIRONDINI, E.; BABADI, B.; WONG, K. F. K.; PIERCE, E. T.; HARRELL, P. G.; WALSH, J. L.; SALAZAR-GOMEZ, A. F.; CASH, S. S.; ESKANDAR, E. N. et al. A transition in brain state during propofol-induced unconsciousness. *Journal of Neuroscience*, Soc Neuroscience, v. 34, n. 3, p. 839–845, 2014.

MUNOZ, M. A. Colloquium: Criticality and dynamical scaling in living systems. *Reviews of Modern Physics*, APS, v. 90, n. 3, p. 031001, 2018.

MYUNG, I. J. Tutorial on maximum likelihood estimation. *Journal of mathematical Psychology*, Elsevier, v. 47, n. 1, p. 90–100, 2003.

NORTHCUTT, R. G.; KAAS, J. H. The emergence and evolution of mammalian neocortex. *Trends in neurosciences*, Elsevier Current Trends, v. 18, n. 9, p. 373–379, 1995.

PARASURAM, H.; NAIR, B.; D'ANGELO, E.; HINES, M.; NALDI, G.; DIWAKAR, S. Computational modeling of single neuron extracellular electric potentials and network local field potentials using lfpsim. *Frontiers in Computational Neuroscience*, Frontiers Media SA, v. 10, p. 65, 2016.

PARISI, G. Statistical physics and biology. *Physics World*, IOP Publishing, v. 6, n. 9, p. 42, 1993.

PAXINOS, G.; WATSON, C. *The rat brain in stereotaxic coordinates: hard cover edition*. [S.l.]: Elsevier, 2006.

PETERMANN, T.; THIAGARAJAN, T. C.; LEBEDEV, M. A.; NICOLELIS, M. A.; CHIALVO, D. R.; PLENZ, D. Spontaneous cortical activity in awake monkeys composed of neuronal avalanches. *Proceedings of the National Academy of Sciences*, National Acad Sciences, v. 106, n. 37, p. 15921–15926, 2009.

POULET, J. F.; CROCHET, S. The cortical states of wakefulness. *Frontiers in systems neuroscience*, Frontiers Media SA, v. 12, p. 64, 2019.

POULET, J. F.; FERNANDEZ, L. M.; CROCHET, S.; PETERSEN, C. C. Thalamic control of cortical states. *Nature neuroscience*, Nature Publishing Group US New York, v. 15, n. 3, p. 370–372, 2012.

PRIESEMANN, V.; VALDERRAMA, M.; WIBRAL, M.; QUYEN, M. L. V. Neuronal avalanches differ from wakefulness to deep sleep–evidence from intracranial depth recordings in humans. *PLoS computational biology*, Public Library of Science San Francisco, USA, v. 9, n. 3, p. e1002985, 2013.

PRIESEMANN, V.; WIBRAL, M.; VALDERRAMA, M.; PRÖPPER, R.; QUYEN, M. L. V.; GEISEL, T.; TRIESCH, J.; NIKOLIĆ, D.; MUNK, M. H. Spike avalanches in vivo suggest a driven, slightly subcritical brain state. *Frontiers in systems neuroscience*, Frontiers Media SA, v. 8, p. 108, 2014.

REY, H. G.; PEDREIRA, C.; QUIROGA, R. Q. Past, present and future of spike sorting techniques. *Brain research bulletin*, Elsevier, v. 119, p. 106–117, 2015.

REZAEI, S.; DAROONEH, A. H.; LOTFI, N.; ASAADI, N. The earthquakes network: Retrieving the empirical seismological laws. *Physica A: Statistical Mechanics and its Applications*, Elsevier, v. 471, p. 80–87, 2017.

RIBEIRO, T. L.; COPELLI, M.; CAIXETA, F.; BELCHIOR, H.; CHIALVO, D. R.; NICOLELIS, M. A.; RIBEIRO, S. Spike avalanches exhibit universal dynamics across the sleep-wake cycle. *PloS one*, Public Library of Science San Francisco, USA, v. 5, n. 11, p. e14129, 2010.

ROSSANT, C.; KADIR, S. N.; GOODMAN, D. F.; SCHULMAN, J.; HUNTER, M. L.; SALEEM, A. B.; GROSMARK, A.; BELLUSCIO, M.; DENFIELD, G. H.; ECKER, A. S. et al. Spike sorting for large, dense electrode arrays. *Nature neuroscience*, Nature Publishing Group US New York, v. 19, n. 4, p. 634–641, 2016.

SACHDEV, S.; MA, H. U. C. Quantum phase transitions. 2011.

SACKS, O. *Alucinações musicais: relatos sobre a música e o cérebro*. [S.l.]: Editora Companhia das Letras, 2007.

SAKATA, S.; HARRIS, K. D. Laminar structure of spontaneous and sensory-evoked population activity in auditory cortex. *Neuron*, Elsevier, v. 64, n. 3, p. 404–418, 2009.

SCHNEIDMAN, E.; BERRY, M. J.; SEGEV, R.; BIALEK, W. Weak pairwise correlations imply strongly correlated network states in a neural population. *Nature*, 2006.

SCHUSTER, H. G. *Criticality in neural systems*. [S.l.]: John Wiley & Sons, 2014.

SENZAI, Y.; FERNANDEZ-RUIZ, A.; BUZSÁKI, G. Layer-specific physiological features and interlaminar interactions in the primary visual cortex of the mouse. *Neuron*, Elsevier, v. 101, n. 3, p. 500–513, 2019.

SETHNA, J. P.; DAHMEN, K. A.; MYERS, C. R. Crackling noise. *Nature*, Nature Publishing Group UK London, v. 410, n. 6825, p. 242–250, 2001.

SHEW, W. L.; CLAWSON, W. P.; POBST, J.; KARIMIPANAH, Y.; WRIGHT, N. C.; WESSEL, R. Adaptation to sensory input tunes visual cortex to criticality. *Nature Physics*, Nature Publishing Group UK London, v. 11, n. 8, p. 659–663, 2015.

SHEW, W. L.; PLENZ, D. The functional benefits of criticality in the cortex. *The neuroscientist*, SAGE Publications Sage CA: Los Angeles, CA, v. 19, n. 1, p. 88–100, 2013.

SHEW, W. L.; YANG, H.; PETERMANN, T.; ROY, R.; PLENZ, D. Neuronal avalanches imply maximum dynamic range in cortical networks at criticality. *Journal of neuroscience*, Soc Neuroscience, v. 29, n. 49, p. 15595–15600, 2009.

SHEW, W. L.; YANG, H.; YU, S.; ROY, R.; PLENZ, D. Information capacity and transmission are maximized in balanced cortical networks with neuronal avalanches. *Journal of neuroscience*, Soc Neuroscience, v. 31, n. 1, p. 55–63, 2011.

SIEGLE, J. H.; LÓPEZ, A. C.; PATEL, Y. A.; ABRAMOV, K.; OHAYON, S.; VOIGTS, J. Open ephys: an open-source, plugin-based platform for multichannel electrophysiology. *Journal of neural engineering*, IOP Publishing, v. 14, n. 4, p. 045003, 2017.

SMITH, R. L.; IKEDA, A. K.; ROWLEY, C. A.; KHANDHADIA, A.; GORBACH, A. M.; CHIMALIZENI, Y.; TAYLOR, T. E.; SEYDEL, K.; ACKERMAN, H. C. Increased brain microvascular hemoglobin concentrations in children with cerebral malaria. *Science Translational Medicine*, American Association for the Advancement of Science, v. 15, n. 713, p. eadh4293, 2023.

SOMOGYI, P.; TAMAS, G.; LUJAN, R.; BUHL, E. H. Salient features of synaptic organisation in the cerebral cortex. *Brain research reviews*, Elsevier, v. 26, n. 2-3, p. 113–135, 1998.

SPORNS, O. Contributions and challenges for network models in cognitive neuroscience. *Nature neuroscience*, Nature Publishing Group US New York, v. 17, n. 5, p. 652–660, 2014.

SQUIRE, L.; BERG, D.; BLOOM, F. E.; LAC, S. D.; GHOSH, A.; SPITZER, N. C. *Fundamental neuroscience*. [S.l.]: Academic press, 2012.

STANLEY, H. E. *Phase transitions and critical phenomena*. [S.l.]: Clarendon Press, Oxford, 1971.

STEVENSON, I. H.; KORDING, K. P. How advances in neural recording affect data analysis. *Nature neuroscience*, Nature Publishing Group US New York, v. 14, n. 2, p. 139–142, 2011.

SUR, M.; RUBENSTEIN, J. L. Patterning and plasticity of the cerebral cortex. *Science*, American Association for the Advancement of Science, v. 310, n. 5749, p. 805–810, 2005.

TAGLIAZUCCHI, E.; CARHART-HARRIS, R.; LEECH, R.; NUTT, D.; CHIALVO, D. R. Enhanced repertoire of brain dynamical states during the psychedelic experience. *Human brain mapping*, Wiley Online Library, v. 35, n. 11, p. 5442–5456, 2014.

TALKNER, P.; WEBER, R. O. Power spectrum and detrended fluctuation analysis: Application to daily temperatures. *Physical Review E*, APS, v. 62, n. 1, p. 150, 2000.

TANG, H.; SCHRIMPF, M.; LOTTER, W.; MOERMAN, C.; PAREDES, A.; CARO, J. O.; HARDESTY, W.; COX, D.; KREIMAN, G. Recurrent computations for visual pattern completion. *Proceedings of the National Academy of Sciences*, National Acad Sciences, v. 115, n. 35, p. 8835–8840, 2018.

TEETER, C.; IYER, R.; MENON, V.; GOUWENS, N.; FENG, D.; BERG, J.; SZAFER, A.; CAIN, N.; ZENG, H.; HAWRYLYCZ, M. et al. Generalized leaky integrate-and-fire models classify multiple neuron types. *Nature communications*, Nature Publishing Group UK London, v. 9, n. 1, p. 709, 2018.

TIMME, N. M.; MARSHALL, N. J.; BENNETT, N.; RIPP, M.; LAUTZENHISER, E.; BEGGS, J. M. Criticality maximizes complexity in neural tissue. *Frontiers in physiology*, Frontiers Media SA, v. 7, p. 425, 2016.

TINKER, J.; VELAZQUEZ, J. L. P. Power law scaling in synchronization of brain signals depends on cognitive load. *Frontiers in systems neuroscience*, Frontiers Media SA, v. 8, p. 73, 2014.

TKAČIK, G.; MARRE, O.; AMODEI, D.; SCHNEIDMAN, E.; BIALEK, W.; BERRY, M. J. Searching for collective behavior in a large network of sensory neurons. *PLoS computational biology*, Public Library of Science San Francisco, USA, v. 10, n. 1, p. e1003408, 2014.

TKAČIK, G.; MARRE, O.; MORA, T.; AMODEI, D.; II, M. J. B.; BIALEK, W. The simplest maximum entropy model for collective behavior in a neural network. *Journal of Statistical Mechanics: Theory and Experiment*, IOP Publishing, v. 2013, n. 03, p. P03011, 2013.

TKAČIK, G.; MORA, T.; MARRE, O.; AMODEI, D.; PALMER, S. E.; BERRY, M. J.; BIALEK, W. Thermodynamics and signatures of criticality in a network of neurons. *Proceedings of the National Academy of Sciences*, National Acad Sciences, v. 112, n. 37, p. 11508–11513, 2015.

TORQUATO, S.; TORQUATO, S. Statistical mechanics of many-particle systems. *Random Heterogeneous Materials: Microstructure and Macroscopic Properties*, Springer, p. 59–95, 2002.

TOUSSAINT, M.; SEELEN, W. von. Complex adaptation and system structure. *BioSystems*, Elsevier, v. 90, n. 3, p. 769–782, 2007.

VOLLENWEIDER, F. X.; KOMETER, M. The neurobiology of psychedelic drugs: implications for the treatment of mood disorders. *Nature Reviews Neuroscience*, Nature Publishing Group UK London, v. 11, n. 9, p. 642–651, 2010.

VYŠATA, O.; PROCHÁZKA, A.; MAREŠ, J.; RUSINA, R.; PAZDERA, L.; VALIŠ, M.; KUKAL, J. Change in the characteristics of eeg color noise in alzheimer's disease. *Clinical EEG and neuroscience*, Sage Publications Sage CA: Los Angeles, CA, v. 45, n. 3, p. 147–151, 2014.

WHEATLEY, M. Searching for order in an orderly world: A poetic for post-machine-age managers. *Journal of Management Inquiry*, Sage Publications Sage CA: Thousand Oaks, CA, v. 1, n. 4, p. 337–342, 1992.

WOOLSEY, T. A.; LOOS, H. Van der. The structural organization of layer iv in the somatosensory region (si) of mouse cerebral cortex: the description of a cortical field composed of discrete cytoarchitectonic units. *Brain research*, Elsevier, v. 17, n. 2, p. 205–242, 1970.

WORRELL, G. A.; CRANSTOUN, S. D.; ECHAUZ, J.; LITT, B. Evidence for self-organized criticality in human epileptic hippocampus. *Neuroreport*, LWW, v. 13, n. 16, p. 2017–2021, 2002.

YAGHOUBI, M.; GRAAF, T. de; ORLANDI, J. G.; GIROTTO, F.; COLICOS, M. A.; DAVIDSEN, J. Neuronal avalanche dynamics indicates different universality classes in neuronal cultures. *Scientific reports*, Nature Publishing Group UK London, v. 8, n. 1, p. 3417, 2018.

YEOMANS, J. M. *Statistical mechanics of phase transitions*. [S.l.]: Clarendon Press, 1992.

YIZHAR, O.; FENNO, L. E.; DAVIDSON, T. J.; MOGRI, M.; DEISSEROTH, K. Optogenetics in neural systems. *Neuron*, Elsevier, v. 71, n. 1, p. 9–34, 2011.

ZIMMERN, V. Why brain criticality is clinically relevant: a scoping review. *Frontiers in neural circuits*, Frontiers, v. 14, p. 54, 2020.

APPENDIX A – RECORDED DATA

A.1 CV TEMPORAL SERIES

The coefficient of variability, CV, is a measure of how a spike temporal series is variable concerning its mean. It is expected, for this specific experiment protocol that the CV calculated at every 10 seconds presents a great variability itself. This could be seen in 43.

Figure 43 – CV calculated during 9000s of the recording at every 10 seconds for the 5 datasets. On the right of each CV plot, there is a CV value distribution. The y-axis is shared between the CV temporal series and the histogram.

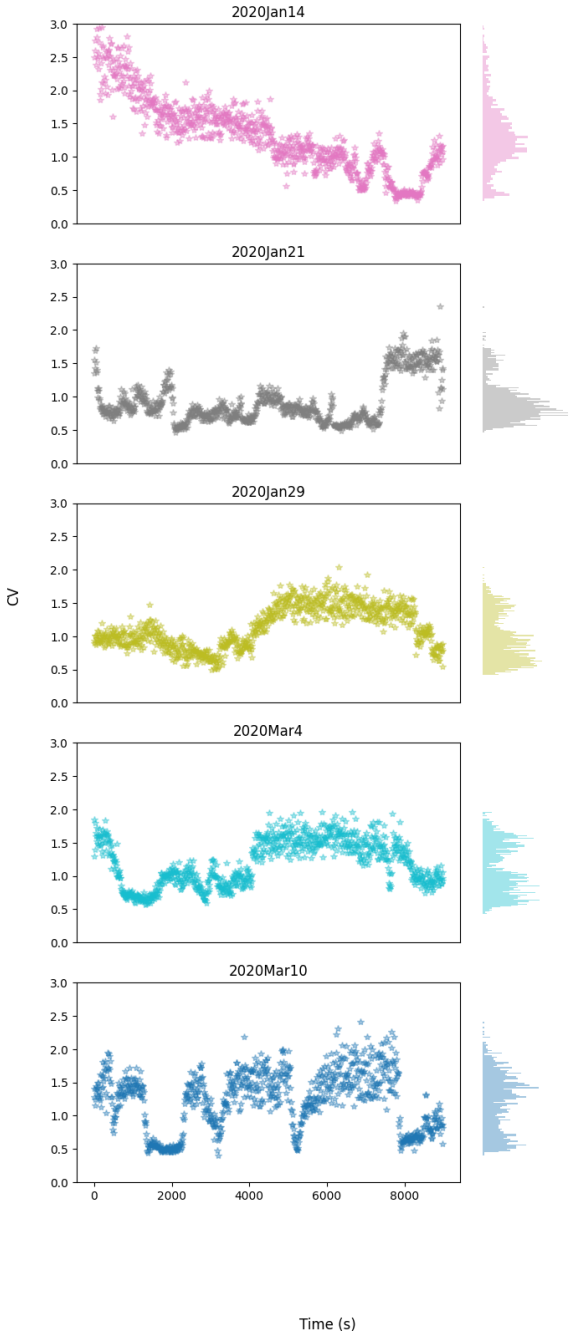

Source: The author (2023)

A.2 NUMBER OF NEURONS, RECORDING DURATION, NUMBER OF SPIKES

Table 1 – Table displaying the number of Single Unit Activity clusters and the Multi Unit Activity clusters for each dataset. It is shown in minutes the duration of each recording.

Experiment	SUA	MUA	Spikes	Duration (min)
2020Jan14	76.0	147.0	10176745.0	190.085404
2020Jan21	88.0	84.0	7716918.0	195.014969
2020Jan29	76.0	291.0	27270750.0	243.558400
2020Mar4	73.0	211.0	12908127.0	186.954667
2020Mar10	144.0	168.0	5637017.0	180.286720

Source: The author (2023)

Figure 44 – Neurons Firing rate distribution for each recording.

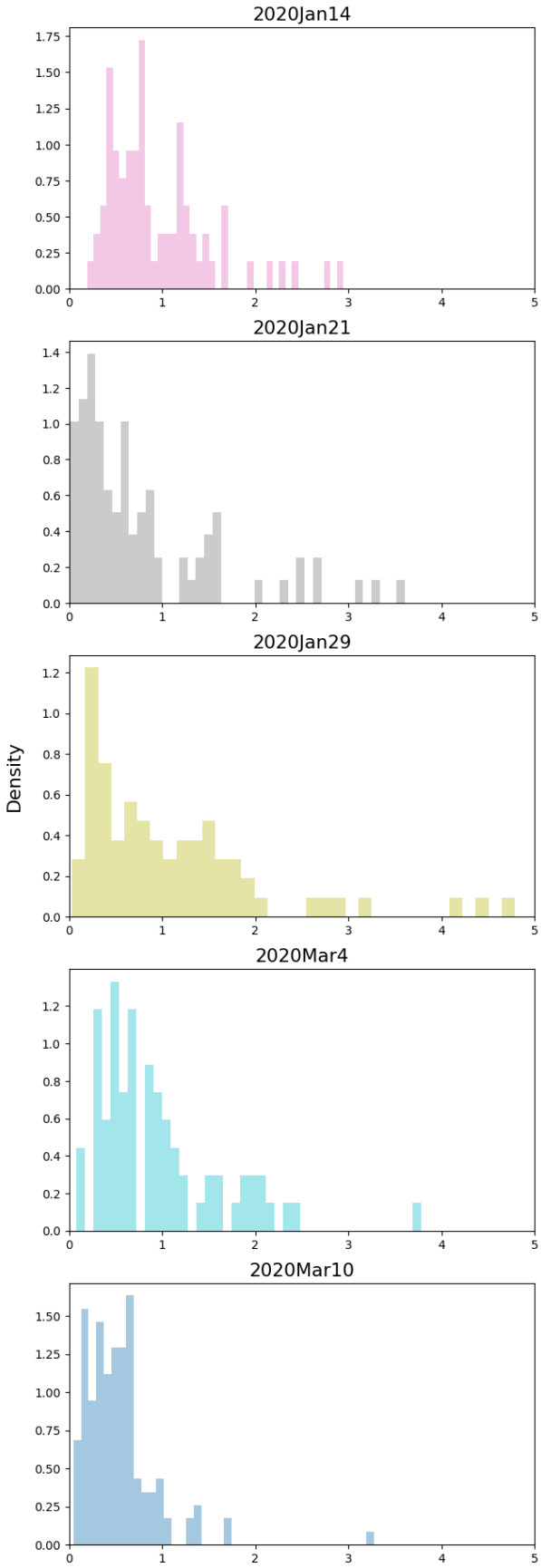

A.3 WAVEFORMS EXAMPLES

Figure 45 – More active cluster waveform example for each shank. The experiment was performed on January 14th 2020.

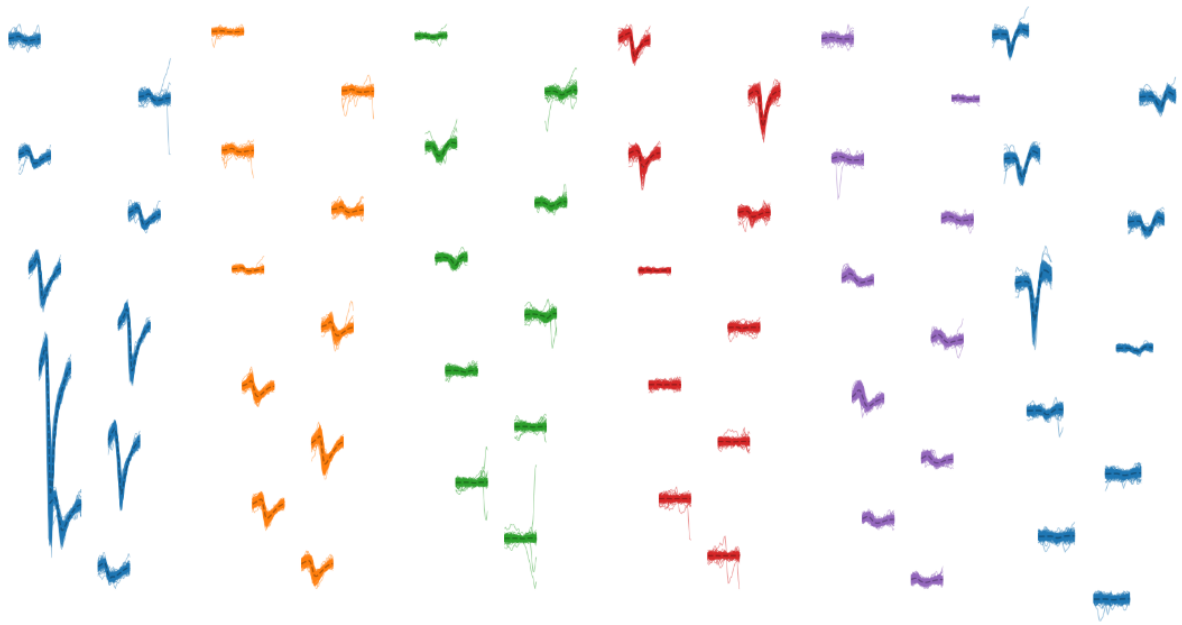

Source: The author (2023)

Figure 46 – More active cluster waveform example for each shank. The experiment was performed on January 21st 2020.

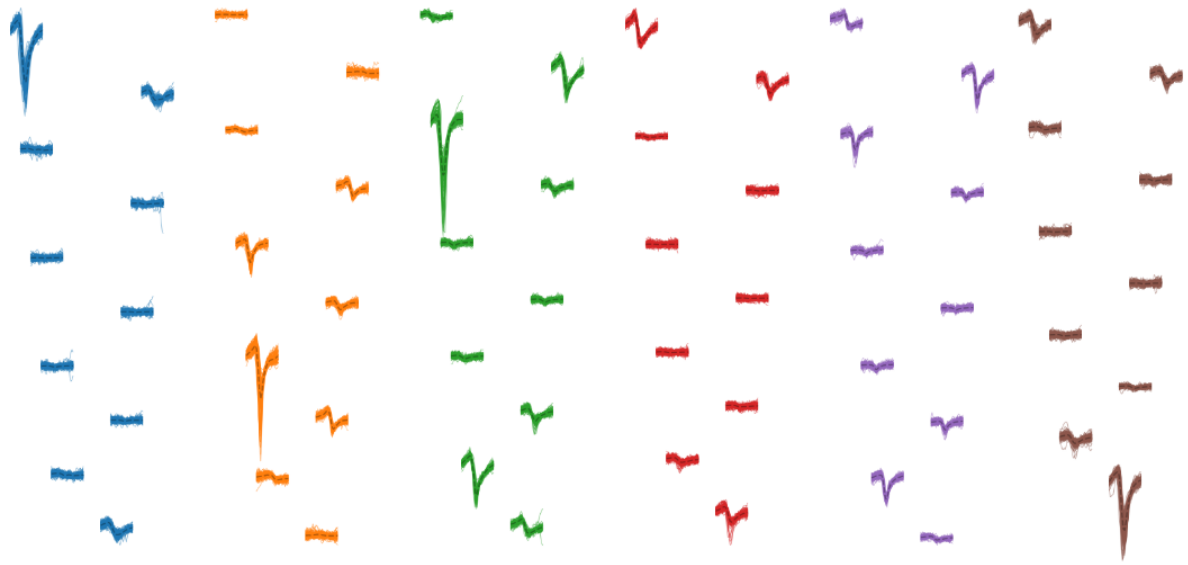

Source: The author (2023)

Figure 47 – More active cluster waveform example for each shank. The experiment was performed on January 29th 2020.

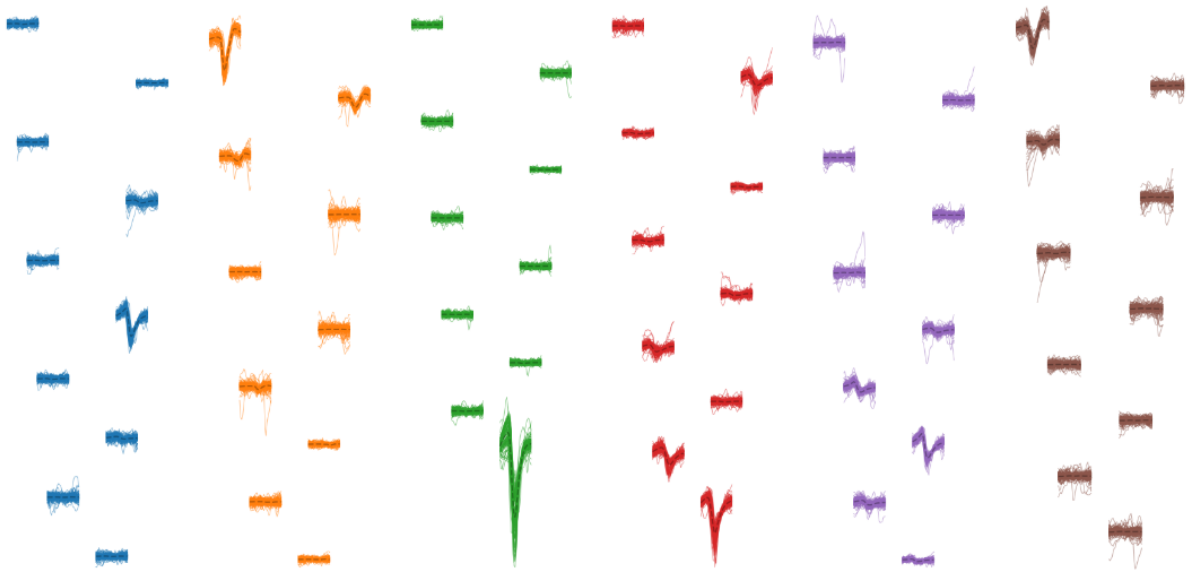

Source: The author (2023)

Figure 48 – More active cluster waveform example for each shank. The experiment was performed on March 4th 2020.

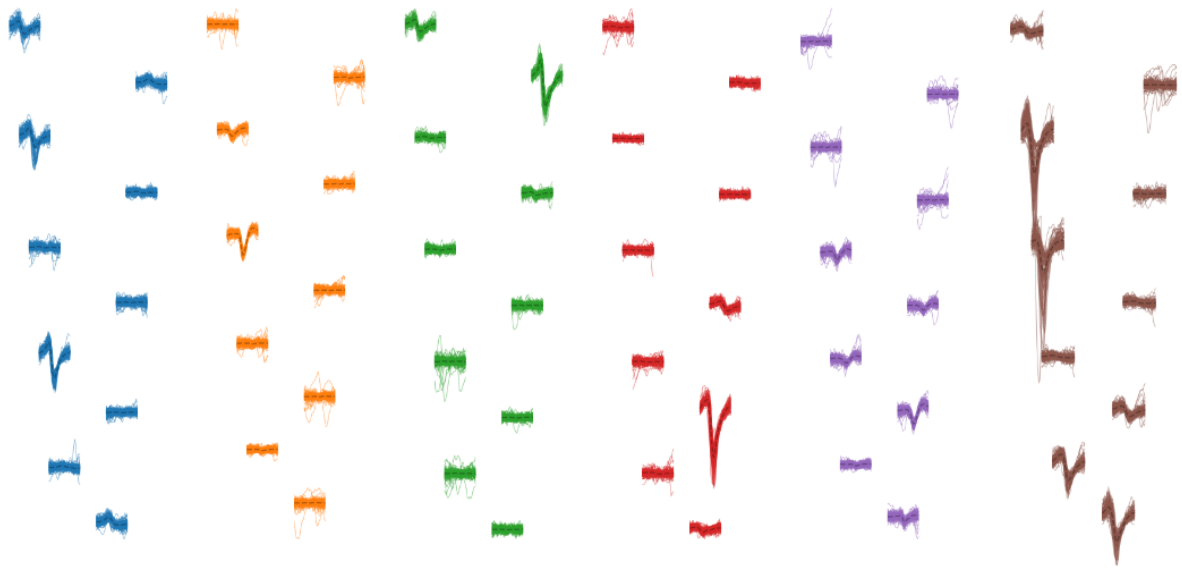

Source: The author (2023)

Figure 49 – More active cluster waveform example for each shank. The experiment was performed on March 10th 2020.

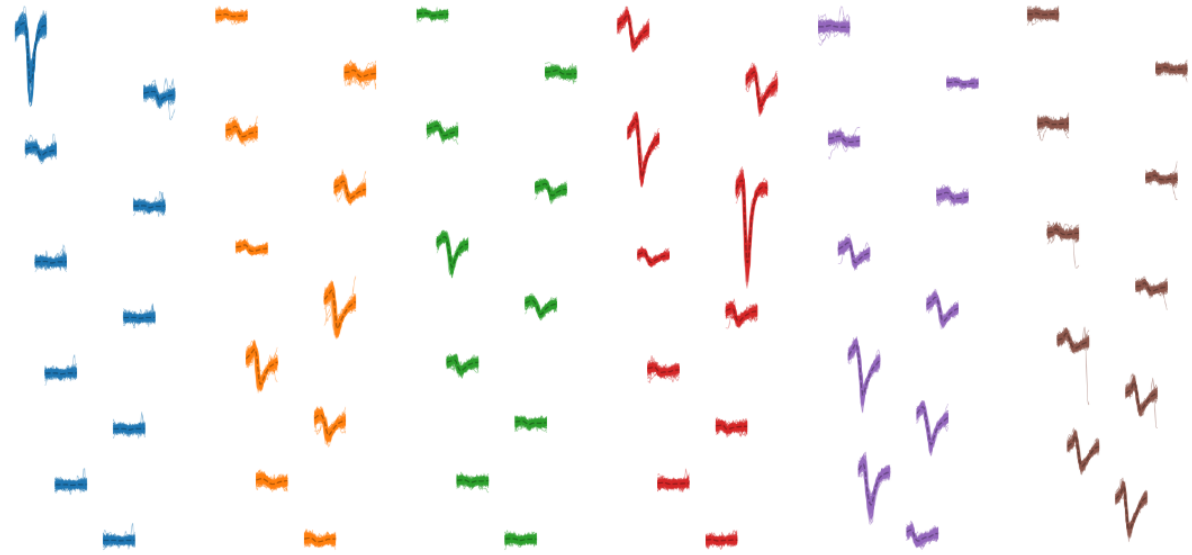

Source: The author (2023)

A.4 IN RASTER PLOT, WE TRUST

Figure 50 – 4 seconds of spike activity displayed as a raster plot for three different levels of variability. Each color is a different shank. This experiment was performed on January 14th 2020

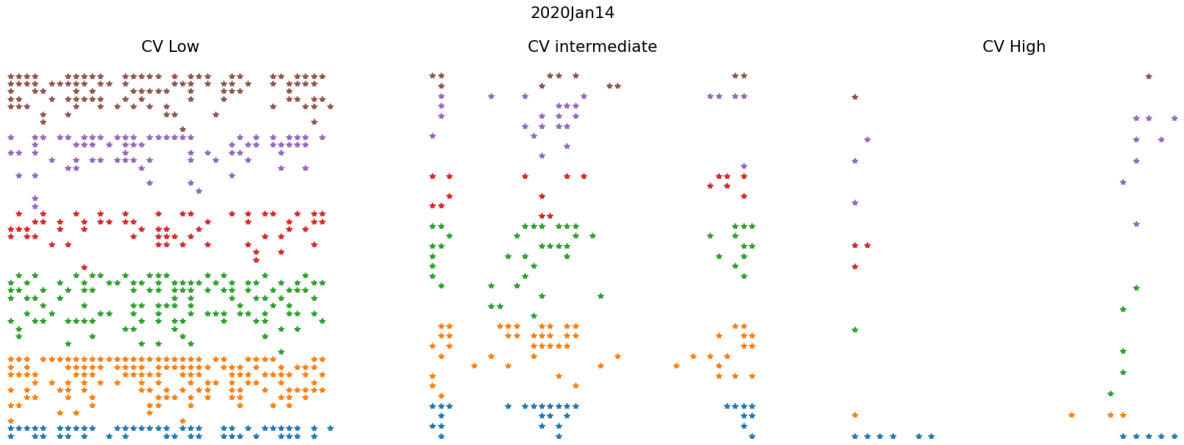

Source: The author (2023)

Figure 51 – 4 seconds of spike activity displayed as a raster plot for three different levels of variability. Each color is a different shank. This experiment was performed on January 21st 2020

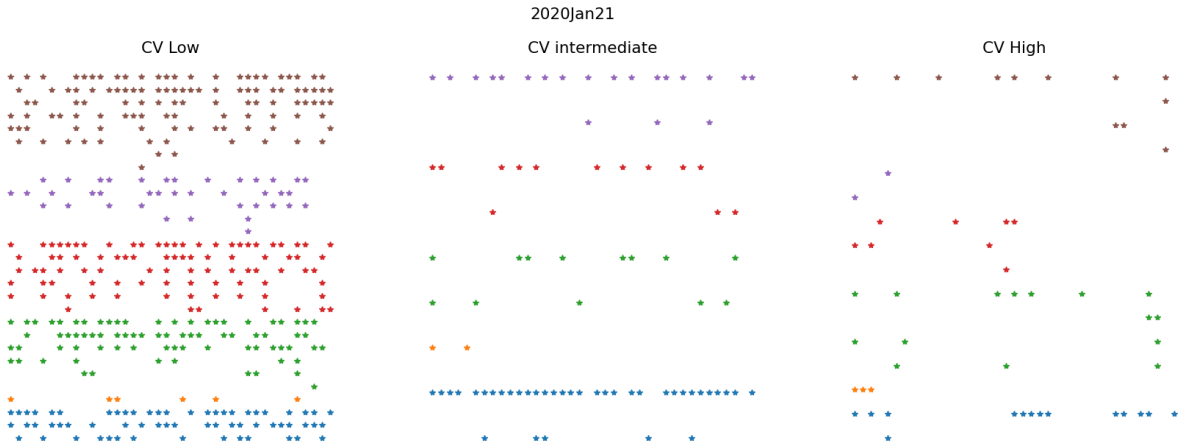

Source: The author (2023)

Figure 52 – 4 seconds of spike activity displayed as a raster plot for three different levels of variability. Each color is a different shank. This experiment was performed on January 29th 2020

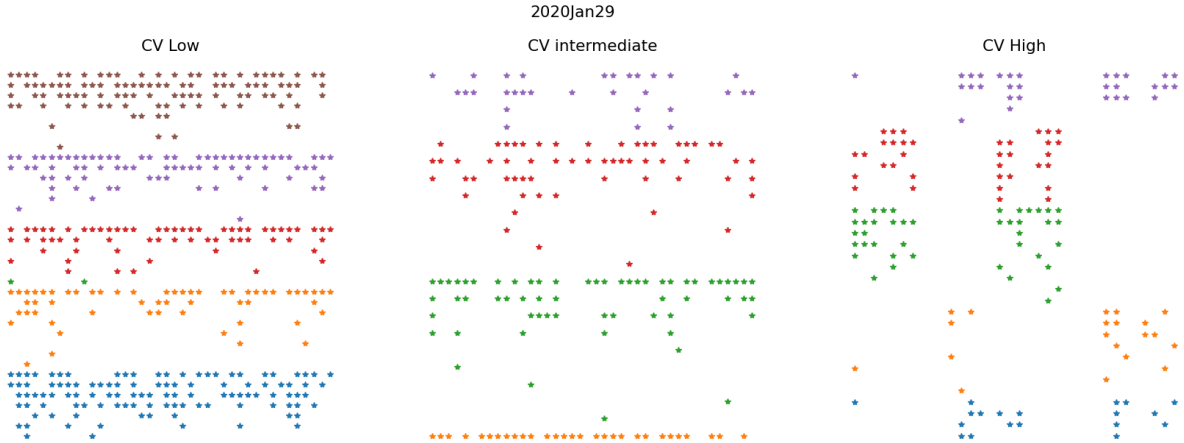

Source: The author (2023)

Figure 53 – 4 seconds of spike activity displayed as a raster plot for three different levels of variability. Each color is a different shank. This experiment was performed on March 4th 2020

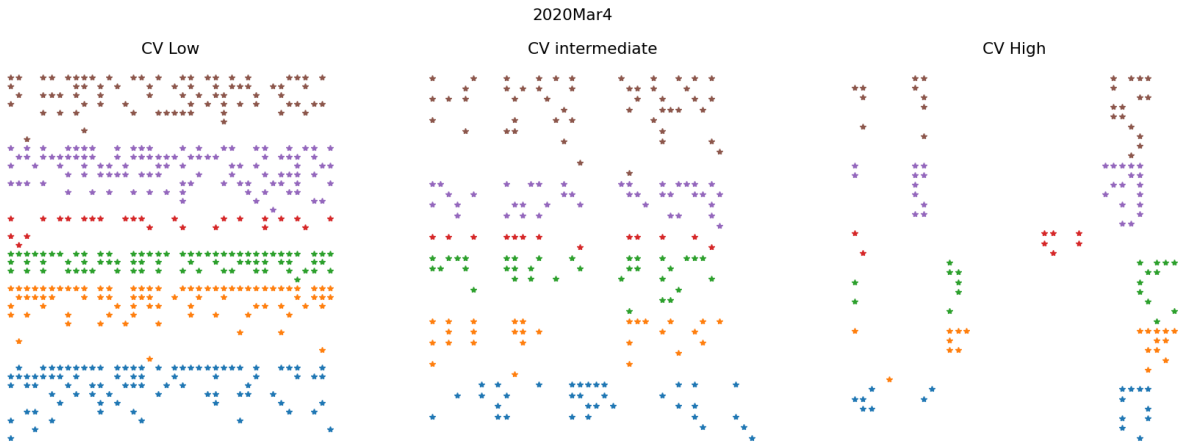

Source: The author (2023)

Figure 54 – 4 seconds of spike activity displayed as a raster plot for three different levels of variability. Each color is a different shank. This experiment was performed on March 10th 2020

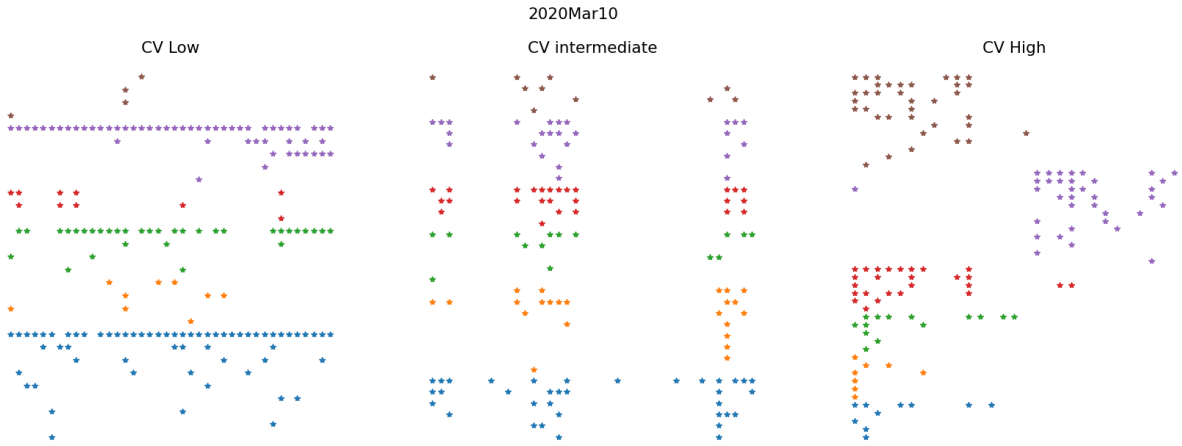

Source: The author (2023)

A.5 RAW DATA

Figure 55 – 4 seconds of raw data acquired. Each color represents 10 channels of a different shank. Each column represents 4 seconds of different levels of CV. The experiment was performed on January 14th 2020.

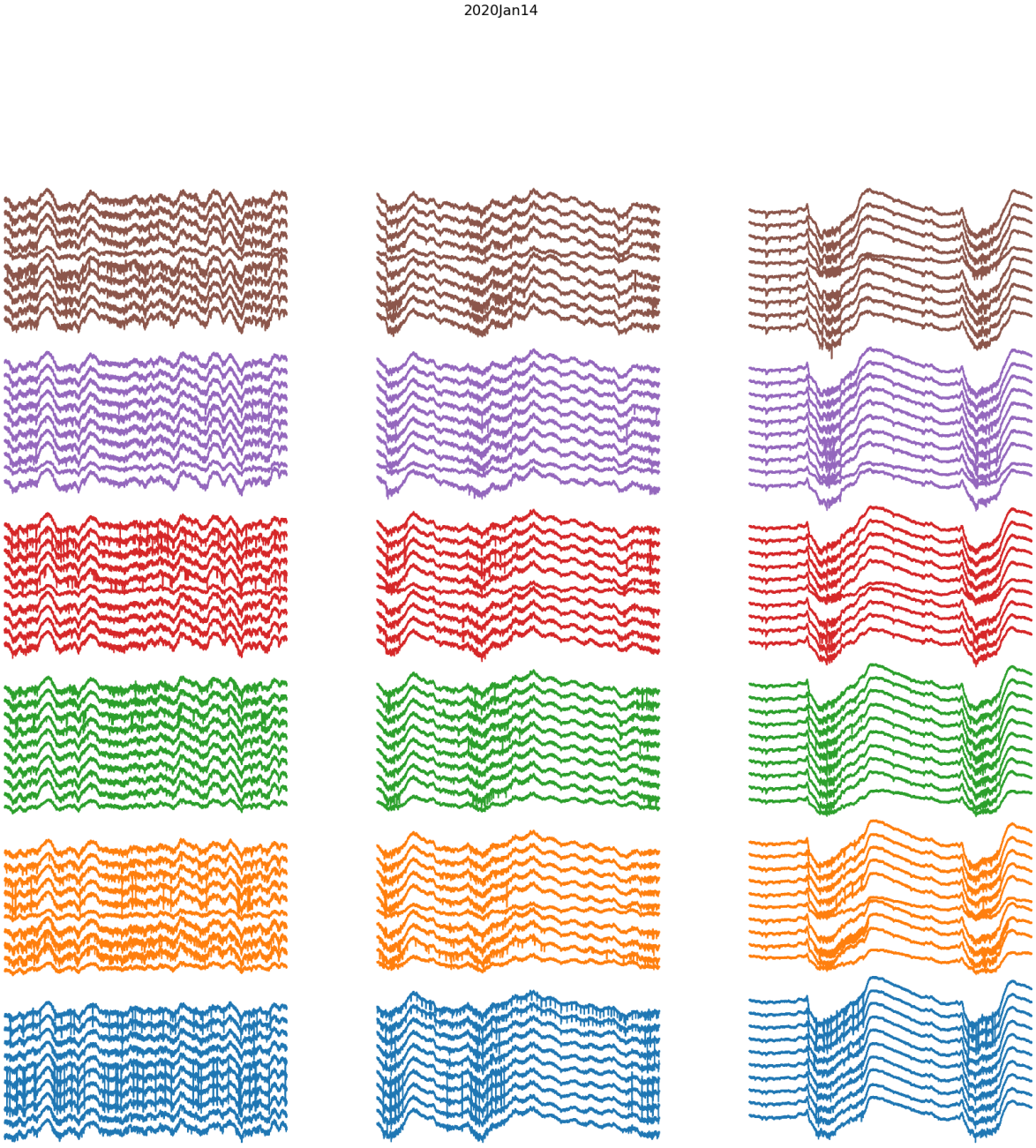

Source: The author (2023)

Figure 56 – 4 seconds of raw data acquired. Each color represents 10 channels of a different shank. Each column represents 4 seconds of different levels of CV. The experiment was performed on January 21st 2020.

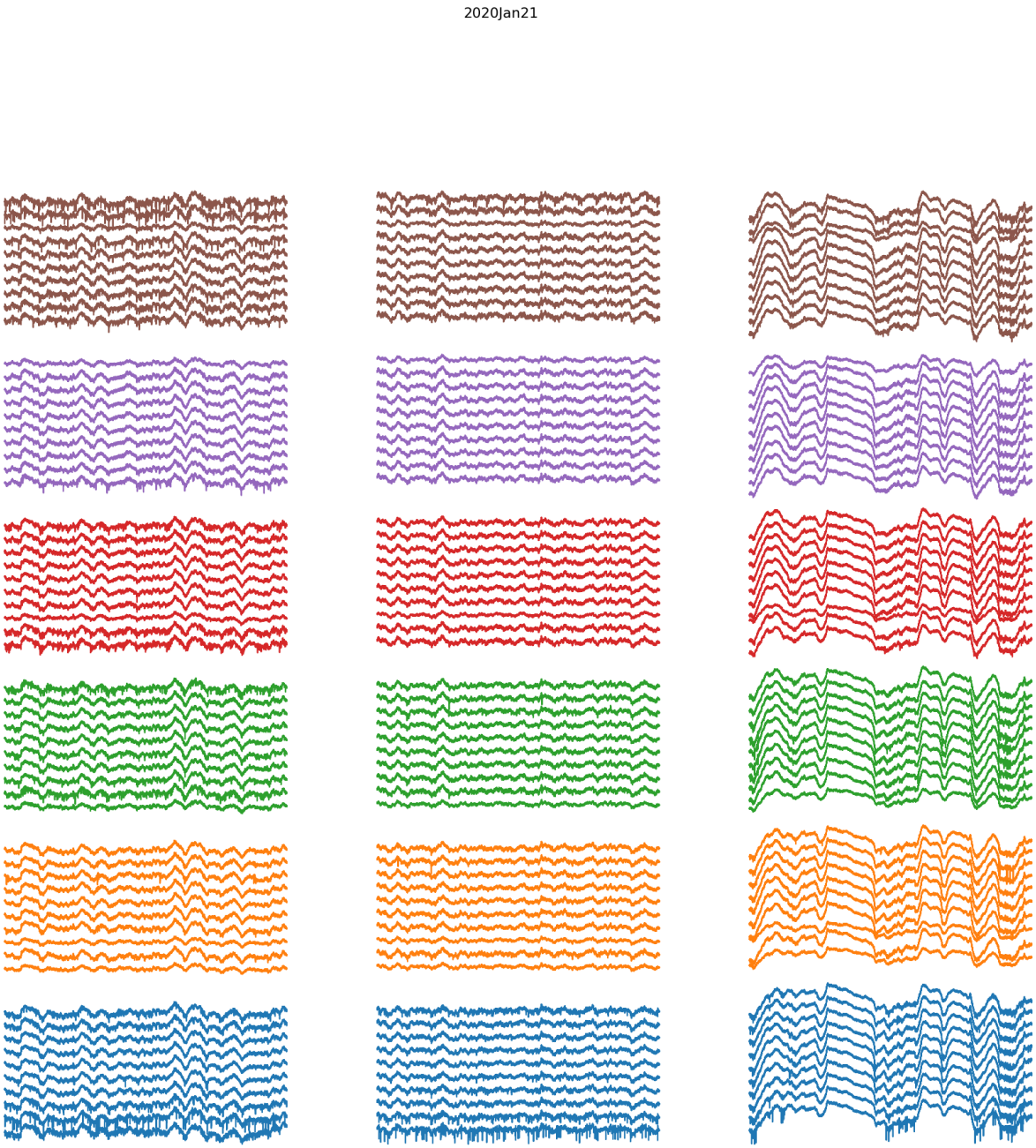

Source: The author (2023)

Figure 57 – 4 seconds of raw data acquired. Each color represents 10 channels of a different shank. Each column represents 4 seconds of different levels of CV. The experiment was performed on January 29th 2020.

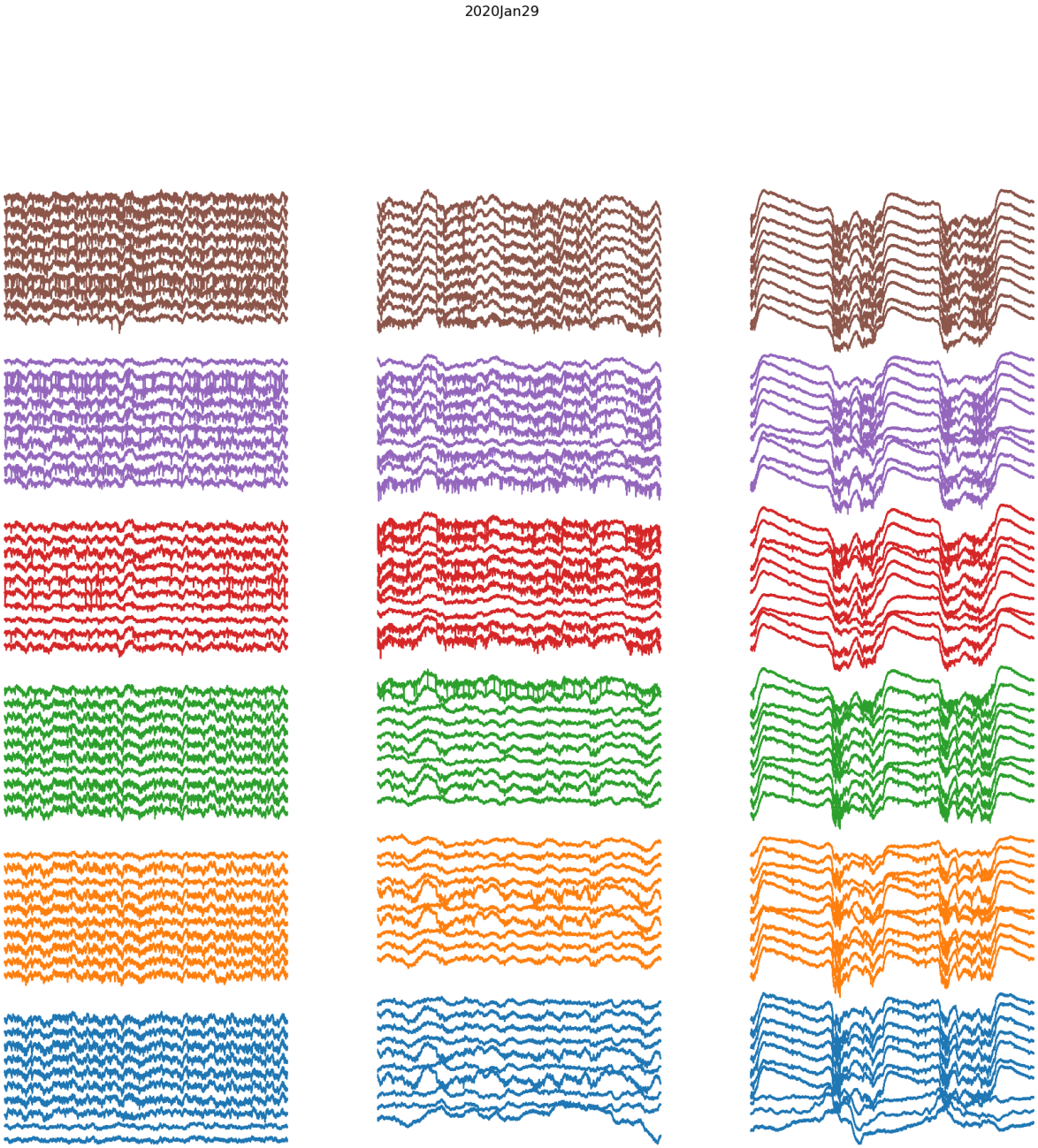

Source: The author (2023)

Figure 58 – 4 seconds of raw data acquired. Each color represents 10 channels of a different shank. Each column represents 4 seconds of different levels of CV. The experiment was performed on March 4th 2020.

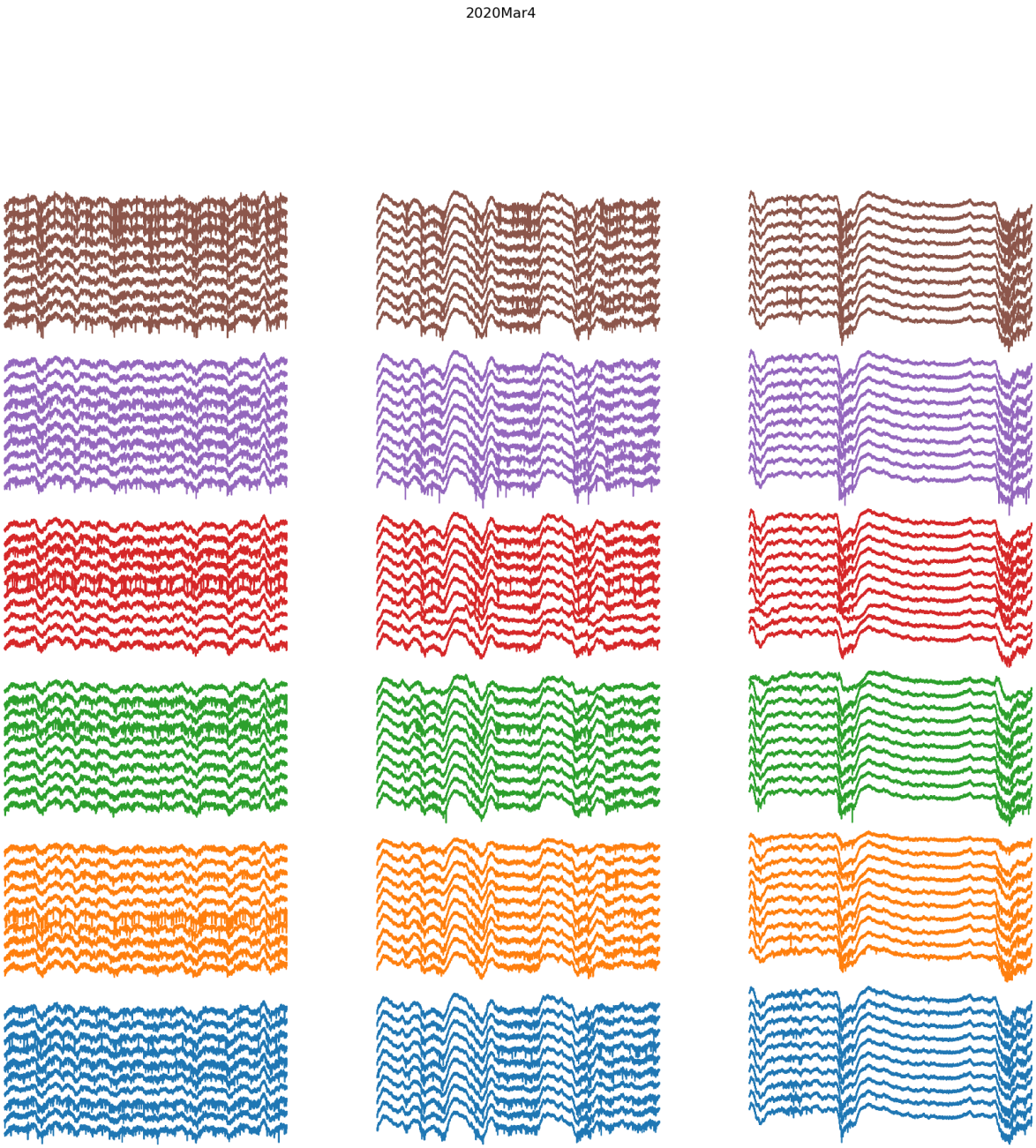

Source: The author (2023)

Figure 59 – 4 seconds of raw data acquired. Each color represents 10 channels of a different shank. Each column represents 4 seconds of different levels of CV. The experiment was performed on March 10th 2020.

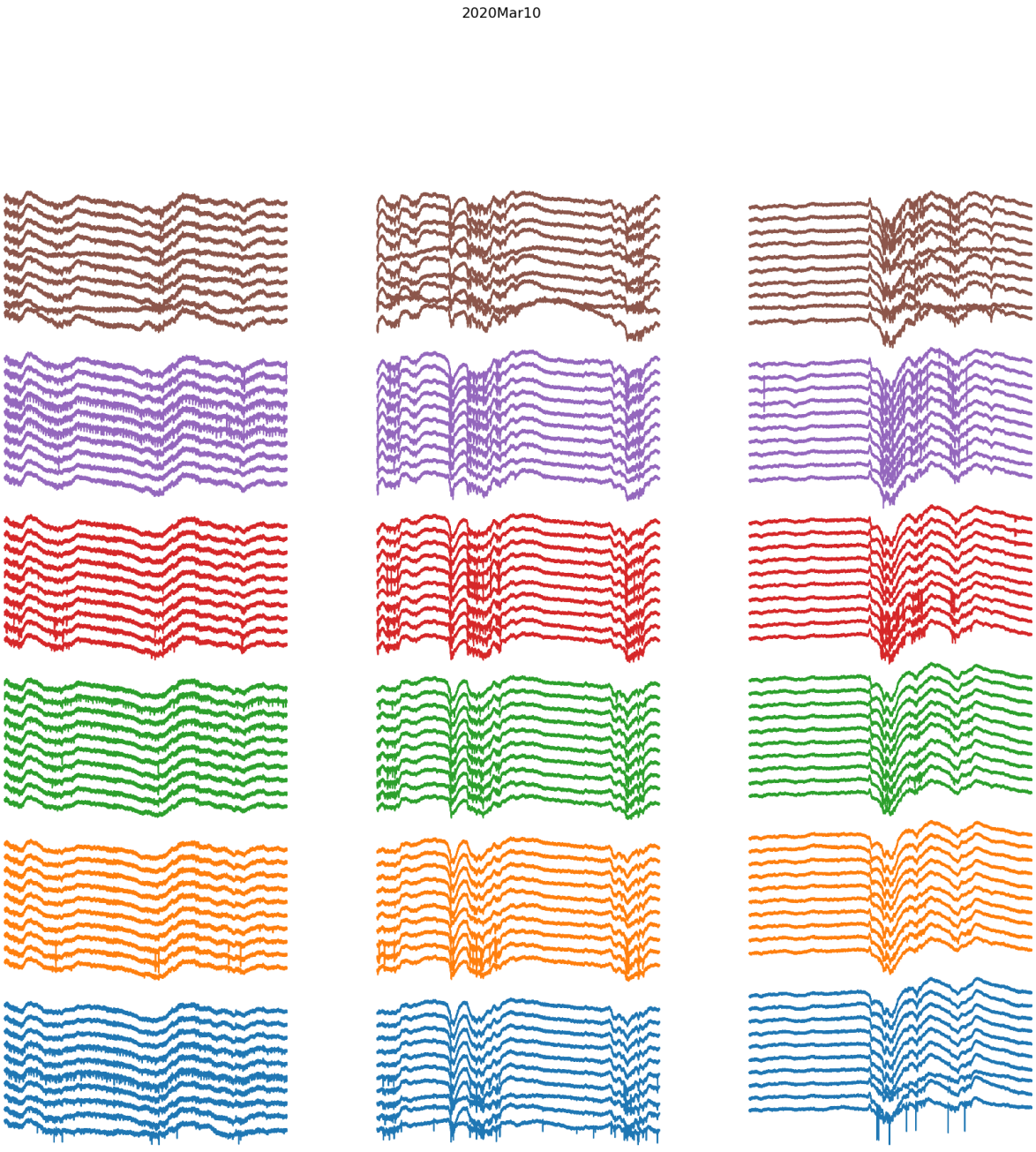

Source: The author (2023)